DISTRIBUTION, MINERALOGY, AND POTENTIAL RECOVERY OF RUTILE FROM THE CHUQUICAMATA PORPHYRY COPPER DEPOSIT OF NORTHERN CHILE

Trevor William Finlayson

Submitted in Partial Fulfillment of the Requirements
For the Degree of Bachelor of Science, Honours
Department of Earth Sciences
Dalhousie University, Halifax, Nova Scotia
May 10, 2002

Dalhousie University

Department of Earth Sciences
Halifax, Nova Scotia
Canada B3H 3J5
(902) 494-2358
FAX (902) 494-6889

DATE May 10, 2002

AUTHOR Trevor William Finlayson

TITLE Distribution, mineralogy, and potential recovery of rutile from the Chuquicarrata porphyry copper deposit of northern Chile.

Degree BSc Convocation May Year 2002

Permission is herewith granted to Dalhousie University to circulate and to have copied for non-commercial purposes, at its discretion, the above title upon the request of individuals or institutions.

Abstract

Rutile is a common accessory phase in altered porphyry copper ores (up to 1 wt. % of the host rock), yet it is generally lost to tailings, despite its relatively high price. Ti metal (*sponge*) is about 5 times the price of Cu, and high-grade rutile concentrate for pigment is comparable in price to copper-sulphide concentrate. This pilot study assesses the feasibility of rutile recovery from ores going through the mill of the Chuquicamata porphyry copper deposit. As a first step, ores and heavy mineral concentrates were analysed using microscopy, and electron probe microanalysis, as well, various statistical analyses were completed on a large database of major metal and mineralogical content of heavy mineral concentrate samples.

Rutile commonly forms by alteration of titanite, titanium-bearing magnetite, or biotite. In the potassic alteration zone of Chuquicamata, rutile occurs as individual grains surrounding biotite or pseudomorphing titanite, in habits that could lead to easy liberation. In the quartz-sericite alteration zone rutile is intergrown with pyrite, thus decreasing the likelihood of effective separation.

Statistically, there is a high positive correlation r between rutile and chalcopyrite, rutile and bornite, and a consistently high negative correlation between rutile and pyrite. This behaviour mimics a high positive correlation between Ti and Cu in the least overprinted potassic alteration zone (Cu/Ti ~15/1; $r = 0.82$). Geochemically, the element Ti behaved as immobile element during alteration. A high negative correlation between Ti and Cu observed in the quartz-sericite alteration zone, suggests a fresh input of Cu into a constant reservoir of Ti during this hydrothermal event.

The geochemical characterization of trace elements could facilitate the use of refractory rutile in geochemical exploration for porphyry copper deposits. U, and Th content detected in rutile suggest it is datable by U/Pb methods. Image analysis in the microprobe allows determining the relative morphology and size of rutile in polished grain mounts of heavy mineral concentrates, and permits useful imaging of degree of liberation. The results suggest that full liberation of rutile would require excessively fine milling (to ca. 10 μm) making it uneconomic, however an investigation into the possibility of partial recovery via a series of froth flotation circuits may be warranted.

Keywords: *Titanium, Rutile, Porphyry Copper Deposits, Hydrothermal Alteration, Froth Flotation*

Table of Contents

Table of Appendices

Table of Figures

Table of Tables

Acknowledgements

First and foremost, I would like to thank my supervisor Dr. Marcos Zentilli for his ongoing enthusiasm and support throughout the duration of this project.

I am grateful to Cuesta Research Ltd. for allowing me the use of their heavy mineral concentrate samples, which was a crucial source of information for this project. As well I would like to extend my thanks to graduate student Lexie Arnott for lending me all of her relevant microprobe data, polished thin sections, and providing a wealth of knowledge pertaining to the Chuquicamata area, and to Milton Graves for answering many of my questions and taking the time to just chat about the project.

I would also like to thank Bob MacKay at the microprobe lab for all of his assistance, and to Gordon Brown for the production of the excellent polished sections.

Chapter 1

Introduction

1.1. General statement

As technology continues to advance, the element titanium is playing an increasingly important role in our lives. It has gained this importance because of its unique economic significance both as a metal and as an oxide. The majority of titanium mined today is from the exploitation of placer beach deposits. This thesis, however, examines the possibility of recovering titanium as a by-product of porphyry copper mining from already crushed ore during the milling process, which is particularly attractive from both an ecological and environmental standpoint. This is achieved through consideration of mineralogical, geochemical, and metallurgical aspects of titanium at the Chuquicamata porphyry copper deposit of northern Chile.

1.2. Objectives

The primary objective of this thesis is to determine the possibility of recovering titanium, in the form of rutile (TiO_2), from copper ore that is passing through the milling process at Chuquicamata. Studying the mineralogy, geochemical distribution, and grain size distribution of rutile within this area will complete this objective. As a secondary objective, I will describe how the titanium behaves geologically in the ores that comprise this deposit.

1.3. Introduction

Titanium is a lustrous silver-white metal. It has a very high strength to weight ratio and is resistant to dilute sulphuric and hydrochloric acid, most organic acids, chlorine gas, and chloride, making it extremely resistant to corrosion, a very useful

property that it is being used more and more for various marine applications and is the metal of choice for offshore oil structures. Titanium oxide is brittle, but titanium metal is ductile, and when heated it becomes malleable. The metal is also combustible in air, forming TiO_2, and is the only element that will ignite in nitrogen, producing titanium nitride (National Materials Advisory Board, 1983).

Titanium metal production only accounts for approximately 5-6% of the total titanium ore mined today. The majority of this product is used in the aerospace industry because of its unique high strength and low weight.

Based on the above properties, and the fact that titanium metal is nontoxic with a greater biocompatibility than stainless steel or cobalt chrome, it is highly used as hip and joint replacements, heart valves, pacemaker cases, and other prosthetic devices (Titanium Industries Inc., 1998). With an aging population, an increased demand for these products is inevitable (Hibberd and Smith, 1999).

Pure titanium dioxide has an extremely high refractive index (2.6 to 2.9, or higher than diamond (Force, 1991)), great inertness, and a negligible colour (pure white as powder), all qualities that make it close to an ideal pigment. For these reasons it is used heavily in the paper, rubber, plastic, paint, and even in the food industry. It has replaced lead-based pigments (proven health hazards) in many of these roles and commonly forms more than 20% by weight of some paints (Force, 1991). Titanium dioxide for use in the pigment industry consumes approximately 90% of the total titanium ore mined today (Force, 1991). Titanium dioxide also has uses outside of the pigment industry. It is also an excellent reflector, and is used as a sunblock in sunscreen (Hummel, 2000).

1.4. History of titanium

The element titanium was discovered just over 200 years ago as the result of independent investigations in England and Germany (Rose, 1969). Robinson (1922) reported that the Rev. William Gregor, a Scottish scientist, was investigating the black sand occurrence at Menachan, Cornwall around 1790. He named this sand *menoschite* (Rose, 1969). In 1794 or 1795 M.H. Klaproth, a chemist from Germany was investigating the composition of a mineral known as Hungarian *red schorl* (now known as rutile). He anticipated the presence of a new chemical element, which he called titanium after the titans of Greek mythology because of its great chemical bonding strength (Rose, 1969). In 1797, that Klaproth was working on the mineral Ilmenite, named after the Ilmen Mountains of the Urals in Russia, and recognized that his titanium element was the same as the element Gregor called menaschite (Rose, 1969).

Repeated attempts throughout the nineteenth century were undertaken to produce titanium metal from these compounds; however, only the nitride and sub-oxides were successfully obtained (McQuillian and McQuillian, 1956). At the end of the century, Moissian (1896) and Nilson and Pettersson (1887) succeeded in producing a metal containing about 95% titanium (McQuillian and McQuillian, 1956). The first moderately pure sample, which was reported as being 99.9% titanium, was prepared in 1910 by M.A. Hunter and associates at the General Electric Company while searching for a new material for lamp filaments (McQuillian and McQuillian, 1956). Hunter's process involved the heating of titanium chloride and sodium together in a vacuum to produce a metal that when cold was brittle, but when heated became malleable. Unfortunately, this new metal had a melting point of only 1800° C and was not suitable as lamp filament

material. Hunter's process, however, became the standard for titanium production during the next thirty years (McQuillian and McQuillian, 1956). In 1925, van Arkel and de Boer produced small quantities of titanium free from non-metallic impurities with a newly developed iodide dissociation method. It gradually became clear that titanium metal would have great advantages as a construction material if an economical process for its production could be created. W.J. Kroll (1940) solved this problem. Kroll devised a method of reducing titanium tetrachloride by passing it into a bath of molten magnesium, thereby launching the industrial exploitation of titanium (McQuillian and McQuillian, 1956).

1.5. Mineralogy of titanium: an overview

Titanium (Ti) has an atomic number of 22, making it a transitional metal on the periodic table. Titanium is a dispersed lithophile element (Van Baalen, 1993), and is the ninth most abundant element in the Earth's crust (0.86 percent Ti or 1.4 percent TiO_2); however, it does not occur in nature in its metallic form but is found in silicate and oxide minerals (Force, 1991). In igneous rocks, TiO_2 can be present up to 3.3 percent by weight in rocks of alkalic composition. Metamorphic rocks of eclogite composition can host up to 6 percent TiO_2 by weight, and shales can host up to 0.7 percent TiO_2 by weight (Force, 1991).

Titanium can be considered both a trace element as well as a minor element in a rock. If Ti reaches a sufficient concentration as a minor element (>0.1 wt%), it may form separate accessory minerals, the most common of which are titanite, rutile, and the Fe-Ti oxides (e.g. ilmenite) (Appendix 1 provides a complete list of the most common titanium bearing minerals). Trace elements are too dilute to form separate mineral phases, instead

they substitute for major and minor elements in common rock-forming minerals such as biotite and amphiboles (Winter, 1999).

Rock types	TiO_2 (%)	TiO_2 in oxide minerals (as % of total TiO_2)
Igneous rocks		
Ultramafic	0.2–0.8	1–4
Mafic	0.9–2.7	50
Felsic	0.2–0.8	3–30
Alkalic	0.1–3.3	3–50
Charnockitic	0.4–1.6	50–95
Anorthositic	0.1–0.5	50–95
Metamorphic rocks		
Gneiss	0.6	5–100
Schist and phyllite	0.6	1–70
Amphibolite	1.4	15–70
Serpentinite	0.0	n.a.
Eclogite	1.0–6.0	50–90
Sedimentary rocks		
Sandstone	0.2–0.6	10–100
Shale	0.6–0.7	?
Limestone	0.1–0.2	?

Table 1.1: Average titanium dioxide percentages of common igneous metamorphic and sedimentary rocks (After Force, 1991).

Titanium is an *incompatible* element and, based on the ratio of valence charge to ionic ratio it is defined as a *small, highly charged* element. Therefore, it is considered part of the group of *high field strength* (HFS) elements, along with the elements Th, U, Ce, Pb^{4+}, Zr, Hf, Nb, Ta, and the REE. Under subsolidus conditions, alteration, or metamorphism, these elements, including titanium, are considered to be relatively immobile in the presence of a fluid phase (Winter, 1999).

In silicates, titanium is most commonly found in **titanite**, biotite, calcic amphiboles (hornblende), and titanian augite (Force, 1976A). Ideally **titanite** ($CaTiSiO_5$) has 41 % by weight TiO_2, but is commonly fairly rich in REE, especially in late-stage

granites and pegmatites where significant amounts of niobium, tantalum, and vanadium have been analyzed (Deer et al., 1992).

Biotite ($K(Fe,Mg)_2(Fe,Al,Ti)Si_3AlO_{10}(OH,F)_2$) and hornblende ($Ca_2(Fe,Mg,Ti,Al)_5Si_7AlO_{22}(OH,F)_2$) do not contain relatively large amounts of titanium, but, because they are usually found in greater abundance than the titanium-rich accessory minerals, they become significant hosts of titanium in a mass balance calculation (Force, 1976A). Biotite and hornblende can contain up to 5.9 and 2.7 weight percent TiO_2 respectively in common igneous rocks of calc-alkalic compositions (Force, 1976A).

Titanian augite ($(Ca,Mg,Fe^{2+},Ti,Al)_2[(Si,Al)_2O_6]$) is a characteristic phase in many volcanic and alkalic dike rocks, such as monchiquites and essexites, which may contain as much as 9 percent TiO_2 (Deer et al., 1992).

The above titanium-bearing silicate minerals are important to the geochemical distribution of titanium, however, only titanium-bearing oxide minerals with more than 25 weight percent TiO_2 have economic value (Force, 1991). These minerals include ilmenite, rutile, and leucoxene.

Ilmenite ($FeTiO_3$), along with its alteration products, are the most abundant sources of TiO_2. Hard-rock mining of ilmenite is usually associated with gabbros, diorites, and anorthosites, and is primarily used in the production of TiO_2 slag (Force, 1991). In association with magnetite, ilmenite can be strongly magnetic, however, it still possesses a weak magnetism when magnetite is absent, especially if it contains manganese (Mn).

During the alteration of ilmenite, such as in hydrothermal environments, the leaching of iron (in contrast to the relative immobility of Ti) can cause a relative

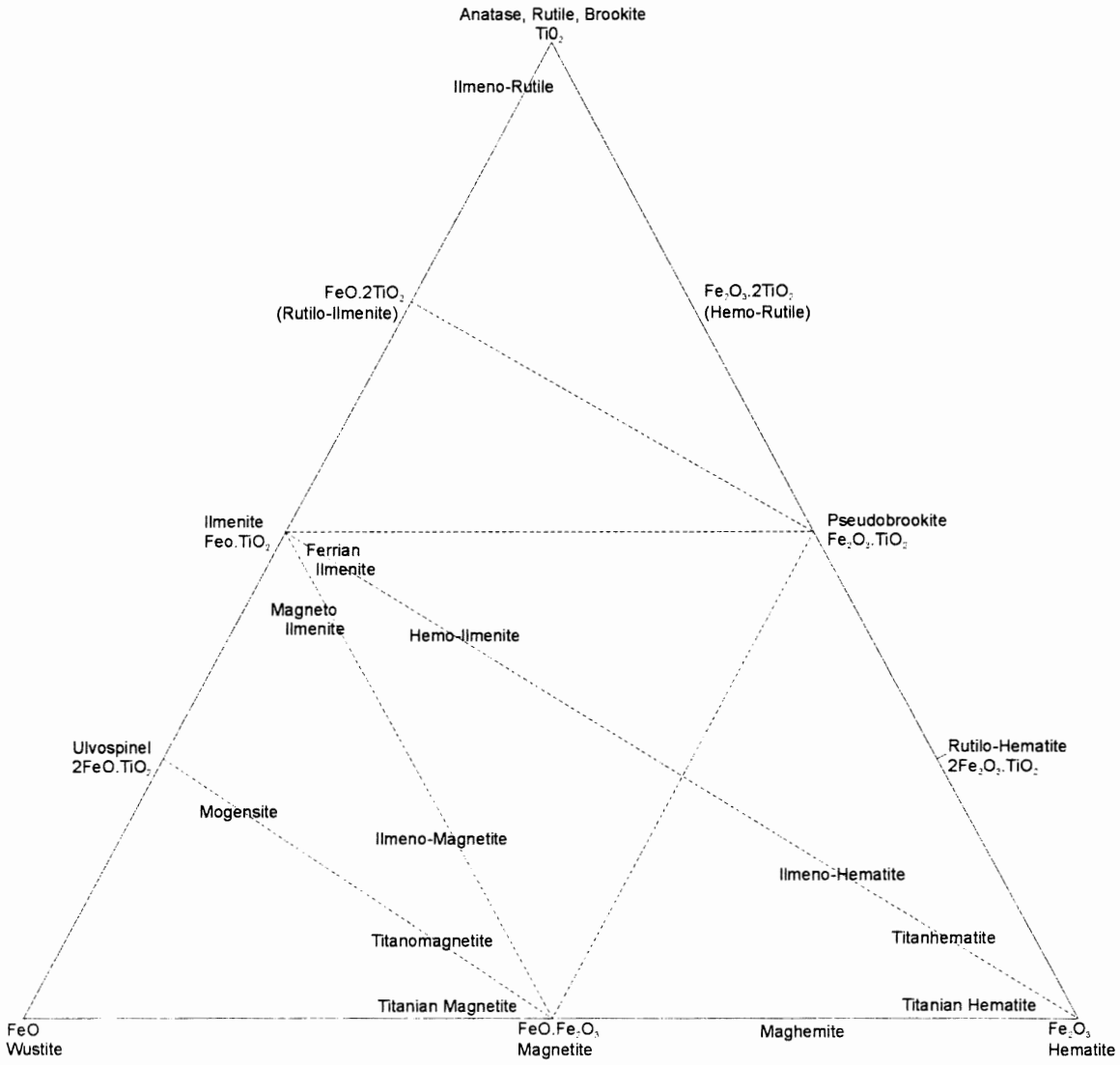

Figure 1.1: FeO-Fe_2O_3-TiO_2 system depicting suggested mineral series names and their approximate chemical compositions (After Rose, 1969).

enrichment in the amount of TiO_2 present (Force, 1976A). As alteration continues, the end product will be one of two polymorphs of TiO_2, **anatase** or, more likely, the highly stable high temperature polymorph **rutile** (Force, 1991). As the alteration progresses and the TiO_2 content becomes greater than 70 percent it is commonly referred to as **leucoxene** (Force, 1991). Leucoxene occurs as hard dark brown films, as a mixture of rutile, hematite, and pseudobrookite in titanium-bearing ores and sands. Leucoxene can also occur as soft creamy white films, as a mixture of titanite and altered feldspar in titanium-bearing rocks (Rose, 1969).

Rutile (TiO_2) is a common accessory mineral in igneous and metamorphic rocks. It has the smallest molecular volume of the TiO_2 polymorphs and tends to occur in high P-T assemblages (Deer et al., 1992). It commonly occurs as widely dispersed minute grains in plutonic rocks, and is also common in some amphibolites, eclogites, and in metamorphosed limestone (Deer et al., 1992). Rutile also occurs as inclusions in ilmenite, biotite, and most notably quartz, where it may take the form of long hair-like needles, (Deer et al., 1992).

1.6. Present knowledge of titanium in porphyry metal deposits

Most authors agree that, in hydrothermal porphyry deposits rutile is the dominant titanium-bearing mineral (Force 1976F, Williams and Cesborn 1977, Czamanske et al., 1981, and Force 1991). A number of articles state that the presence of titanium, in the form of rutile, in porphyry metal deposits. For example, Anderson et al. (1955) highlighted the fact that 6,000,000 lb of rutile was going through the Bagdad (Arizona) mill each year and that "a study of the economics of its recovery should be warranted" (Czamanske et al., 1981). Force (1976 F) discussed two possible reaction types

responsible for the presence of rutile in porphyry copper deposits, as well as the possibility of by-product recovery of coarser-grained rutile. Williams and Cesborn (1977) recorded the distribution and morphology of rutile in porphyry copper deposits as well as their uses as prospecting guides for other porphyry deposits. Czamanske et al. (1981) presented a discussion of the geological occurrence and potential resource aspects of rutile in porphyry metal deposits, with specific reference to the Bingham, San Manual, Bagdad, and Ajo deposits. Force (1991) provided a brief interpretation regarding the formation, use for exploration, and economic significance of rutile in porphyry deposits, with reference to the Bingham mine in Utah. Carson and Jambor (1974) described the presence of titanium oxide in various biotites of the Babine Lake Porphyry deposit of British Columbia.

1.7. Present knowledge of titanium in Chuquicamata

To date, there has been very little work done regarding presence of titanium in the Chuquicamata deposit. However, a report by Graves and Zentilli (1994) on the mineralogical, geochemical and structural aspects of Chuquicamata provided an excellent source of point count (point counting by Myriam Brockway, in CIMM report for CODELCO) and geochemical data of the elemental titanium and rutile mineralogy of concentrates from samples from the potassic zone of alteration, as well as samples from the surrounding MM and RT porphyry copper mines. A PhD thesis by A. Arnott (in progress) also discusses the geochemistry and mineralogy of titanium in Chuquicamata.

1.8. Organization of this thesis

This thesis is written from both the geological and metallurgical perspectives. Chapter 2 is an introduction to porphyry copper deposits, and the processes that lead to

the occurrence of rutile within them. As well it serves as an introduction to the geographic and geologic setting of the study site.

Chapter 3 provides a discussion of the various analytical methods employed to collect the mineralogical, geochemical, and metallurgical data needed to perform this study.

Chapter 4 presents the results of the analyses.

Chapter 5 discusses the geochemistry, mineralogy and distribution of titanium at Chuquicamata. It then presents the conclusions, the possibility of using rutile as a tracer for the exploration of other porphyry copper deposits, and some considerations for future studies.

Chapter 6 focuses on the metallurgical aspects of titanium. It discusses such topics as the grain size distribution, degree of liberation, ore grades, and processes employed at Chuquicamata for extracting copper and molybdenum from raw ore. It also gives a summary of my conclusions and suggests future research.

Chapter 7 serves as a literature review on froth flotation and how it could be utilized for the extraction of fine-grained rutile from the raw ore.

Chapter 2

Porphyry copper deposits, titanium distribution, and regional geology

2.1. Porphyry copper deposits

There has been considerable debate over a precise definition for a porphyry copper deposit. The first widely accepted definition was given by Lowell and Guilbert (1970 p. 374) as follows:

> "A copper and/or molybdenum sulfide deposit consisting of disseminated and stockwork veinlet sulfide mineralization emplaced in various host rocks that have been altered by hydrothermal solutions into roughly concentric zonal patterns. The deposit is generally large, on the scale of several thousands of feet...and...associated with a complex, passively emplaced stock of intermediate composition including porphyry units."

However, since then it has been stated that in hydrothermal ore deposits multiple intrusions are necessary to maintain the activity required to sustain the life of these systems, sometimes for hundreds of thousands of years (Hedenquist and Lowenstern, 1994 and all references therein). The model derived by Lowell and Guilbert (1970) (Figures 2.1(b) and 2.2) should, therefore, serve only as an example of an idealized porphyry copper deposit that has undergone all hydrothermal processes. It assumes that all zones of alteration occur simultaneously, however, this is not true. Reynolds et al. (1998) and Ballard et al. (2001) both agree that the Chuquicamata porphyry deposit is the result of multiple intrusions in which the two most developed alteration zones, the potassic and the quartz-sericite, have distinctly different ages. The potassic zone has an average age of 33.4 ± 0.3 Ma, whereas the quartz-sericite zone averages 31.1 ± 0.3 Ma

(Reynolds et al., 1998 and Ballard et al., 2001). No definition for a porphyry copper has been totally accepted. For instance, a mining geologist may consider a porphyry copper deposit as any large, low-grade copper deposit that can be developed by mass mining methods, regardless of its genesis and host rock type. A geological engineer, on the other hand, may include such properties as joint spacing, and rock mechanics, but again ignoring the geological significance of the deposit. In light of these differences, the revised definition presented by Guilbert and Park (1986, p.406) states

> "A porphyry copper deposit, or PCD, is a large low- to medium-grade deposit, primarily of chalcopyrite and molybdenite, in which hypogene sulfide and silicate zoning spans potassic-propylitic alkali metasomatic and phyllic-argillic hydrolitic alteration, and which is temporally and spatially related to epizonal calc-alkaline porphyritic intrusion."

and captures the most essential characteristics of this type of deposit. However, even this definition neglects the fact that these deposits are, in many cases, the creation of multiple intrusions with alteration zones forming over extended periods of time.

Porphyry deposits are commonly low-grade ore deposits, ranging from 0.5-0.8% Cu and 0.002% Mo for a typical porphyry copper, and 0.3% Mo and 0.05% Cu for a typical molybdenum deposit. The primary ore minerals are sulphides that occur as disseminated grains and veinlets located within, or adjacent to, porphyritic intrusions ranging from silicic to intermediate composition and commonly formed at depths of 2-5 km under lithostatic pressures (Hedenquist and Lowenstern, 1994).

The copper-bearing porphyries (e.g. Chuquicamata, Chile) are commonly found along the magmatic fronts of subducting plate margins, whereas the molybdenum-bearing types (i.e. Climax, Colorado) seem to be more characteristic of extensional zones

associated to back arcs (Craig and Vaughan, 1994). If the hosting country rock has a reasonable permeability a convective interaction with circulating groundwater can be established. This will result in very hot chemically abundant solutions that rise above the stock, simultaneous with an initially cool circulation of solution toward the stock. This convective process will cause the outer rim to crystallize first, forming an outer shell. Once the pressure from trapped groundwater within the melt of the inner core becomes critical, the outer shell becomes fractured, instantaneously reducing this pressure and thus quenching this melt to a porphyry (e.g. Craig and Vaughan, 1994).

Based on this process, subtle thermal gradients are defined from higher temperatures to lower ones nearer the surface and outwards. These temperature gradients that define the zones of hydrothermal alteration and mineralization that are thought to represent deuteric to late stage magmatic conditions (e.g. Lowell and Guilbert, 1970).

2.1.1. Alteration zones

A porphyry copper system is defined by specific zones of hydrothermal alteration (Figure 2.1), which are closely related to the vertical and outward temperature gradients discussed in Section 2.1. These zones were defined by Lowell and Guilbert (1970) as: the potassic zone, phyllic zone, argillic zone, and propylitic zone, for an idealized porphyry copper deposit. Guilbert and Park (1986) have since defined a zone of advanced argillic alteration that was not recognized by Lowell and Guilbert (1970). These zones typically define a sequence consisting of a potassic inner core, outward to a propylitic outer shell.

2.1.1.1. Potassic zone

The innermost zone (core) of alteration in a porphyry copper system is the potassic zone. It is characterized by the replacement of primary minerals by K-feldspar, hydrothermal biotite, quartz, and sericite. To a lesser extent occurrences of magnetite, anhydrite, carbonates, apatite, rutile, fluorite, scheelite, and wolframite are present (Lowell and Guilbert, 1970, Guilbert and Park, 1986).

2.1.1.2. Phyllic zone

Often referred to as the "quartz-sericite zone" or "sericitic zone," the phyllic zone is a dome-shaped zone surrounding the core of potassic alteration and consisting predominantly of the hydrothermal minerals sericite and quartz that have replaced all of the primary rock forming silicates such as feldspars, micas, and mafic minerals (Guilbert and Park, 1986). Common accessory hydrothermal minerals include pyrite, minor chlorite, and traces of rutile. The inner portion of this zone is dominated by sericitic alteration, whereas towards the edge clay minerals and hydromica prevail. There is less abundance of alteration quartz, however, it is commonly associated with anhedral or sagienitic rutile or leucoxene, both of which are thought to represent the displacement of titanium from primary biotite and titanite (Lowell and Guilbert, 1970, Guilbert and Park, 1986).

2.1.1.3. Argillic zone

The argillic zone is the smallest, and usually least developed, zone of alteration. It is characterized by the alteration of plagioclase to the clay minerals kaolinite, and montmorillonite. Kaolinite is the most common reaction product, occurring nearer the

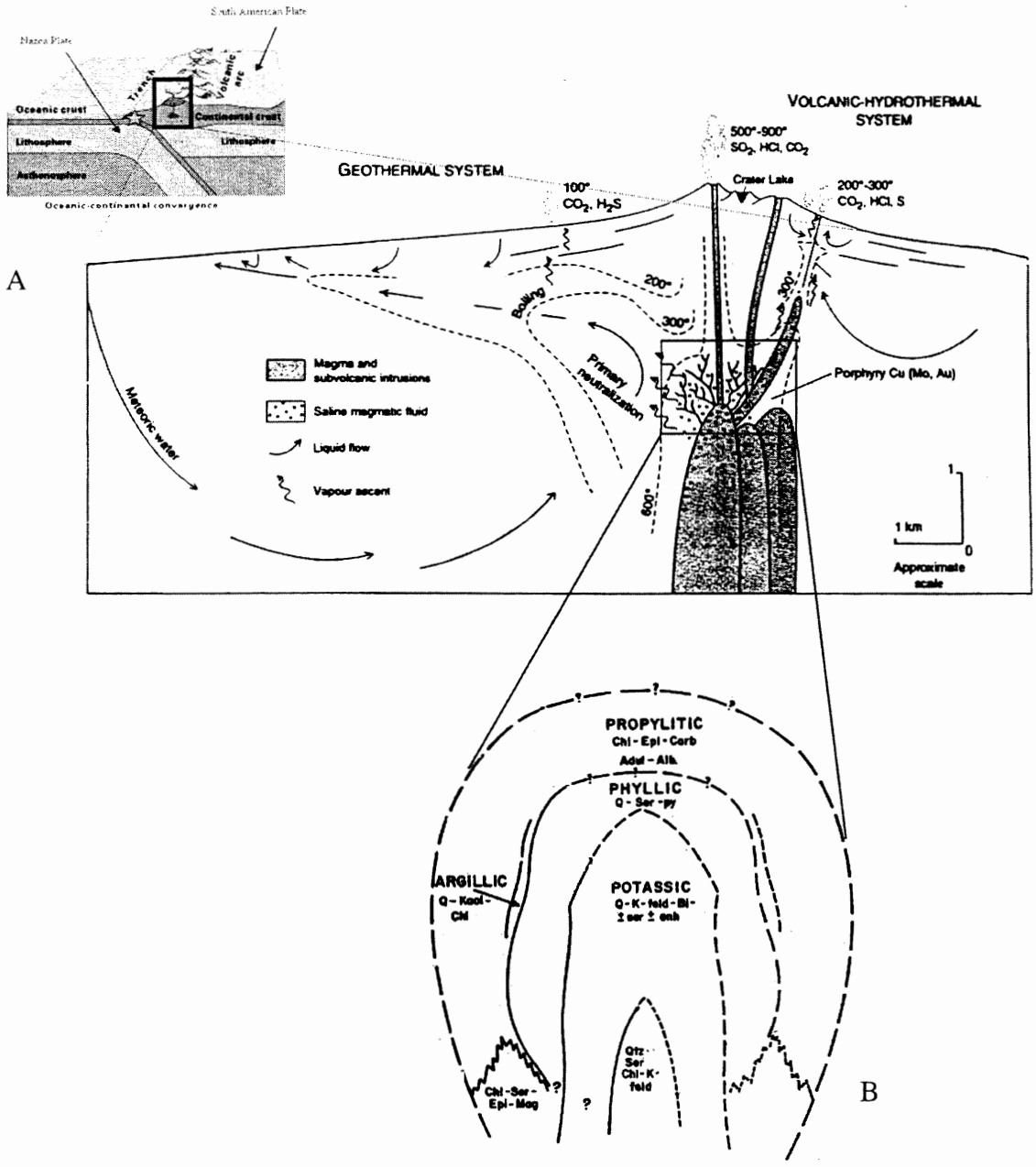

Figure 2.1: (A) Idealized model of the porphyry copper environment along subduction zones with the associated stratovolcano. (B) Concentric zones of alteration that result from the interaction of hydrothermal fluids on intrusive igneous rocks and the surrounding country rock. (After Hedenquist and Lowenstern, 1994, and Lowell and Guilbert, 1970).

orebody, however, it decreases in abundance, with distance from the orebody, giving way to the montmorillonite. Again, pyrite is common but much less abundant than in the phyllic zone. Primary biotite and K-feldspar seem to be generally unaffected, however, the biotite may have minor chlorite alteration along its cleavages, and the K-feldspar may show minor sericitization or kaolinite dusting (Lowell and Guilbert, 1970, Guilbert and Park, 1986).

2.1.1.4. Advanced argillic zone

This zone is characterized by the presence of pyrophyllite or pyrophyllite-andalusite, which occurs at temperatures above about 300°C, or kaolinite or dickite, which become dominant at temperatures below 300°C (Guilbert and Park, 1986). This zone also has an abundance of quartz, and an association with the Cu-As-S minerals enargite and tennanite-tetrahedrite (Guilbert and Park, 1986).

2.1.1.5. Propylitic zone

A wide distribution and least distinctive alteration assemblage is characteristic of this zone. It involves the alteration-generation of epidote, chlorite, and carbonates that are typically replacing plagioclase, and the replacement of hornblende and biotite by epidote, calcite, and montmorillonite (Guilbert and Park, 1986). It is also characterized by the addition of H_2O, H^+, CO_2, and S (Guilbert and Park, 1986).

2.1.2. Mineralization zones

The zones of mineralization are somewhat coherent with the zones of alteration (Fig. 2.2 a & b); therefore, each zone can be distinguished based on its location within the porphyry copper system.

2.1.2.1. Potassic zone

Craig and Vaughan (1994) have divided the potassic zone into two coinciding zones of mineralization. The first, an inner low-grade (<0.3% Cu) core containing pyrite and chalcopyrite at a 1:2 ratio, along with minor magnetite and molybdenite. The second consists of an ore shell (>0.5% Cu) that has a ratio of 1:1 between pyrite and chalcopyrite. The pyrite is generally contained in veinlets, whereas the chalcopyrite occurs as disseminated grains (Lowell and Guilbert, 1970). Minor molybdenite occurs as veinlets and dispersed grains. Discrete grains of bornite, intergrown with chalcopyrite, are also common.

2.1.2.2. Phyllic and argillic zones

The phyllic zone overlaps with the outer region of the ore shell as defined by figure 2.2 (a). However, this shell does not include the entirety of these zones. Surrounding it, but within these zones, has copper mineralization ranging from 0.1% - 0.5% with a pyrite to chalcopyrite ratio of 10:1. The pyrite and chalcopyrite are typically found in veinlets (Lowell and Guilbert, 1970). A zone of pyrite mineralization, known as the pyrite shell, surrounds the previously mentioned copper mineralization, but is still within the phyllic and argillic zones. This shell can range from 6%-25% pyrite by weight (Lowell and Guilbert, 1970), and occurs as coarse anhedral pyretic-quartz veins up to 2 cm thick (Craig and Vaughan, 1994).

2.1.2.3. Propylitic zone

Mineralization in this zone consists of minor, small, high-grade silver, gold, and chalcopyrite veins, as well as veinlets of pervasive pyrite (2%-6% by weight) (Lowell

and Guilbert, 1970). Typical hydrothermal base-metal occurrences, such as galena and sphalerite, are also present in this zone (Craig and Vaughan, 1994).

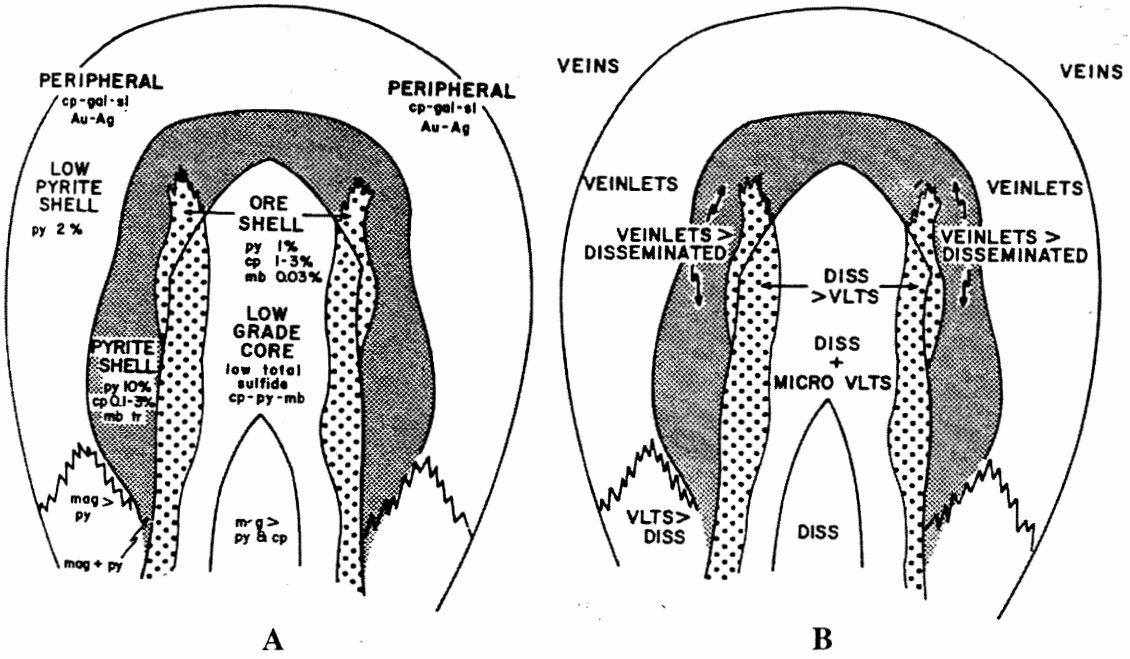

Figure 2.2: Zones of mineralization (A) and types of sulphide occurrence (B) in an idealized porphyry copper deposit. (After Lowell and Guilbert, 1970).

By considering a porphyry copper deposit as a single entity, the significance of erosional and metamorphic processes in defining economically viable amounts of ore at any given deposit becomes clear. Consistent with the model of mineralization established by Lowell and Guilbert (1970), the ore grade increases with depth below surface, possibly dictating the type of mine (open pit vs. underground), depending of the level of erosion and degree of post-ore metamorphism or deformation that it has undergone.

2.2. Hydrothermal fluids

Porphyry copper deposits tend to occur in association with more oxidized magmas, those that contain magnetite (Hedenquist and Lowenstern, 1994 and all references therein). The mineralization in porphyry copper deposits is dominated by the influence of magmatic fluids in the early stages, however, in later stages of its development meteoric water may become a common and critical fluid for enhancing porphyry metal concentrations to ore grade (Hedenquist and Lowenstern, 1994 and all references therein). Hydrothermal fluids related to porphyry copper deposits are classified as high-sulphidation fluids that typically contain CO_2, SO_2, H_2S, and HCl (Hedenquist and Lowenstern, 1994 and all references therein). Fluid inclusion studies have also indicated that these fluids may have a salinity of 2-5 wt% NaCl eq., with a noticeable increase with depth to 20-30 wt% NaCl eq. below the ore zone (Hedenquist and Lowenstern, 1994 and all references therein).

Figure 2.3 shows the stability fields of the major mineral assemblage of the ore zone, chalcopyrite, bornite, and pyrite. This allows for the identification of the ore-depositing environment. The first constraint is the abundance of pyrite along with the absence of pyrrhotite and hematite, so the conditions are within the line labeled Py. Secondly, along with pyrite, chalcopyrite and bornite are also predominant ore assemblage minerals, so the conditions are now moved close to the Bn+Py/Cp line. Another important constraint is the pH, which is generally fixed in the muscovite (sericite) stability field near the feldspar limit (Barnes, 1979), therefore it would be weakly acidic. The absence of graphite puts conditions at aO_2 (or fO_2) above this field, and the presence of varying amounts of hydrothermal barite and anhydrite means that the

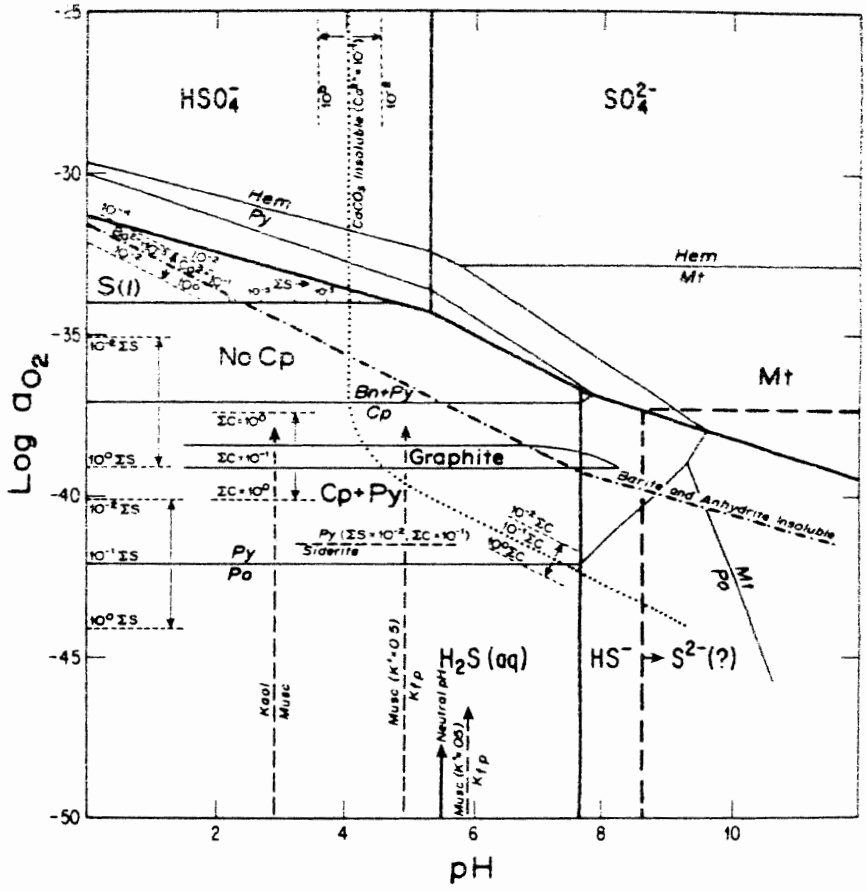

Figure 2.3: Stability diagram of log a O_2 vs. pH for minerals in a porphyry copper deposit at temperatures of 250°C (After Barnes, 1979).

solution must have reached saturation close to the "Barite and Anhydrite Insoluble" curve (Barnes, 1979). Locally calcite also makes an appearance (although not seen at Chuquicamata), occurring in small veins in the ores, thus, indicating solution saturation close to the "$CaCO_3$ Insoluble" curve (Barnes, 1979). Based on these constraints, the preferred zone of deposition is within a triangle comprised of the dotted carbonate line, the dash-dot barite-anhydrite line, and the solid Bn+Py/Cp line (Barnes, 1979).

2.3. Titanium distribution in porphyry copper deposits

Rutile is the most common titanium-bearing mineral in porphyry copper deposits. It is a secondary mineral that is formed by the alteration of primary titaniferous minerals such as magmatic biotite, hornblende, titaniferous magnetite, titanite, and ilmenite (Force, 1991). These host minerals are present in the unaltered parent rock, usually of calc-alkaline granitic composition; however, neither of them is stable in the hydrothermal environment (Force, 1991). They are either altered to new minerals containing lower amounts of TiO_2, such as biotite, hornblende, and magnetite, or they disappear altogether, such as ilmenite and titanite.

Force (1976F) first noted that the reactions responsible for the liberation of titanium from primary minerals to their hydrothermal equivalents are driven predominantly by the introduction of sulphur or carbon dioxide (CO_2). Force (1991) defined five chemical reactions that are responsible for the secondary rutile. In the first type, sulphur reacts with the biotite [Equation 2.1], and hornblende [Equation 2.2] to form pyrite, hydrothermal silicates, and rutile.

Biotite + Sulphur $\Rightarrow$ Phlogopitic Biotite + Pyrite +Rutile

$$K(Fe,Mg)_2(Fe,Al,Ti)Si_3AlO_{10}(OH,F)_2 + S_2 \Rightarrow \quad [2.1]$$

$$K(Mg,Fe)_3Si_3AlO_{10}(OH,F)_2 + FeS_2 + TiO_2$$

Hornblende + Sulphur $\Rightarrow$ Actinolitic Hornblende + Pyrite + Rutile + Alumina

$$Ca_2(Fe,Mg,Ti,Al)_5Si_7AlO_{22}(OH,F)_2 + S_2 \Rightarrow \quad [2.2]$$

$$Ca_2(Mg,Fe)_5Si_8O_{22}(OH,F)_2 + FeS_2 + TiO_2 + Al_2O_3$$

The titaniferous magnetite [Equation 2.3] will react with the sulphur to produce stoichiometric magnetite with pyrite and rutile.

Titaniferous Magnetite + Sulphur $\Rightarrow$ Stoichiometric Magnetite + Pyrite + Rutile

$$2(Fe,Ti)_2O_4 + S_2 \Rightarrow Fe_3O_4 + FeS_2 + TiO_2 \quad [2.3]$$

Also, primary ilmenite [Equation 2.4] reacts with sulphur to produce pyrite and rutile.

Ilmenite + Sulphur $\Rightarrow$ Pyrite + Rutile

$$FeTiO_3 + S_2 \Rightarrow FeS_2 + TiO_2 \quad [2.4]$$

The second type of rutile forming reaction involves the introduction of CO_2. It reacts with primary titanite and produces hydrothermal rutile, calcite, and quartz [Equation 2.5].

Titanite + carbon dioxide $\Rightarrow$ Rutile + Calcite + Quartz

$$CaTiSiO_5 + CO_2 \Rightarrow TiO_2 + CaCO_3 + SiO_2 \quad [2.5]$$

The titanite – carbon dioxide reaction is a function of CO_2 pressure, in which a high pressure will force the reaction toward a rutile and carbonate product (Force 1976F). The problem with this reaction is that carbonate is a rare mineral in porphyries, and at Chuquicamata it is not present; therefore, some other reaction must have controlled the alteration of titanite.

2.3.1. The use of rutile as a prospecting tool for porphyry copper deposits

Rutile in a porphyry copper deposit corresponds relatively well with the change in zones of alteration, by combining this characteristic with its high resistance to weathering in soils, it is not inconceivable to think that rutile could serve as a valuable exploration tool for other porphyry copper deposits. As described above, rutile is the major titanium-bearing mineral phase in porphyry copper deposits. Evidence from this study suggests that it first appears in the potassic zone of alteration and progresses outwards into the quartz-sericite zone and into the argillic zone. As this progression advances, there is a noticeable decrease in the overall abundance and size of this mineral, as well as a general decrease in the total titanium content.

Williams and Cesbron (1977) discussed that rutile in most environments have a high ratio (Nb + Ta)/ (Cr +V), however the reverse is true for rutile related to porphyry copper deposits.

A study by Force et al. (1984) was carried out on the feasibility of using rutile as an exploration tool for porphyry metal deposits based on its distribution in the surrounding soils of the deeply weathered Tangse porphyry of Sumatra. The study proposed two types of tests, a proximal exploration in soils and local streams and a distal exploration in the sediments of larger streams. The results of this study indicated that the proximal methods proved to be a valuable tool while the distal methods did not. The proximal method was most effective because the soil samples showed a rutile distribution that closely related to the intensity of alteration in the parent rock. This distribution of rutile was limited to soils that covered rock that had been affected by quartz-sericite or potassic alteration. As well the coarsest rutile was found to be within the area of

maximum sulphide concentration. The local stream sediment samples all contained rutile as well. The distal method, consisting of samples from large streams did not show any presence of rutile. The two problems that were defined for this result were: 1) there was a massive dilution with other debris, so rutile was extremely hard to locate. 2) Most of the fine-grained rutile had been transported to lower energy depositional sites downstream.

Lawrence and Savage (1975) presented a study of the porphyry copper deposits of Melanesia in which they too found the persistence of rutile in the alteration zones of the deposits. They then stated that upon weathering it would seem likely for rutile to be released into the nearby alluvium or eluvium, cumulating as erosion and weathering progresses, to enable detection form samples in these localities. They also conceived the possibility of titanium halos occurring around porphyry copper deposits. This idea was never confirmed, however, if such a thing existed, they might surround areas of higher copper concentration.

The actual by-product mining of rutile from porphyry copper deposits may in fact turn out to be uneconomical, however, its presence may lead to the discovery of larger copper reserves than was expected at various deposits. It has also proven to be a valuable tool in the exploration for new deposits, which in itself gives it an economic value.

2.4. Regional and geological setting

The Chuquicamata porphyry copper deposit of Northern Chile lies approximately 2,800 m above sea level in the Atacama Desert, about 240 km northeast of the port of Antofagasta, and 16km northeast of the town of Calama (22° 17.5'S, 68° 54.5'W)(Figures

2.4 and 2.5). Located in the Precordillera of Northern Chile, it lies to the west of the modern continental arc volcanoes of the Andean Cordillera (Ossandón et al., 2001).

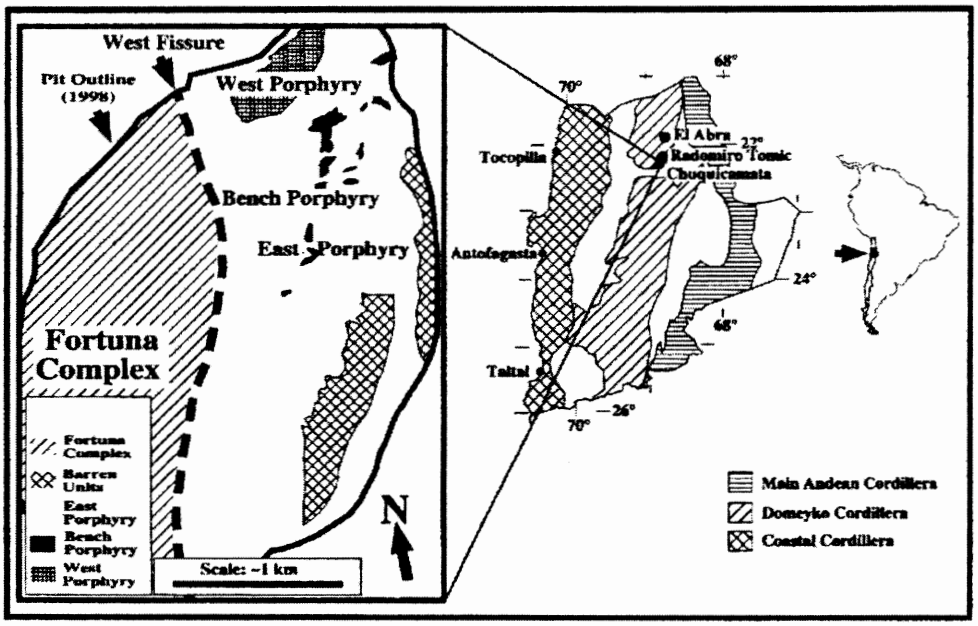

Figure 2.4: Location of Chuquicamata Mine along with East, West, and Banco porphyries (After Ballard et al., 2001).

The porphyry copper deposits of Northern Chile represent the world's premier porphyry copper district where, along with Chuquicamata, several major deposits such as Collahuasi, Spence, Escondida and El Salvador, as well as numerous smaller and sub-economic deposits, occur (Richards et al., 2001). Along with Chuquicamata, two smaller porphyry copper deposits are also studied. These include the Radomiro Tomic (RT) deposit to the north, and the Mansa Mina (MM) deposit to the south (Fig. 2.4). These deposits are all located on a narrow 30-to-50- km wide, orogen-parallel belt stretching over 1,000 km from 28° to 19°S and possibly as far as southern Peru at 18° S (Richards et al., 2001; Clark et al., 1998). This belt is known as the Sistema de Falla de Domeyko

(Domeyko Fault System) because its western boundary is defined by the intersection of the Cordillera Domeyko and the Depression Intermedia (Central Valley) (Richards et al., 2001). Of all the porphyry deposits in Northern Chile, Chuquicamata is the most closely related to this fault system in space and time (Ossandón et al., 2001). The reason for this relation is that magmatism in the Eocene-Oligocene resulted in a weakening of crust in the Chuquicamata district, creating a west fissure zone of strike-slip deformation known as the Falla Oeste (West Fault), which is a branch of the more extensive Domeyko fault system (Maksaev & Zentilli, 1988; Lindsay et al., 1995; Lindsay, 1998). The West Fault is responsible for the juxtaposition of the non-economic Fortuna complex against the ore-bearing Chuquicamata porphyry in the central part of the pit (Lindsay et al., 1995; Lindsay, 1998).

2.4.1. Chuquicamata Porphyry Complex

Practically all of the Chuquicamata orebody occurs at the southern end of the 3 km x 12 km NNE trending Chuquicamata Porphyry Complex (Fig. 2.5) (Ossandón, et al., 2001). This complex is comprised of the East, West, and Banco (Bench) porphyries (Figure 2.4), all of which, in their least altered state contain plagioclase, quartz, K-feldspar, biotite, and hornblende, with accessory titanite and magnetite (Ossandón et al., 2001). Each exposure has been affected to some degree of hydrothermal alteration and pervasive cataclastic deformation, therefore, textures are widely varied, and sharp intrusive contacts have only been observed between the East and Banco porphyries (Ossandón et al., 2001).

Of these three porphyries, the East porphyry is the largest and presumably the oldest (Ossandón et al., 2001). It is classified as a granodiorite to monzogranite

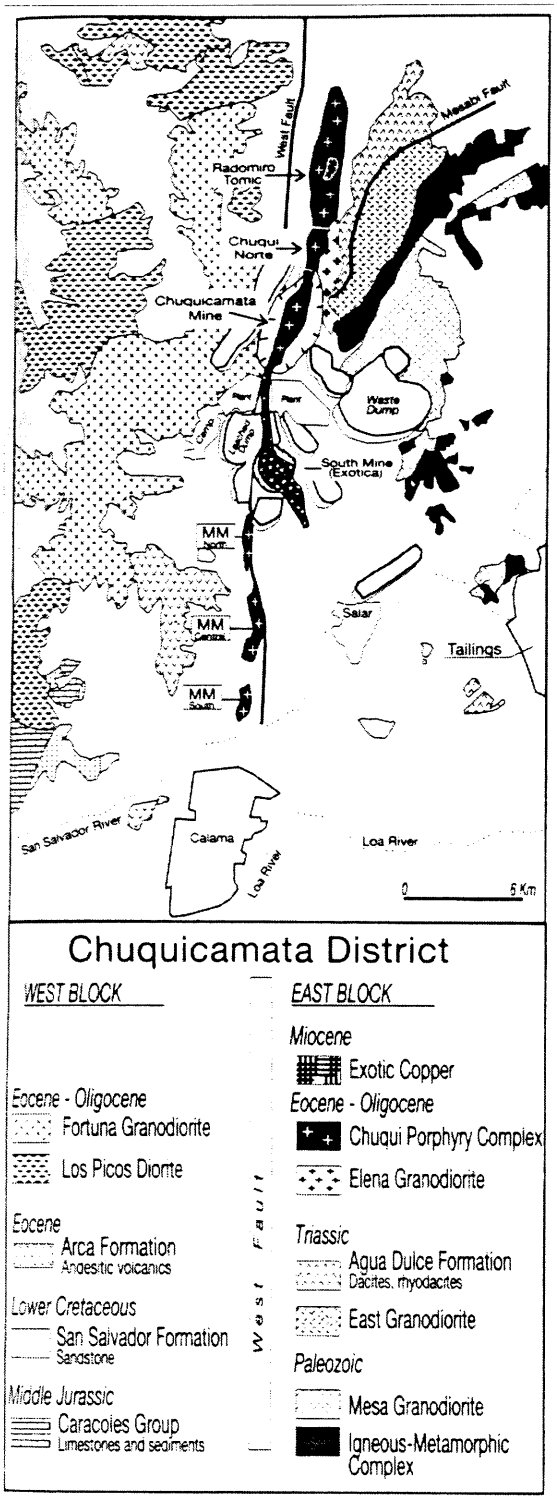

Figure 2.5: Geological Map of the Chuquicamata Mining district, showing the Radomiro Tomic (RT) and Mansa Mina (MM) mines to the north and south respectively of the Chuquicamata mine (After Ossandón et al., 2001).

displaying a hypidiomorphic-granular texture (Ossandón et al., 2001), with medium to coarse grains in a scarce matrix (Lindsay, 1998). The Banco and West porphyries have only minor occurrences (Lindsay, 1998). There are outcrops of the West porphyry in the northern end of the pit; however, its boundaries have not yet been clearly defined (Ballard et al., 2001). It has been classified as a monzogranite to granodiorite containing visibly spaced phenocrysts occurring in a saccaroidal matrix (Lindsay, 1998). The Banco porphyry intrudes into the East porphyry (Ossandón et al., 2001) along the eastern flank of the pit in a series of north-trending dike-like bodies offset by later faulting (Lindsay et al., 1995; Lindsay, 1998). It has been classified as a monzodiorite that contains a bimodal distribution of phenocryst size distribution set in an aphanitic matrix (Lindsay, 1998).

To the west of the Chuquicamata Porphyry Complex, adjacent to the mine, is the Fortuna Intrusive Complex (Fig. 2.4), which contains only a low-grade mineralization and has been structurally displaced against the heavily mineralized Chuquicamata Porphyry Complex by regional, post-mineral movement along the West Fault (Ossandón et al., 2001). The volumetrically dominant lithological unit within the Fortuna Intrusive Complex is the Fiesta Granodiorite. It shows weak mineralization, mainly around contacts of the intruding San Lorenzo porphyries, comprised of weak chalcopyrite-(bornite) disseminations and veinlets, minor chalcopyrite-magnetite veinlets, and molybdenite on the fractures; however, all of the rock west of the West Fault are shipped to the waste dumps, and mapping is only for slope stability purposes (Ossandón et al., 2001).

To the east of the Chuquicamata Porphyry Complex, at the eastern margin of the pit are the Elena and East Granodiorites (Fig. 2.4), both of which intrude metasedimentary rocks that were originally shale and sandstone with minor limestone (Ossandón et al., 2001). Compared to the spatially dominant East porphyry of the Chuquicamata Porphyry Complex, the East Granodiorite is unmistakably different texturally and clearly older; however, the Elena Granodiorite is both mineralogically and texturally similar (Ossandón et al., 2001). Regardless of this similarity all of the rocks occurring at the eastern edge of the mine are essentially barren, although geological activity has been highly concentrated within and adjacent to the orebody extending 800-1200 m east of the West Fault (Ossandón et al., 2001).

2.4.2. Radomiro Tomic (RT)

The Radomiro Tomic (RT) porphyry deposit is also located along the north-south trending West Fault. The reason for its importance in this study is that the host rock is part of the Chuquicamata Porphyry Complex and consists predominantly of potassium-altered rocks (Cuadra and Rojas, 2001). This zone of alteration is responsible for the majority of ore grade mineralization (Lowell and Guilbert, 1970). The deposit itself is located beneath a flat desert valley 5 km north of the Chuquicamata mine (Figure 2.5). The deposit is of granodioritic-to-monzodioritic composition with hydrothermal alteration dated to Early Oligocene (Pemberton, 1997).

2.4.3. Mansa Mina (MM)

The third porphyry copper deposit that will be included in this study is the Mansa Mina (MM) deposit. The MM deposit is a completely concealed porphyry, covered by a large piedmont gravel plain and is located about 10 km south of the Chuquicamata mine

(Figure 2.5) (Sillitoe et al., 1996). This deposit, based on its similarities with Chuquicamata, is regarded as part of the Chuquicamata Porphyry Complex, the displacement of which occurred along the West Fault. The alteration within this deposit is predominantly quartz-sericite that was developed pervasively, which commonly resulted in the destruction of primary igneous textures of the host granodiorite (Sillitoe et al., 1996). As well, near the West Fault minor anhydrite that has been hydrated to supergene gypsum can be found locally (Sillitoe et al., 1996).

Chapter 3

Data acquisition and analytical methods

3.1. Sample/data acquisition

The data for this report was compiled from two separate sources. The first consisted of heavy mineral concentrate samples. These samples were prepared by CIMM in Santiago from drill core (Chuquicamata and Mansa Mina) and muck (Radomiro Tomic). Samples were taken from the portions of half drillcore sampled fro assay by CODELCO, but not assayed. These samples were randomly subsampled and crushed. Crushing varied with liberation, but the resulting samples usually contained sand-sized particles. Enough sample was run through heavy liquid separation with a centrifuge under controlled grinding to avoid fines <-200 Ty. This process generated approximalty 50 grams of heavy mineral concentrates and a few light fractions for subsequence mineralogical examination. From these concentrates mineralogical and geochemical analyses were carried out.

Six grams of each heavy mineral concentrate was used for grain mounts, in which mineralogical studies were preformed on. Myriam Brockway, CIMM, using reflected light microscopy of polished grain mounts prepared from the heavy mineral concentrates, did the mineralogy. Mineral proportions were done by point counting at least 1500 points on each sample. The results have been reproduced in Appendix 1 of this report.

CIMM analyzed the heavy mineral concentrates for major metals using conventional atomic absorption analyses. The results are to be found in the original CIMM reports; extracts are reproduced in Appendix 2 of this report.

The second source for this dataset came from the work of PhD student Alexandra Arnott of Dalhousie University. She provided microprobe data of rutile (Appendix 4) and titanite (Appendix 5) grains from polished thin sections taken from the Chuquicamata mine. She also provided the polished thin sections, representing various degrees of hydrothermal alteration at the Chuquicamata mine.

3.2. Analytical methods

In order to understand the mineralogical distribution of titanium bearing minerals within the Chuquicamata Porphyry Complex a number of analytical techniques were utilized. These included transmitted and reflected light petrography, X-ray diffraction, microprobe and image analysis, grain size distributions, and various statistical methods.

3.2.1. Microscopy

For this study both, transmitted light and reflected light microscopy was used for the identification of titanium-bearing minerals and their relationship to other minerals in thin sections, polished sections, and polished grain mounts. The majority of oxide minerals are opaque; however, rutile is one of the few exceptions that, because of high internal reflections it is possible to view it under both types of light. Titanite, which is a silicate, can undoubtedly be distinguished by transmitted light microscopy; however, it cannot be identified in reflected light. The importance of studying ore-gangue relationships and translucent ore minerals that is best suited for transmitted light microscopy has led to the use of both types of microscopes for the completion of this study. All microscopy was performed with microscopes of the Fission Track Research Laboratory at Dalhousie University.

3.2.2. X-ray diffraction (XRD)

X-ray diffraction analysis was done at the Fission Track Laboratory, Dalhousie University for the purpose of identifying the magnetic minerals present in the least altered composite sample from the Radomiro Tomic mine. The X-ray diffraction process used at Dalhousie University makes use of the powder diffraction method. Sample preparation for this method is done by grinding the sample in acetone in a hand-held mortar. Accurate X-ray diffraction analysis from a powder sample require that it be ground to under 50 μm for simple analysis, to 10 μm or smaller for more complex tests (Bish and Reynolds, 1989). The reason is that the sample has to be sufficiently crushed so that there are no aggregates of different minerals because the whole process relies on individual crystallographic composition to get accurate readings. The powdered sub-samples were then placed on a frosted glass microscope slide where the acetone was allowed to evaporate and then placed in a diffractometer. The sample and the X-ray detector are then rotated at a known rate with respect to the CuK$\propto$ X-ray source and the energy detected is recorded and processed. The data output consists of a list of peaks that are characteristic for each mineral. The values of these peaks are compared with known mineral values in order to make a positive identification. An automated Philips 100kV generator and diffractometer unit was used for mineral identification by powder diffractometry.

3.2.3. Electron microprobe analysis

Both the old and new electron microprobe at Dalhousie University's Earth Sciences Department were used for the completion of this study. All calibrations and operation were performed with the guidance of Robert MacKay, Technologist. The old

probe was used to determine the geochemical composition of the unaltered titanite minerals, and the hydrothermal rutile minerals. It was also used for the image analysis of rutile and molybdenite grains in grain mount samples. The old probe is a JEOL 733 electron microprobe equipped with four wavelength-dispersive spectrometers and an Oxford Link eXL energy dispersive system, the latter of which was used for all geochemical analyses. The energy dispersive detector has a resolution of 137ev at 5.9Kev. Each point analysis was acquired for 40 seconds with an accelerating voltage of 15Kv and a beam current of 15nA. The width of the microprobe beam is 1 micron.

The new electron microprobe was used for the identification of gangue minerals surrounding hydrothermal rutile that was too fine-grained to be identified under the old probe. This new electron microprobe is a JEOL JXA-8200 with five wavelength dispersive spectrometers (WDS) and a Noran energy dispersive spectrometer (EDS). The WDS and EDS analysis can be combined. The EDS has an operating resolution 133eV @ 5.9Kev. The WDS can analyze elements from uranium through to boron. The instrument is capable of automated unattended operation. High quality (1280x1024) backscattered, secondary electron, and X-Ray images can be produced from this probe. The operating system is Solaris (Unix). Both microprobes will accept standard polished thin sections and polished grain mounts. Because many geological samples are electrically nonconducting, a conducting surface coat provides a path for the incident electrons to flow to ground (Reed, 1995). In this case vacuum-evaporated carbon is used because it has a minimal effect on the X-ray intensities; as a result of its low atomic number, it does not add unwanted peaks to the X-ray spectrum or cause significant absorption of X-rays generated by the sample (Reed, 1995).

3.2.3.1. Image analysis

Image analysis is a technique for classifying and characterizing images by using numerical values and specific properties of features that are highlighted in the image (Petruk, 1990). The main properties of these features include the length, width, area, perimeter, boundary irregularities, roundness, and sphericity. For this study, image analysis was carried out on images produced from the electron microprobe. The image analysis of rutile was achieved using backscatter electron (BSE) images from the probe that were transferred to an image analyzer as black and white representations, then subdivided into 256 shades of gray (0-255), where 0 represents pure black, and 255 represents pure white, known as gray-level images. Prior to setting up for image analysis with the electron microprobe, a positive mineral identification is required for each mineral being analyzed by normal x-ray analysis, and their gray-level range determined. Once this is complete the gray-level in the BSE will remain constant as long as the beam current and the GAIN and BRIGHTNESS (contrast) is kept constant. Each mineral or group of minerals has different shades of gray depending on its composition. Minerals with multi-element formulas have BSE images that exhibit a wide gray-level range, as opposed to those with simple formulas and no substitutions that have a narrow range (Petruk, 1990). Each mineral is then isolated from the original BSE image based on its gray-level.

The molybdenite grains did not produce a good BSE contrast for image analysis; therefore, these minerals were analyzed based on their X-ray signatures. Instead of identifying a mineral based on the gray-level, the microprobe takes a rudimentary X-ray analysis of the grain to make a positive identification. The only limitation in using this

method for the analysis of molybdenite is that lead has the same X-ray signature. However, the samples used contained very little lead, so its use can be justified. Both the BSE image and the X-ray method can be used to calculate specific mineral shapes determined from shape factors calculated from measurements of grain area, perimeter, maximum diameter, and minimum diameter.

3.2.4. Grain size distribution

Particle sizing is extremely important in the mining industry. It may ultimately differentiate between an economical or non-economical deposit. In order to get an accurate description of the grain size distribution of typical crushed ore concentrate at Chuquicamata, MM, and RT mines, Cuesta Research Ltd. provided composite samples of each location. These three samples were taken to the Minerals Engineering Centre at Dalhousie University where they were analyzed in a Malvern Mastersizer 2000 grain size analyzer (Figure 3.1), which determines the diameter of each grain in the sample based on the system of laser diffraction (Cyril Cole, Analyst).

The process of laser diffraction (Figure 3.2), or low angle laser light scattering (LALLS), incorporates the use of a He-Ne laser that provides light at a wavelength of 0.663 μm. This scattered light is then focused by an optical system on to a photosensitive silicon detector. The sample can either enter in a dry or suspension form.
The samples for this report were put into suspension with water where they were recirculated via a pump across the path of the laser beam. As each grain passed through the path of the laser, the path became deflected. It is this deflection that determines the diameter of each grain. After the entire sample has passed through the beam a complete breakdown of grain size distribution is achieved.

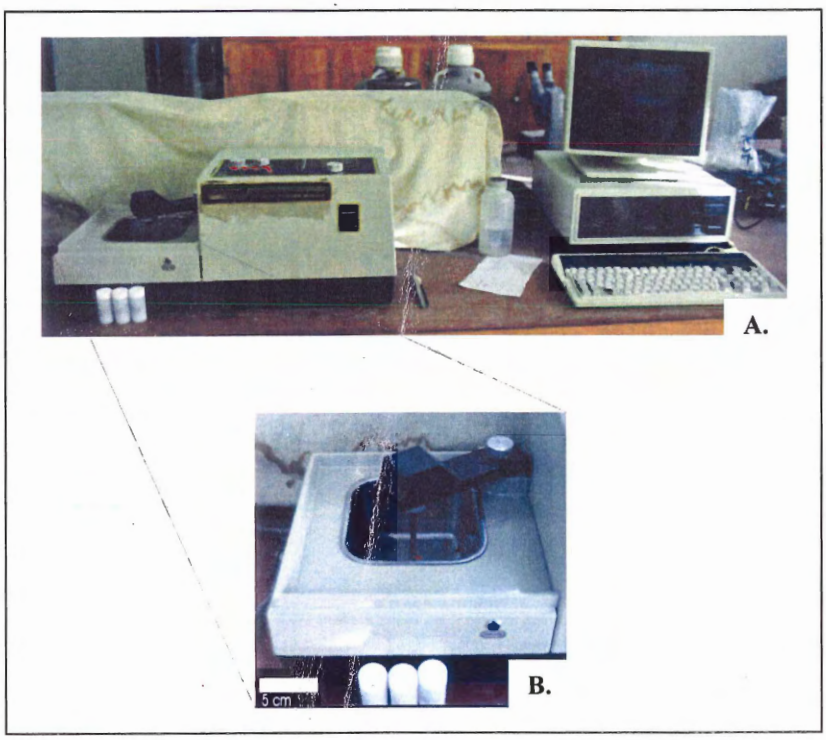

Figure 3.1: A) Malvern Mastersizer 2000 Grain Size Analyzer. B) Close-up of sample bowl where sample grains are thoroughly separated prior to analysis.

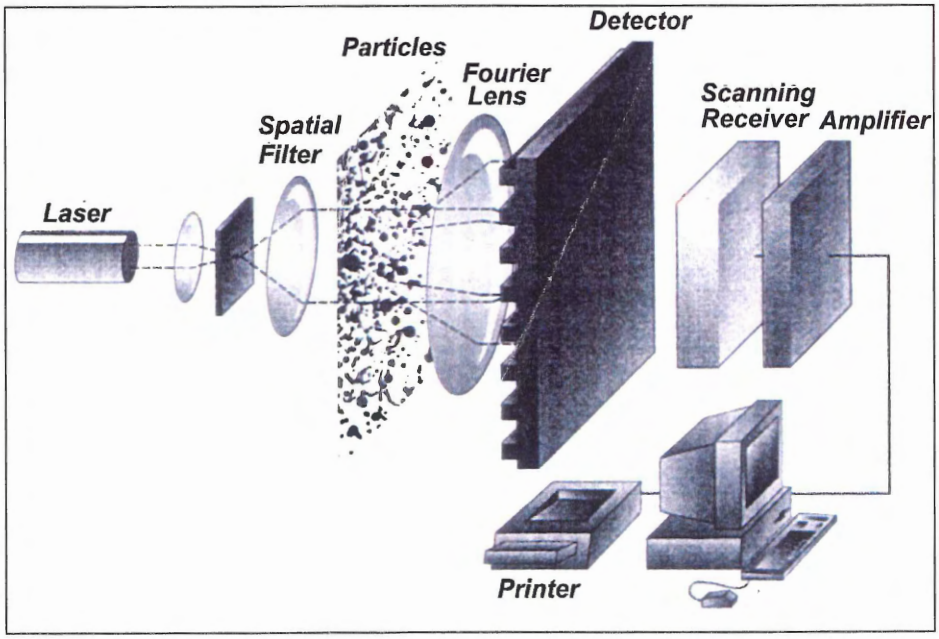

Figure 3.2: Schematic diagram highlighting the basic principles of particle analysis via laser diffraction (After Spectra Research Corporation).

There was, however, a problem when this test was ran on the composite samples. When first put through the analyzer, it was found that the majority of particles were too coarse to get any appreciable information about the pattern of distribution. To solve this problem, all material greater than 45 μm was sieved by hand using screens of 500, 250, 150, 75, and 45 microns respectively. If this were to be done on a much larger scale, a Ro-Tap Testing Sieve Shaker would have been used (Figure 3.3); however, theses samples (<100g each) were too small to warrant its use.

Figure 3.3: Ro-Tap Sieve Shaker; samples are placed into the upper sieve and are shaken through a series of downwards fining sieve sizes to produce a grain size distribution for the sample.

Chapter 4

Results

4.1. CIMM heavy mineral concentrate samples

4.1.1. Sample selection

The entire geochemical (Appendix 8) and mineralogical (Appendix 9) databases were used for the statistical analysis of titanium and rutile in the CIMM heavy mineral concentrate samples. Six grain mount samples were created for the image analysis of rutile. They consisted of three of the CIMM concentrates, and three composite samples comprised of equal portions of concentrate samples from each of the three mining locations (Table 4.1). These concentrate samples were selected based on their high titanium and rutile percentages. Mineralogical studies were then performed on two of these concentrate samples (Table 4.1). A seventh grain mount was created from the magnetic minerals separated from the RT composite sample for mineralogical and XRD analysis.

Sample	Database Number.	DDH	Meter Interval	Location
TF1	Composite			Chuquicamata
TF1A	4136-149	3033	66.50-83.00	Chuquicamata
TF2	Composite			Mansa Mina
TF2A	4136-121	3366	251.00-252.50	Mansa Mina
TF3	Composite			Radomiro Tomic
TF3A	4136-62	NIMS 350-188	249.40-250.70	Radomiro Tomic
TF3M	Magnetics			Radomiro Tomic

Table 4.1: Sample type and location of selected CIMM heavy mineral concentrates used in this study.

4.1.2. Statistical analysis of heavy mineral concentrates

The results of the statistical analysis are based on two sources. The first, which was used for the titanium analysis, is the geochemical results obtained by atomic absorption of the major metals in the heavy mineral concentrate samples. This was carried out by CIMM and reproduced here as Appendix 2. The second source, which was used for the rutile analysis, comes from the mineralogical point counting data produced for CIMM by Myriam Brockway and reproduced here as Appendix 1. All statistics were computed using the SPSS 10.1™ statistics program (See Appendix 6 for a glossary of the statistical terms used). For this study I will be focusing on the titanium and rutile statistics.

4.1.2.1. Chuquicamata mine samples

Rutile Statistics: A total of 57 samples were used for the statistical analysis of rutile (Table 4.2). The statistical mean is 1.16% with a standard deviation of 0.704 and variance about the mean of 0.496. The standard error of the mean is 0.0932. The median, also referred to as the 50^{th} percentile, is 1.080, while the most occurring percentage (mode) is 0.290. The range of data is 3.01, with a minimum of 0.180 and a maximum of 3.19. The 25^{th} percentile is 0.560, indicating that 25% of all the data points are below this value. The 75^{th} percentile is 1.655, indicating that 25% of the data points are greater than this value. A histogram of the percentage distribution compared to a normal curve (Figure 4.1) shows that the data has a positive skewness of 0.864 and a

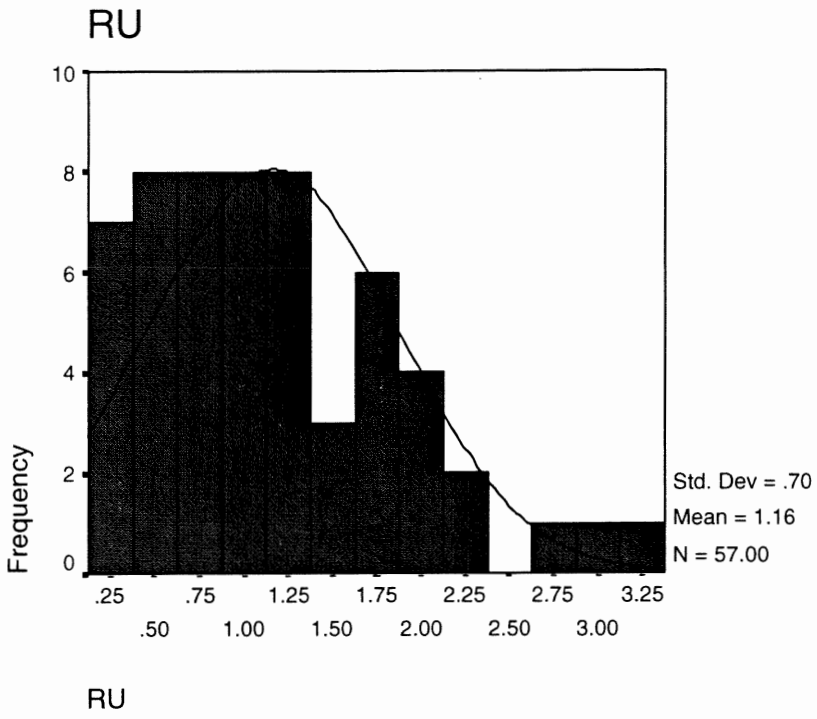

Figure 4.1: Frequency distribution along with normal curve of rutile (RU) based on the Chuquicamata mine concentrate samples.

Statistics

RU

N	Valid	57
	Missing	2
Mean		1.1598
Std. Error of Mean		.09327
Median		1.0800
Mode		.29[a]
Std. Deviation		.70416
Variance		.49584
Skewness		.864
Std. Error of Skewness		.316
Kurtosis		.487
Std. Error of Kurtosis		.623
Range		3.01
Minimum		.18
Maximum		3.19
Percentiles	25	.5600
	50	1.0800
	75	1.6550

a. Multiple modes exist. The smallest value is shown

Table 4.2: Rutile (RU) statistics in Vol.% based on concentrate samples from the Chuquicamata mine.

standard error of skewness of 0.316. Because the skewness is greater than twice its standard error it is an indication of the departure form symmetry. Also, the ratio of skewness to standard error of skewness, which is a test of normality, where values less than +2 or greater than –2 represent a normal distribution, is 2.66. However, by looking at the histogram, the high degree of skewness and asymmetry is a result of a single anomalously high data point. Kurtosis is another numerical representation of the graphical output. It has a value of 0.487, with a standard error of 0.623. A normal curve has a value of 0 and the positive value defined here indicates that the values are clustered more around the mean and have longer tails. Similar to the ratio of skewness to its standard error, the ratio of kurtosis to its standard error can also be used as a test of normality. Normality can be rejected if the ratio is greater than +2 or lower than –2. In this case it is +1.5, so normality can be retained.

Titanium Analysis: The same statistical tests were done on the major element data as was done on the above-described mineralogical data. A total of 59 samples were used for the analysis of titanium at the Chuquicamata mine (Table 4.3). It was found that the mean percentage of titanium was 1.258 with a standard error of 0.0714, standard deviation of 0.549, and a variance of 0.301. The median is 1.10, while the most occurring percentage (mode) is 0.900. The range of data is 2.20, with a minimum of 0.100 and a maximum of 2.30. The 25^{th} percentile is 0.900, indicating that 25% of all the data points are below this value. The 75^{th} percentile is 1.800, indicating that 25% of the data points are greater than this value. A histogram of the percentage distribution compared to a normal curve (Figure 4.2) shows that the data has a very slight positive

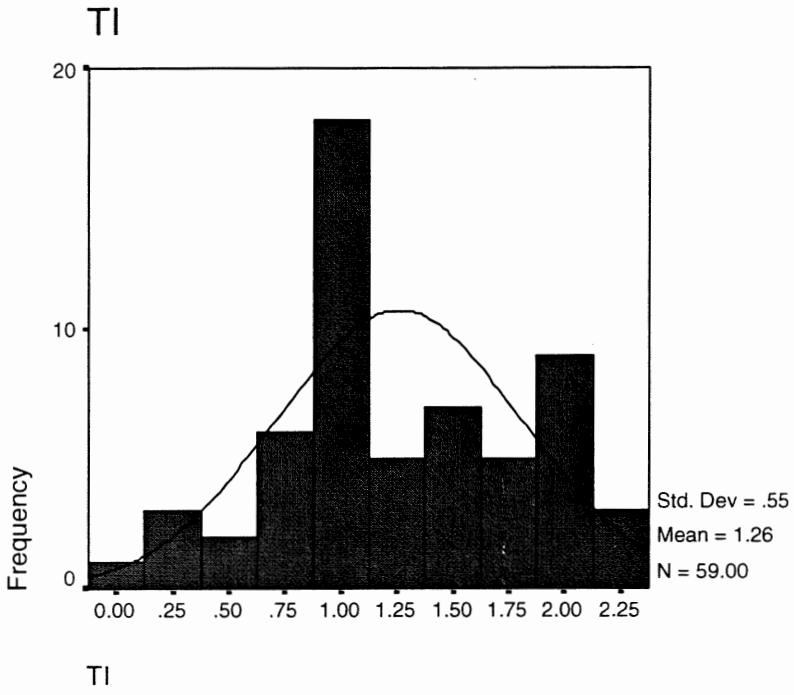

Figure 4.2: Frequency distribution along with normal curve of titanium (Ti) based on the Chuquicamata mine concentrate samples.

Statistics

TI

N	Valid	59
	Missing	0
Mean		1.2576
Std. Error of Mean		.07144
Median		1.1000
Mode		.90[a]
Std. Deviation		.54873
Variance		.30110
Skewness		.070
Std. Error of Skewness		.311
Kurtosis		-.739
Std. Error of Kurtosis		.613
Range		2.20
Minimum		.10
Maximum		2.30
Percentiles	25	.9000
	50	1.1000
	75	1.8000

a. Multiple modes exist. The smallest value is shown

Table 4.3: Titanium (Ti) statistics in Wt. % based on concentrate samples from the Chuquicamata mine.

skewness of 0.070 and a standard error of skewness of 0.0.311. Because the skewness is greater than twice its standard error it is an indication of the departure form symmetry. Also, the ratio of skewness to standard error of skewness, which is a test of normality, is 4.44. Kurtosis is another numerical representation of the graphical output. It has a value of –0.739, with a standard error of 0.613. A normal curve has a value of 0 and the negative value defined here indicates that the values are poorly clustered around the mean and have shorter tails. Similar to the ratio of skewness to its standard error, the ratio of kurtosis to its standard error is -1.2, so normality can be retained.

4.1.2.2. Radomiro Tomic mine samples

Rutile Statistics: A total of 18 samples were used for the statistical analysis of rutile (Table 4.4). The statistical mean is 1.024% with a standard deviation of 1.183 and variance about the mean of 1.401. The standard error of the mean is 0.279. The median, also referred to as the 50^{th} percentile, is 0.350, while the most occurring percentage (mode) is 0.350. The range of data is 4.030, with a minimum of 0.060 and a maximum of 4.09. The 25^{th} percentile is 0.203 indicating that 25% of all the data points are below this value. The 75^{th} percentile is 1.713, indicating that 25% of the data points are greater than this value. A histogram of the percentage distribution compared to a normal curve (Figure 4.3) shows that the data has a highly positive skewness of 1.449 and a standard error of skewness of 0.536. Because the skewness is greater than twice its standard error it is an indication of the departure form symmetry. Also, the ratio of skewness to standard error of skewness, which is a test of normality, where values greater than +2 or less than –2, is 2.57. However, by looking at the histogram, the high degree of skewness and asymmetry is a result of a single anomalously high data point. Kurtosis is

another numerical representation of the graphical output. It has a value of 1.269, with a standard error of 1.038. A normal curve has a value of 0 and the positive value defined here indicates that the values are clustered more around the mean and have longer tails. Similar to the ratio of skewness to its standard error, the ratio of kurtosis to its standard error can also be used as a test of normality. Normality can be rejected if the ratio is greater than +2 or lower than –2. In this case it is +1.22, so normality can be retained.

Titanium Analysis: The same statistical tests were done on the major element data as was done on the above-described mineralogical data. A total of 23 samples were used for the analysis of titanium at the Radomiro Tomic mine (Table 4.5). It was found that the mean percentage of titanium was 1.417 with a standard error of 0.233, standard deviation of 1.117, and a variance of 1.247. The median is 1.200, while the most occurring percentage (mode) is 0.10. The range of data is 4.00, with a minimum of 0.100 and a maximum of 4.10. The 25^{th} percentile is 0.600, indicating that 25% of all the data points are below this value. The 75^{th} percentile is 2.100, indicating that 25% of the data points are greater than this value. A histogram of the percentage distribution compared to a normal curve (Figure 4.4) shows that the data has a positive skewness of 0.975 and a standard error of skewness of 0.481. Because the skewness is greater than twice its standard error it is an indication of the departure form symmetry. Also, the ratio of skewness to standard error of skewness, which is a test of normality, is 2.02. Kurtosis is another numerical representation of the graphical output. It has a value of +0.458, with a standard error of 0.935. A normal curve has a value of 0 and the positive value defined here indicates that the values are more clustered around the mean and have longer tails

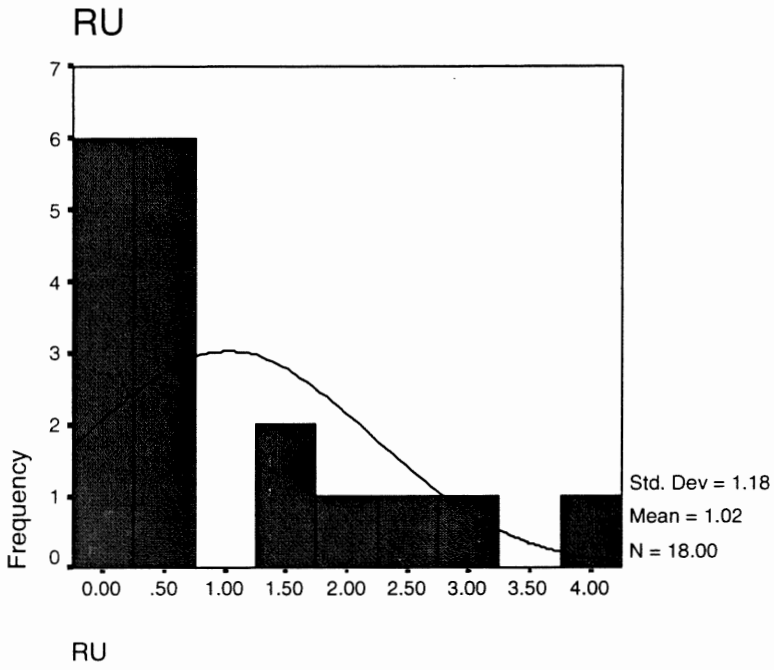

Figure 4.3: Frequency distribution along with normal curve of rutile (RU) based on the Radomiro Tomic mine concentrate samples.

Statistics

RU

N	Valid	18
	Missing	5
Mean		1.0239
Std. Error of Mean		.27897
Median		.3500
Mode		.35
Std. Deviation		1.18358
Variance		1.40087
Skewness		1.449
Std. Error of Skewness		.536
Kurtosis		1.269
Std. Error of Kurtosis		1.038
Range		4.03
Minimum		.06
Maximum		4.09
Percentiles	25	.2025
	50	.3500
	75	1.7125

Table 4.4: Rutile (RU) statistics in Vol.% based on concentrate samples from the Radomiro Tomic mine.

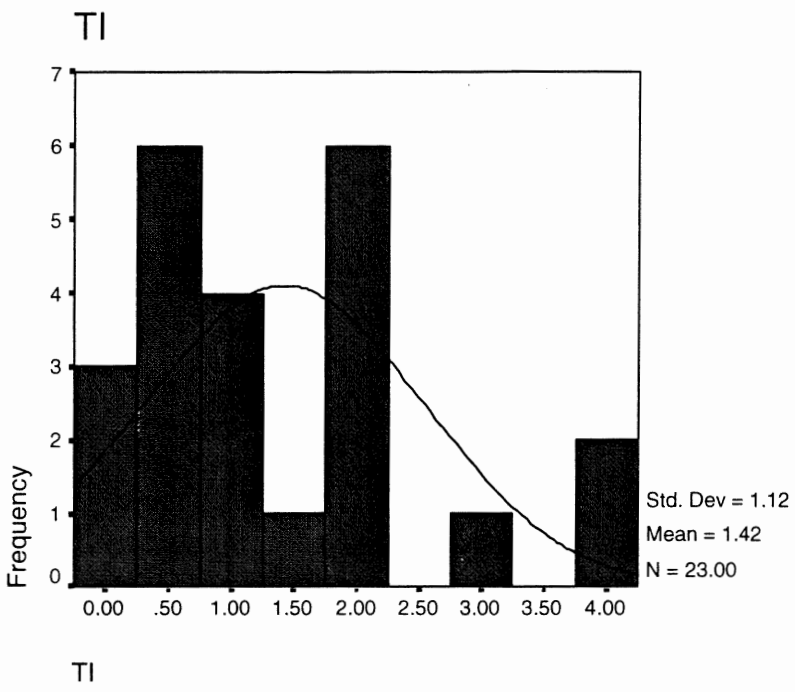

Figure 4.4: Frequency distribution along with normal curve of titanium (Ti) based on the Radomiro Tomic mine concentrate samples.

Statistics

TI

N	Valid	23
	Missing	4
Mean		1.4174
Std. Error of Mean		.23284
Median		1.2000
Mode		.10[a]
Std. Deviation		1.11667
Variance		1.24696
Skewness		.975
Std. Error of Skewness		.481
Kurtosis		.458
Std. Error of Kurtosis		.935
Range		4.00
Minimum		.10
Maximum		4.10
Percentiles	25	.6000
	50	1.2000
	75	2.1000

a. Multiple modes exist. The smallest value is shown

Table 4.5: Titanium (Ti) statistics in Wt. % based on concentrate samples from the Radomiro Tomic mine

than a normal curve. Similar to the ratio of skewness to its standard error, the ratio of kurtosis to its standard error is 2.04; this is an indication that this data is not normally distributed.

4.1.2.3. Mansa Mina mine samples

Rutile Statistics: A total of 56 samples were used for the statistical analysis of rutile (Table 4.6). The statistical mean is 0.339% with a standard deviation of 0.326 and variance about the mean of 0.106. The standard error of the mean is 0.0436. The median, also referred to as the 50^{th} percentile, is 0.260, while the most occurring percentage (mode) is 0.0800. The range of data is 1.83, with a minimum of 0.040 and a maximum of 1.87. The 25^{th} percentile is 0.110 indicating that 25% of all the data points are below this value. The 75^{th} percentile is 0.4625, indicating that 25% of the data points are greater than this value. A histogram of the percentage distribution compared to a normal curve (Figure 4.5) shows that the data has a highly positive skewness of 2.448 and a standard error of skewness of 0.319. Because the skewness is greater than twice its standard error it is an indication of the departure form symmetry. Also, the ratio of skewness to standard error of skewness, which is a test of normality, where values greater than +2 or less than –2, is 7.67. However, by looking at the histogram, the high degree of skewness and asymmetry is a result of a single anomalously high data point. Kurtosis is another numerical representation of the graphical output. It has a value of 8.362, with a standard error of 0.628. A normal curve has a value of 0 and the positive value defined here indicates that the values are clustered more around the mean and have longer tails. Similar to the ratio of skewness to its standard error, the ratio of kurtosis to its standard

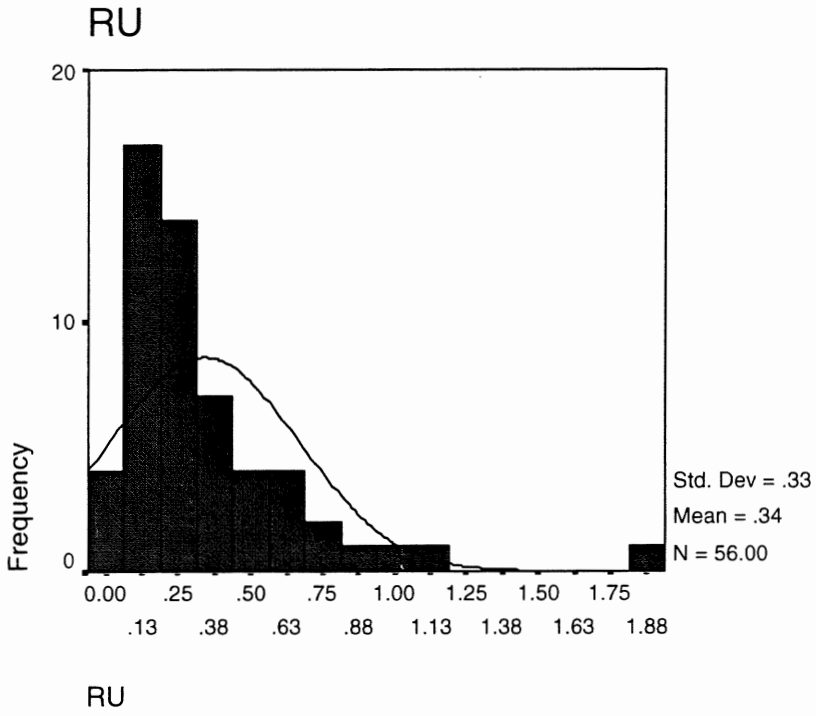

Figure 4.5: Frequency distribution along with normal curve of rutile (RU) based on the Mansa Mina mine concentrate samples.

Statistics

RU

N	Valid	56
	Missing	10
Mean		.3389
Std. Error of Mean		.04355
Median		.2600
Mode		.08
Std. Deviation		.32589
Variance		.10620
Skewness		2.448
Std. Error of Skewness		.319
Kurtosis		8.362
Std. Error of Kurtosis		.628
Range		1.83
Minimum		.04
Maximum		1.87
Percentiles	25	.1100
	50	.2600
	75	.4625

Table 4.6: Rutile (RU) statistics in Vol.% based on concentrate samples from the Mansa Mina mine.

error can also be used as a test of normality. Normality can be rejected if the ratio is greater than +2 or lower than –2. In this case it is +13.32, indicating that the data is not normally distributed.

Titanium Analysis: The same statistical tests were done on the major element data as was done on the above-described mineralogical data. A total of 75 samples were used for the analysis of titanium at the Mansa Mina mine (Table 4.7). It was found that the mean percentage of titanium was 0.353 with a standard error of 0.0234, standard deviation of 0.202, and a variance of 0.0409. The median is 0.300, while the most occurring percentage (mode) is 0.300. The range of data is .0900, with a minimum of 0.100 and a maximum of 1.00. The 25^{th} percentile is 0.200, indicating that 25% of all the data points are below this value. The 75^{th} percentile is 0.400, indicating that 25% of the data points are greater than this value. A histogram of the percentage distribution compared to a normal curve (Figure 4.6) shows that the data has a positive skewness of 1.310 and a standard error of skewness of 0.277. Because the skewness is greater than twice its standard error it is an indication of the departure form symmetry. Also, the ratio of skewness to standard error of skewness, which is a test of normality, is 4.73. Kurtosis is another numerical representation of the graphical output. It has a value of 1.886, with a standard error of 0.548. A normal curve has a value of 0 and the positive value defined here indicates that the values are more clustered around the mean and have longer tails than a normal curve. Similar to the ratio of skewness to its standard error, the ratio of kurtosis to its standard error is 3.44; this is an indication that this data is not normally distributed.

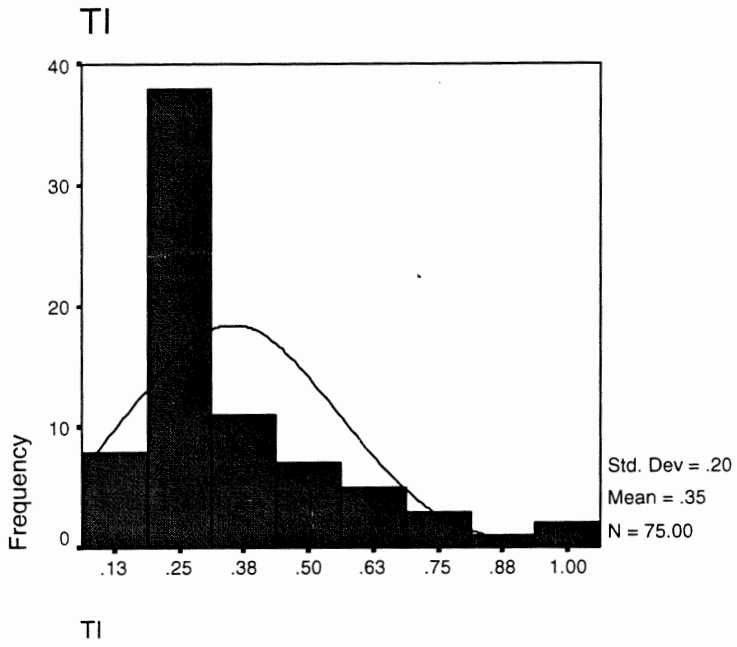

Figure 4.6: Frequency distribution along with normal curve of titanium (Ti) based on the Mansa Mina mine concentrate samples.

Statistics

TI

N	Valid	75
	Missing	3
Mean		.3533
Std. Error of Mean		.02335
Median		.3000
Mode		.30
Std. Deviation		.20224
Variance		.04090
Skewness		1.310
Std. Error of Skewness		.277
Kurtosis		1.886
Std. Error of Kurtosis		.548
Range		.90
Minimum		.10
Maximum		1.00
Percentiles	25	.2000
	50	.3000
	75	.4000

Table 4.7: Titanium (Ti) statistics in Wt. % based on concentrate samples from the Radomiro Tomic mine

4.1.3. Mineralogical and major metal correlations

Correlation charts were created to compare the trends of rutile and titanium against the other minerals and major metals respectively within the CIMM heavy mineral concentrate databases (Appendices 8 and 9). The significance of which follows the significance table from Brooks et al. (1972.) (Appendix 7) For this study I am focusing on the comparison of rutile to chalcopyrite (CP), bornite (BN), pyrite (PY), and molybdenite (MO) (Appendix 8), and the comparison of titanium to the elements copper (Cu), iron (Fe), and molybdenum (Mo) (Appendix 9).

Rutile: The rutile from the Chuquicamata mine concentrates (Figure 4.7) exhibits a very highly significant positive correlation with chalcopyrite and a very highly significant negative correlation with pyrite. When correlated against bornite, and molybdenite there is no significance between the two. The rutile from the Mansa Mina mine concentrates (Figure 4.8) exhibits a very highly significant positive correlation with chalcopyrite. It also exhibits a significant negative correlation with pyrite. There is no statistical significance in the correlation between the rutile and the bornite and molybdenite. However, there is a significant negative correlation with chalcocite, as noticed in the Chuquicamata mine data.

Unlike the previous two correlations, the rutile from the Radomiro Tomic mine concentrates (Figure 4.9) does not exhibit any significant correlation with chalcopyrite; instead there is a very highly significant positive correlation with bornite. The correlation between rutile and pyrite is analogous to the previous two localities in that it has a very highly significant negative correlation. There is no significance between the rutile and molybdenite, or any of the other minerals present in this locality.

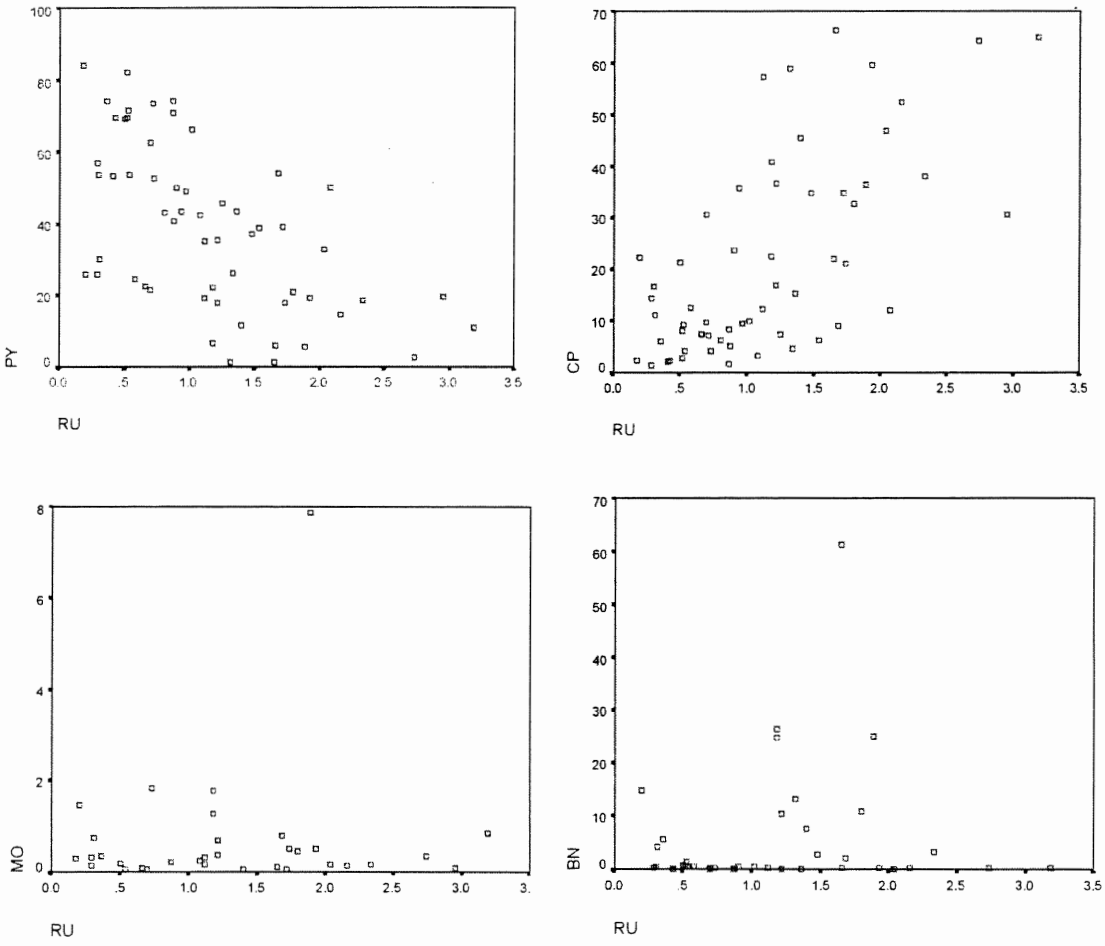

Figure 4.7: Scatter plots of rutile (RU) against pyrite (PY), chalcopyrite (CP), molybdenite (MO), and bornite (BN) from CIMM mineralogical point count data on Chuquicamata heavy mineral concentrate samples (Appendix 1B)

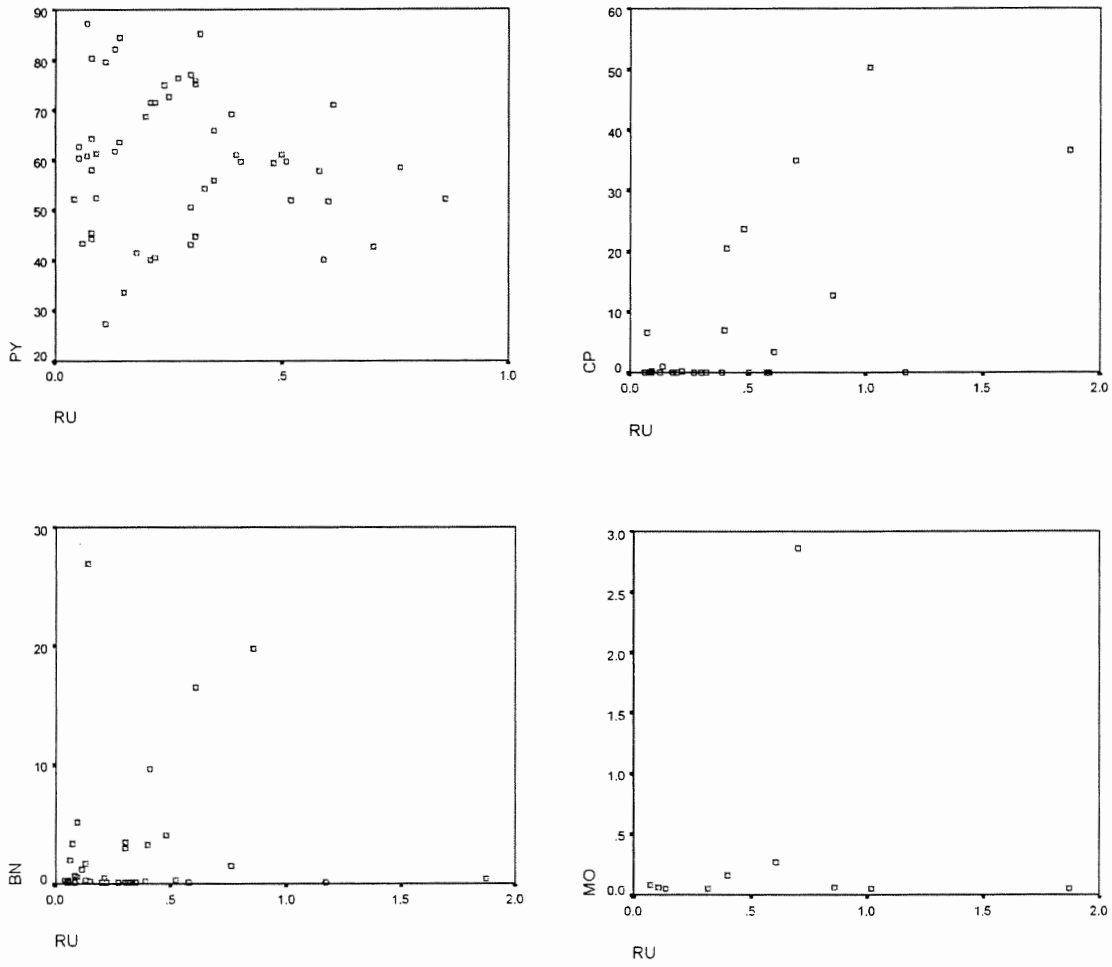

Figure 4.8: Scatter plots of rutile (RU) against pyrite (PY), chalcopyrite (CP), molybdenite (MO), and bornite (BN) from CIMM mineralogical point count data on MM heavy mineral concentrate samples (Appendix 1C)

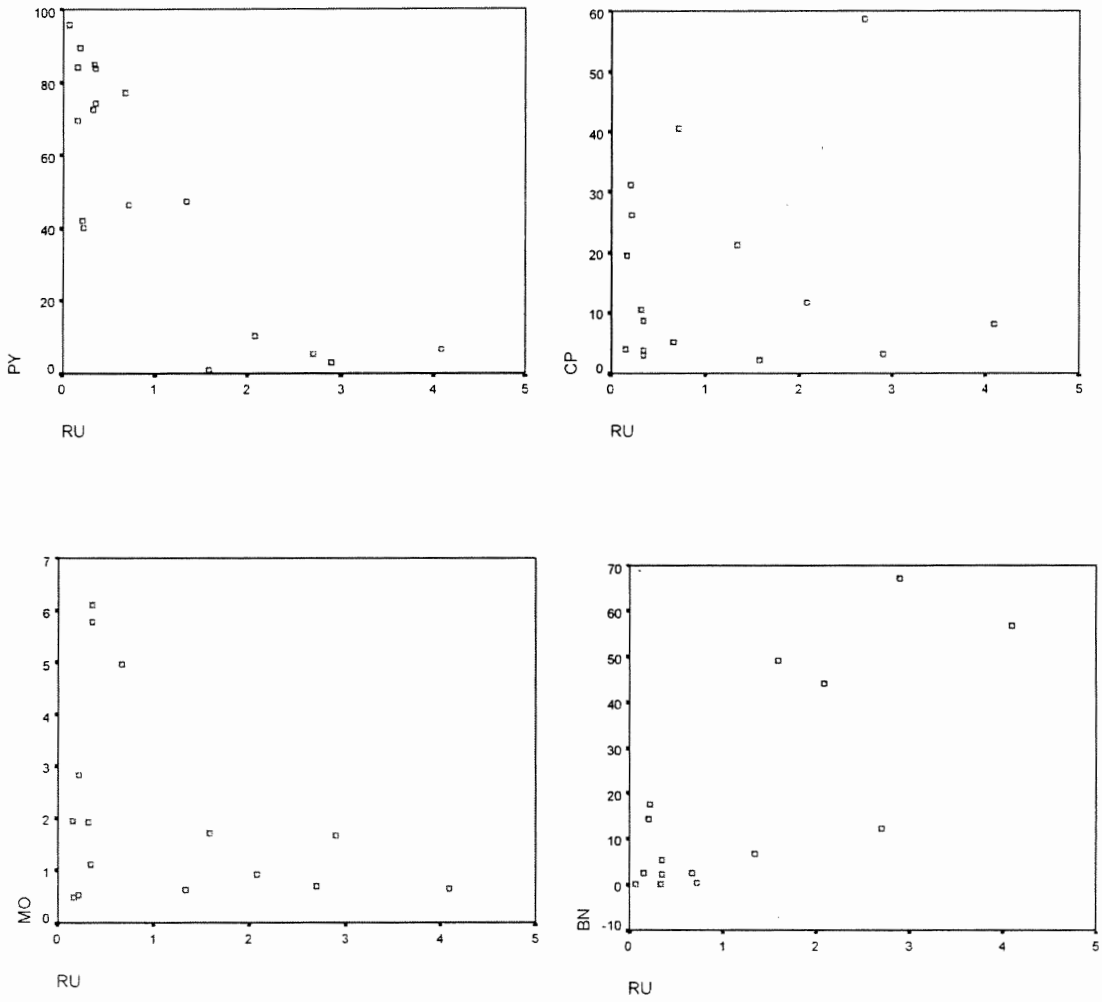

Figure 4.9: Scatter plots of rutile (RU) against pyrite (PY), chalcopyrite (CP), molybdenite (MO), and bornite (BN) from CIMM mineralogical point count data on RT heavy mineral concentrate samples (Appendix 1A)

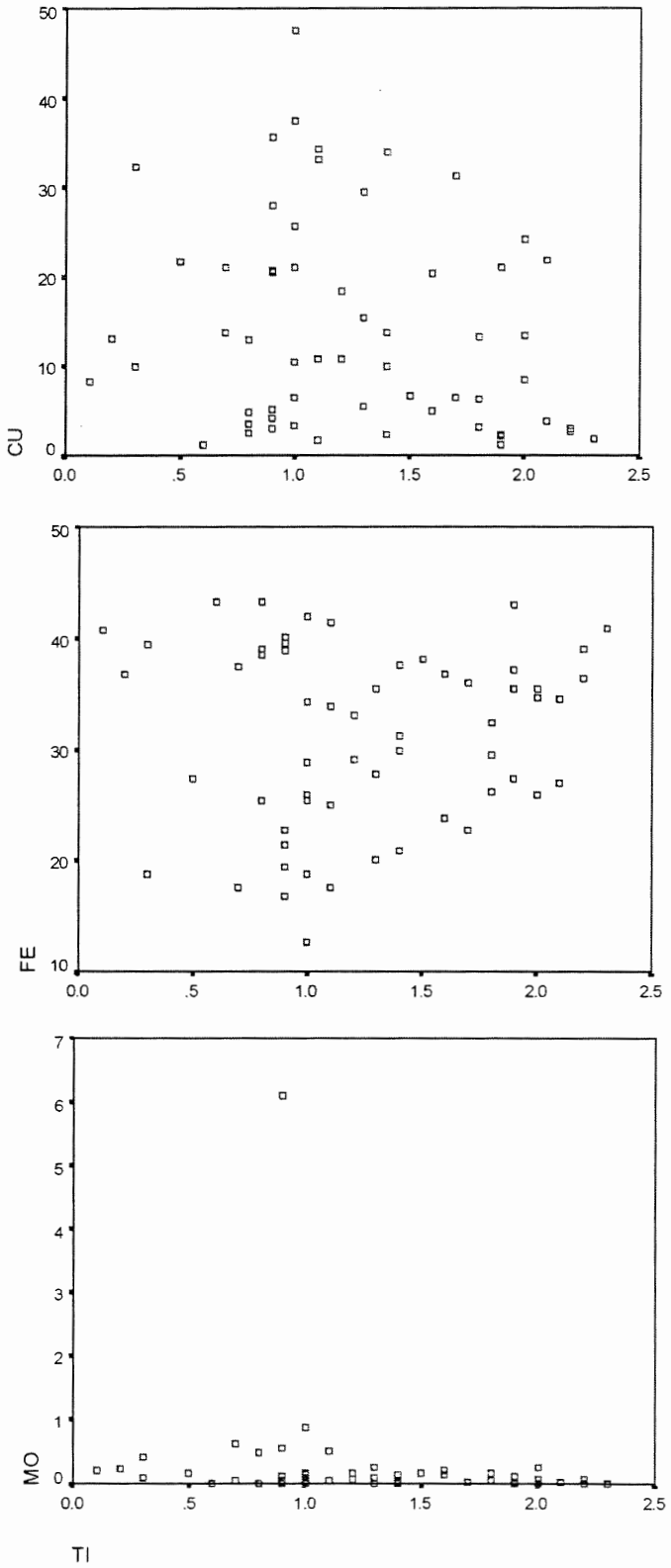

Figure 4.10: Scatter plots of titanium (TI) against copper (CU), iron (FE), and molybdenum (MO) from CIMM major metal geochemical data on Chuquicamata heavy mineral concentrate samples (Appendix 2B)

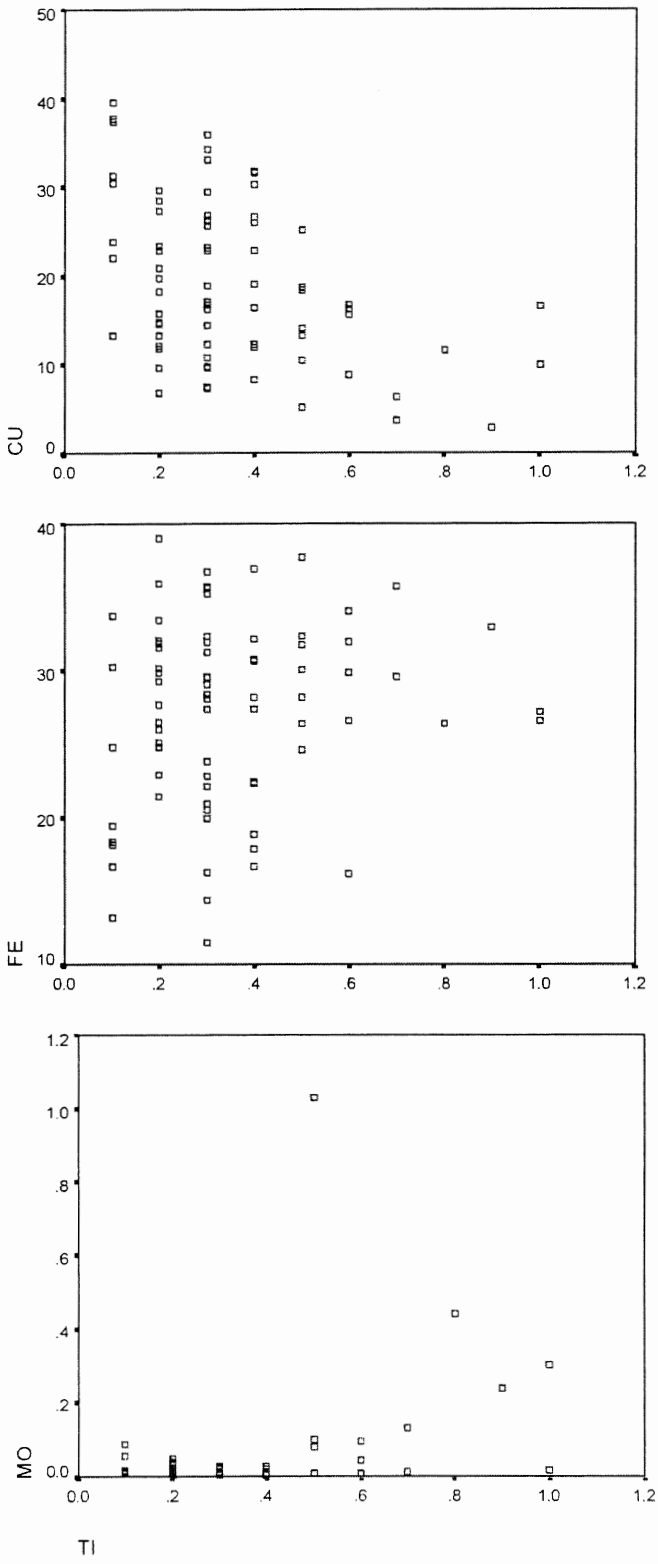

Figure 4.11: Scatter plots of titanium (TI) against copper (CU), iron (FE), and molybdenum (MO) from CIMM major metal geochemical data on MM heavy mineral concentrate samples (Appendix 2C)

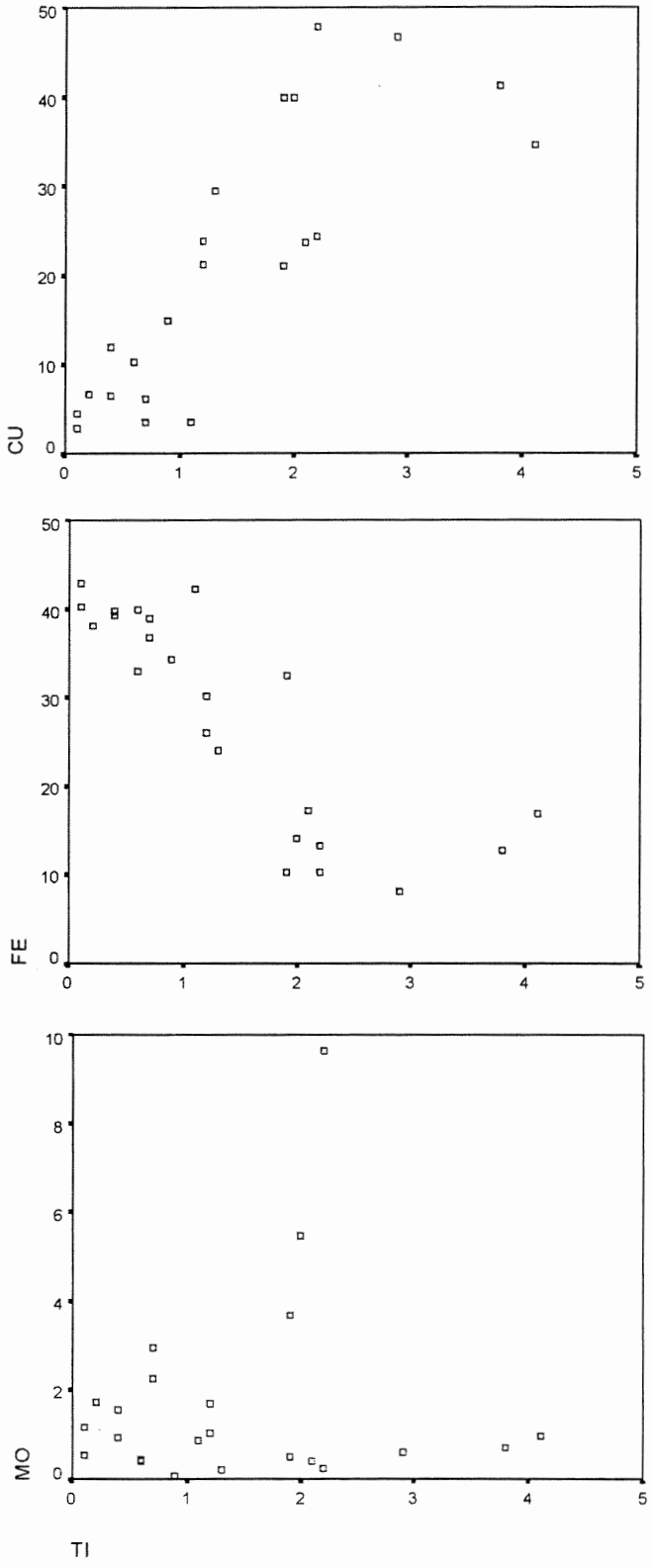

Figure 4.12: Scatter plots of titanium (TI) against copper (CU), iron (FE), and molybdenum (MO) from CIMM major metal geochemical data on RT heavy mineral concentrate samples (Appendix 2A)

Titanium: The titanium metal content from the Chuquicamata mine concentrates (Figure 4.10) does not exhibit any statistically significant correlation with the copper, iron or molybdenum elements present. However, there is a slight negative correlation with copper, but it is not considered to be statistically significant. Also, there is a possibly significant negative correlation with arsenic, lead, zinc, and antimony (Appendix 9B).

The titanium from the Mansa Mina mine locality exhibits a very highly significant negative correlation with copper, as well as a highly significant positive correlation with molybdenum (Figure 4.11). There is, however, no significant correlation with the iron (Figure 4.11). There is also a very highly significant positive correlation with lead, and a highly significant negative correlation with arsenic in these concentrates (Appendix 9C). The titanium in the Radomiro Tomic mine concentrates (Figure 4.12) exhibits a very highly significant statistical positive correlation with copper, and a very highly significant negative correlation with iron. There is no significant correlation with the molybdenum; however, there is a significant positive correlation with the zinc in these concentrates (Appendix 9A).

4.1.4. Mineralogy of CIMM heavy mineral concentrates

TF3M: This sample is a grain mount that was created from the magnetic grains extracted from the RT composite sample (TF3). The rocks at RT have been less overprinted by quartz-sericite alteration than rocks in Chuquicamata, hence represent potassic-altered rocks in the Chuquicamata district. They were separated using a hand magnet. When examined via XRD (Figure 4.13 A) and under the reflected light

Figure 4.13 (Following Page): A) XRD results of RT magnetics in sample TF3M. The "natural" magnetic mineral is magnetite whereas the pyrite is considered to be contamination and the hematite is considered to be a result of magnetite oxidation. B) Sample TF3M. Reflected light grain mount of magnetite (Dark Gray) showing fine exsolution lamellae of ilmenite (Light Gray).

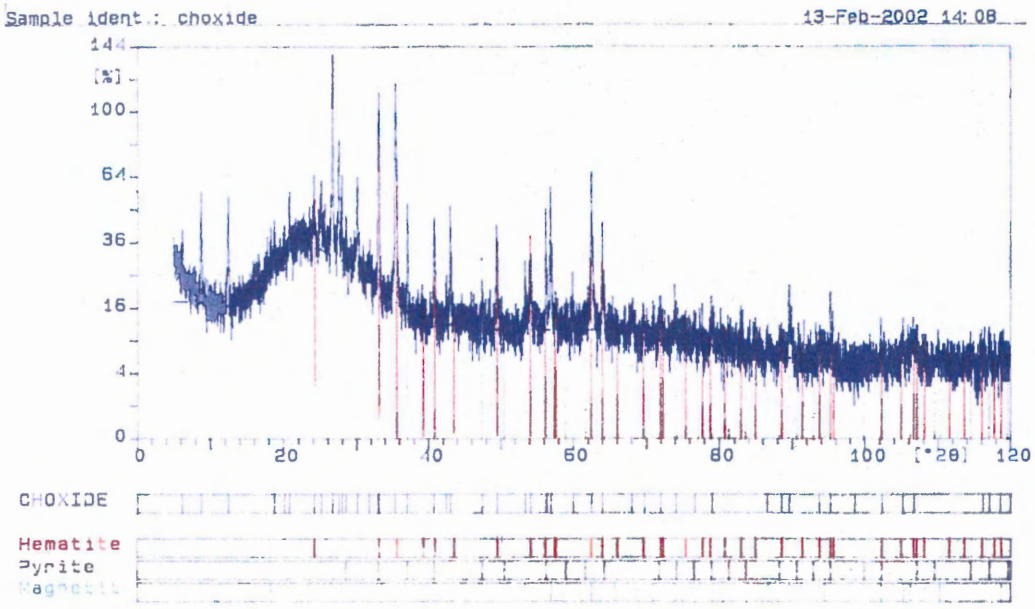
Sample ident.: choxide
13-Feb-2002 14:08
144
[%]
100
64
36
16
4
0
0
20
40
60
80
100
[°2θ]
120
CHOXIDE
Hematite
Pyrite
Magnetit

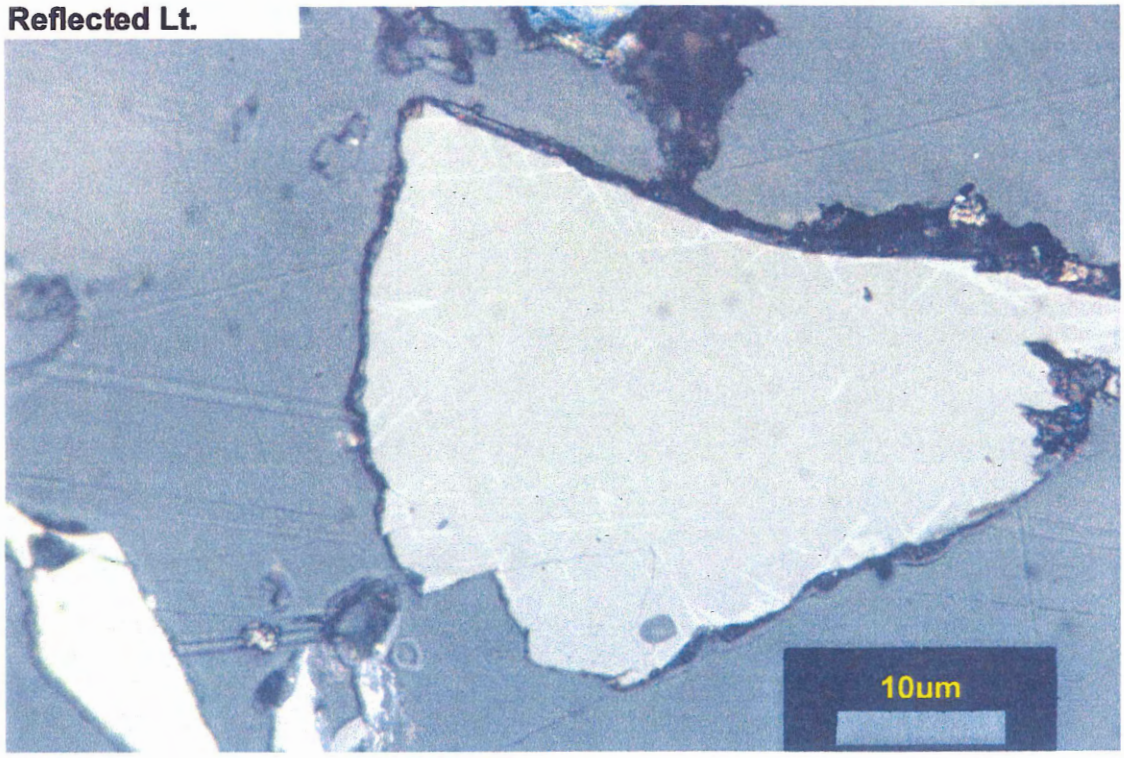
Reflected Lt.
10um

microscope (Figure 4.13 B), the magnetic mineral present is magnetite. These dark gray grains contain exsolution lamellae of a lighter coloured mineral, determined based on its optical properties to be ilmenite (Figure 4.13 B). The exsolution is very fine (~1μm thick) and forms right angle intersections throughout the host magnetite grains.

TF2A: This sample consists of a grain mount made from a MM concentrate sample and represents strictly sericitic alteration in the Chuquicamata district. In this sample rutile occurs as inclusions within and surrounding pyrite grains (Figure 4.14). It also occurs as skeletal grains surrounded by the clay mineral pyrophyllite (Figure 4.15).

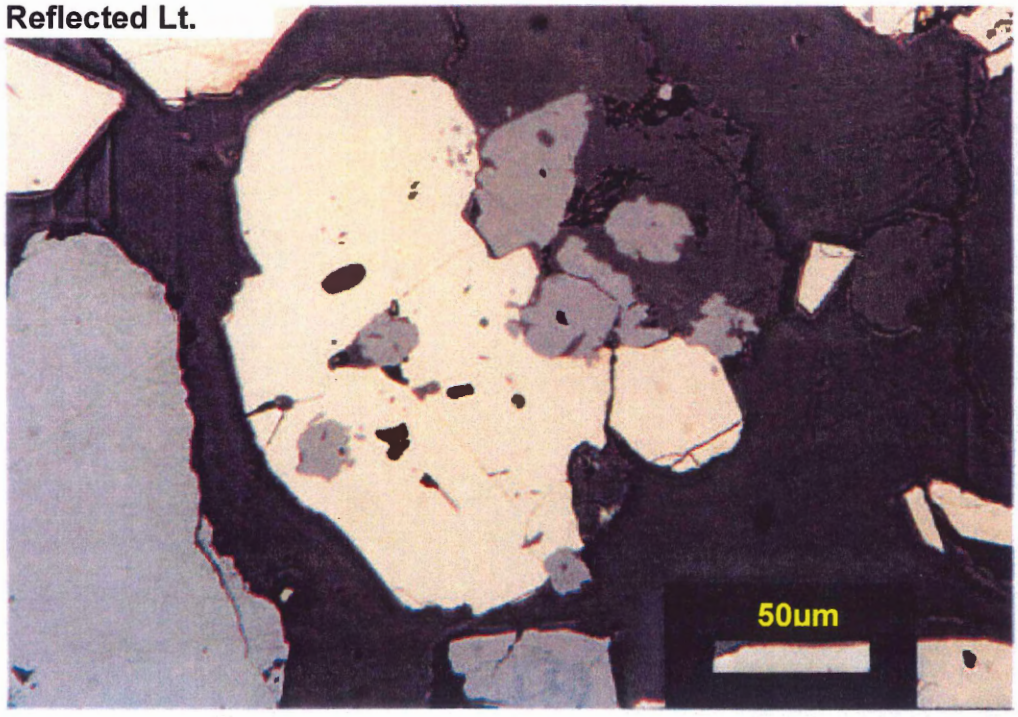

Figure 4.14: Sample TF2A. Reflected light grain mount of rutile grains (Light Gray) occurring as inclusions within and along the perimeter of a pyrite grain (White)

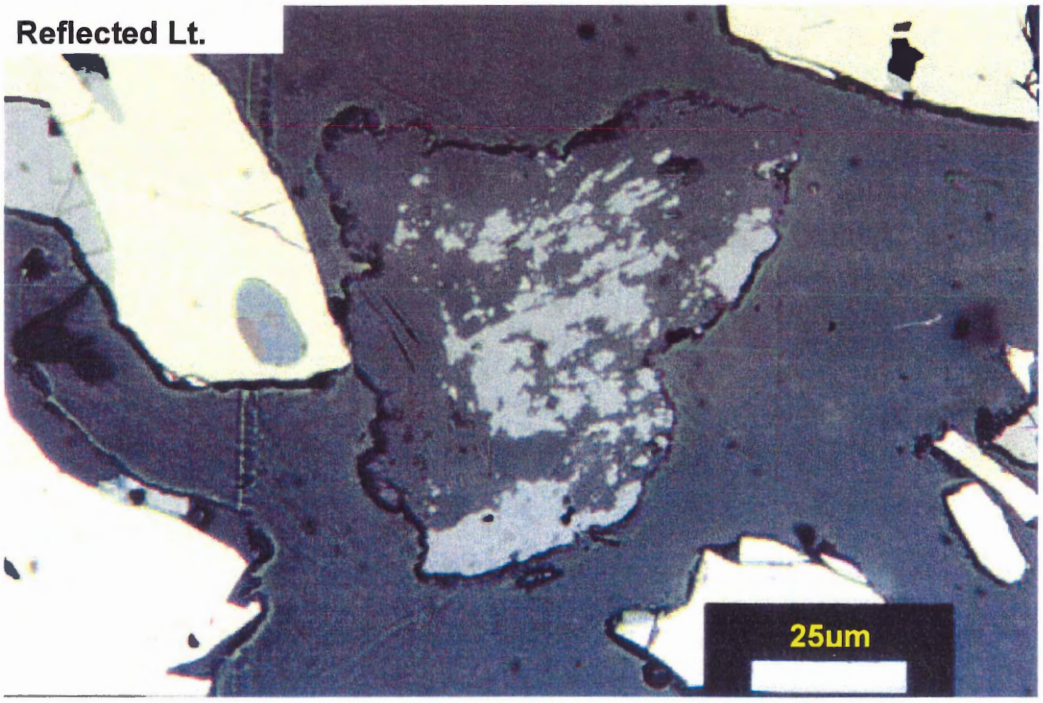

Figure 4.15: Sample TF2A. Reflected light grain mount of a pyrophyllite grain (Dark Grey) hosting inclusions and blebs of rutile grains (Light Gray), surrounded by pyrite grains (White).

4.2. Polished thin section analyses

Samples for this section consist of polished thin sections that were created from rocks at the Chuquicamata mine. The samples that were selected represent both potassic and sericitic alteration at the mine site (Table 4.8).

Sample Number	Field Number	X-Coordinate	Y-Coordinate	Depth (m)	Type of Alteration
CU769	MZ-94-54	N6853	E4397	Surface	"Fresh"
CU790	DL-94-54	N3670	E2475	2671	Potassic
CU1115	AMA-14	3600N	DDH 1843	157.30-157.50	Potassic
CU1101	AMA-01	3600N	DDH 1843	14.77-14.85	Quartz-Sericite
CU448	Z93-869	4500N	DDH 2242	161.04	Quartz-Sericite

Table 4.8: Polished thin section location and degree of hydrothermal alteration

4.2.1. Mineralogy of titanium-bearing minerals

Mineralogical studies were done on polished section from both the potassic and sericitic zones from the Chuquicamata mine (Table 4.8). Rutile was found to be the dominant titanium-bearing mineral throughout the Chuquicamata Porphyry Complex, a result consistent with previous studies on the occurrence of titanium in porphyry deposits (Section 1.5). There is, however, no evidence of magmatic rutile in any of the samples analyzed, therefore, from hereafter all discussion of rutile will be in reference to hydrothermal/secondary rutile.

Mineralogical descriptions of selected samples are arranged in order from the potassic zone to the highly altered samples of the sericitic zone.

CU769: This sample represents the least hydrothermally altered rocks at the Chuquicamata mine; it was collected outside the open pit, from a dike that extends from the Este porphyry to the NNE. It contains abundant biotite, potassium-feldspar, and quartz, with minor amounts of titanite, and opaques. The biotite grains are relatively unaltered, with a distinct brown-to-tan pleochroism and well-defined single cleavage. It also has a minor degree of alteration by opaque minerals occurring as blebs along the cleavage planes and the circumference. When viewed in reflected light these opaques consist of both rutile and pyrite. The titanite grains are also relatively unaltered as they show a characteristic diamond shape and single cleavage plane, however, there are some opaque grains occurring within each of these minerals. In reflected light, the opaques can be identified as grains of rutile (Figure 4.16).

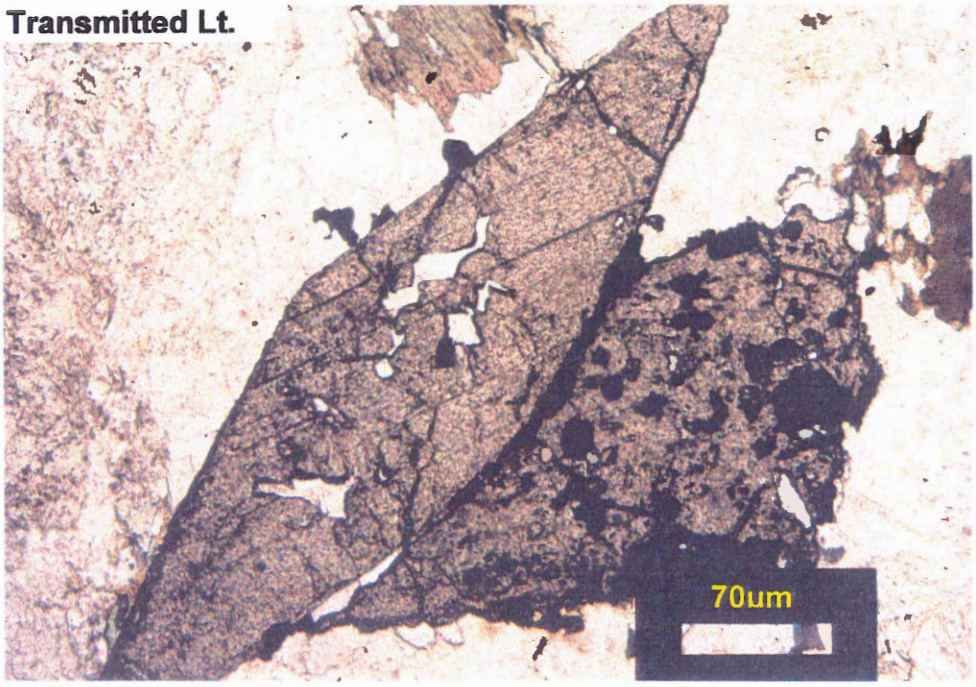

Figure 1

Figure 4.16: Sample CU769. Transmitted light thin section of a relatively unaltered, diamond-shaped titanite grain with single cleavage above another titanite grain that shows a higher degree of alteration and less characteristic shape.

CU790: This sample shows a slightly higher degree of alteration than in CU769; however, it too is from the zone of potassic alteration and reveals the characteristic biotite, potassium-feldspar, and quartz mineralogy one would expect. The biotite grains in this sample have undergone a stronger alteration than the above samples, and consist of a larger proportion of opaque minerals surrounding or rimming the grain. When viewed in reflected light they are pyrite and rutile (Figure 4.17). This sample does not contain any titanite grains.

CU1115: This sample represents the highest degree of potassic alteration found at Chuquicamata. The abundance of potassium-feldspars and biotite has decreased, and the quartz is still relatively abundant. The biotite grains have been severely altered to opaque minerals throughout each of the grains. When viewed in reflected light the

opaques are again pyrite and rutile, as well as chalcopyrite in some incidences (Figure 4.18). All of the titanite present has been altered to aggregates of rutile and quartz; however, the primary crystal shape is retained for each grain (Figure 4.19).

CU1101: This sample represents the quartz-sericitic zone of alteration at Chuquicamata. The mineralogy consists predominantly of quartz and sericite with opaque minerals. There is still a minor amount of biotite and potassium feldspars, however, for the most part they have been altered to sericite. When viewed in reflected light, the opaques are predominantly pyrite with some chalcopyrite, and minor amounts of rutile. As in the previous sample, all of the titanite has been altered to rutile, however, retaining the primary titanite crystal shape. It is important to note that the rutile forms skeletal grains and does not completely pseudomorph the titanite grains. A quartz vein has crosscut one of the altered titanite grains (Figure 4.20). These quartz veinlets are characteristic of rocks that have undergone sericitic alteration.

CU448: This sample represents the highest degree of sericitic alteration present at Chuquicamata. The mineralogy consists predominantly of quartz and sericite. All the biotite and potassium-feldspars have been altered to sericite. There is only a minor occurrence of rutile in this sample. It is seen as a typical pseudomorph of primary titanite as well as single grains within the quartz-sericite matrix (Figure 4.21). The single grains show high internal reflections, giving them the characteristic deep red colour in transmitted light, as opposed to the rutile grains that are replacing the titanite and biotite. These grains are completely opaque with no apparent internal reflections.

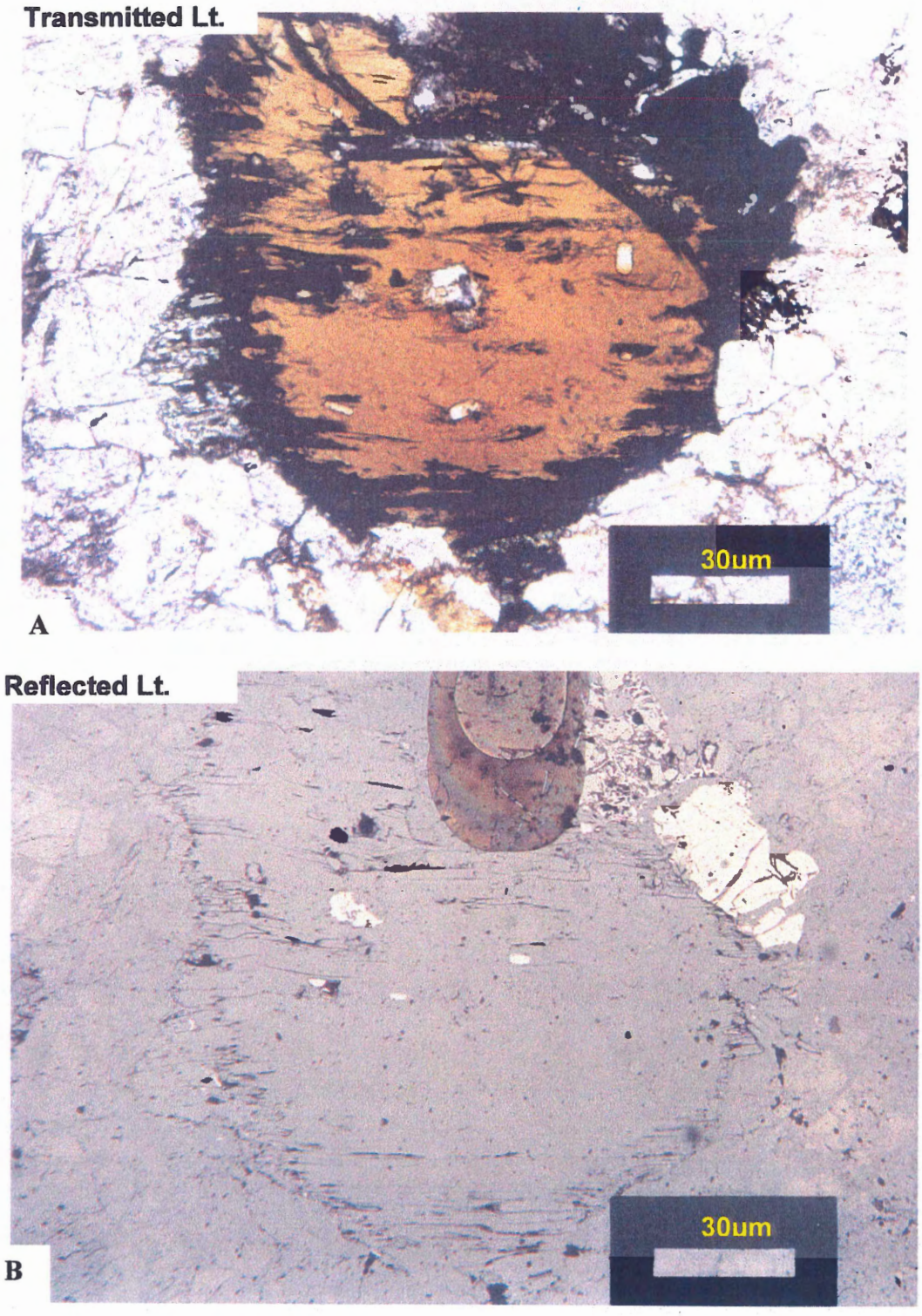

Figure 1

Figure 4.17: Sample CU790. A) Transmitted light view of a biotite grain that has undergone a moderate degree of hydrothermal alteration as defined by the presence of opaque minerals surrounding the perimeter of the grain. B) The same grain as in A, but viewed in reflected light. This reveals that the opaques consist of rutile and pyrite.

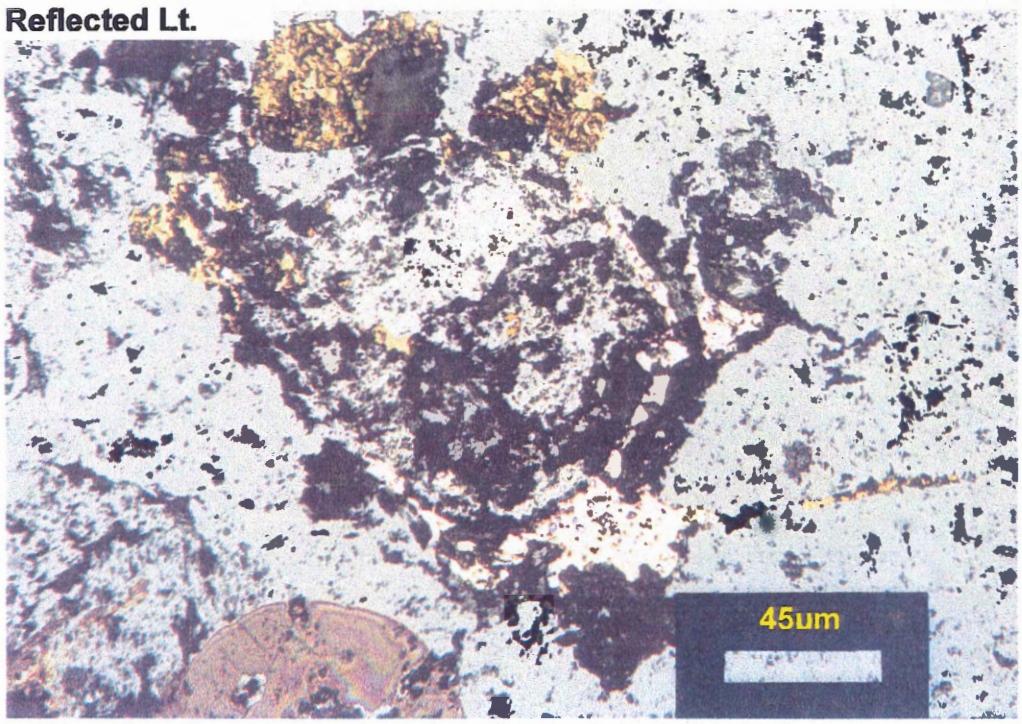

Figure 4.18: Sample CU1115. Reflected light thin section of an altered biotite grain that has been replaced predominantly by rutile (Light Gray), pyrite (White), and chalcopyrite (Yellow).

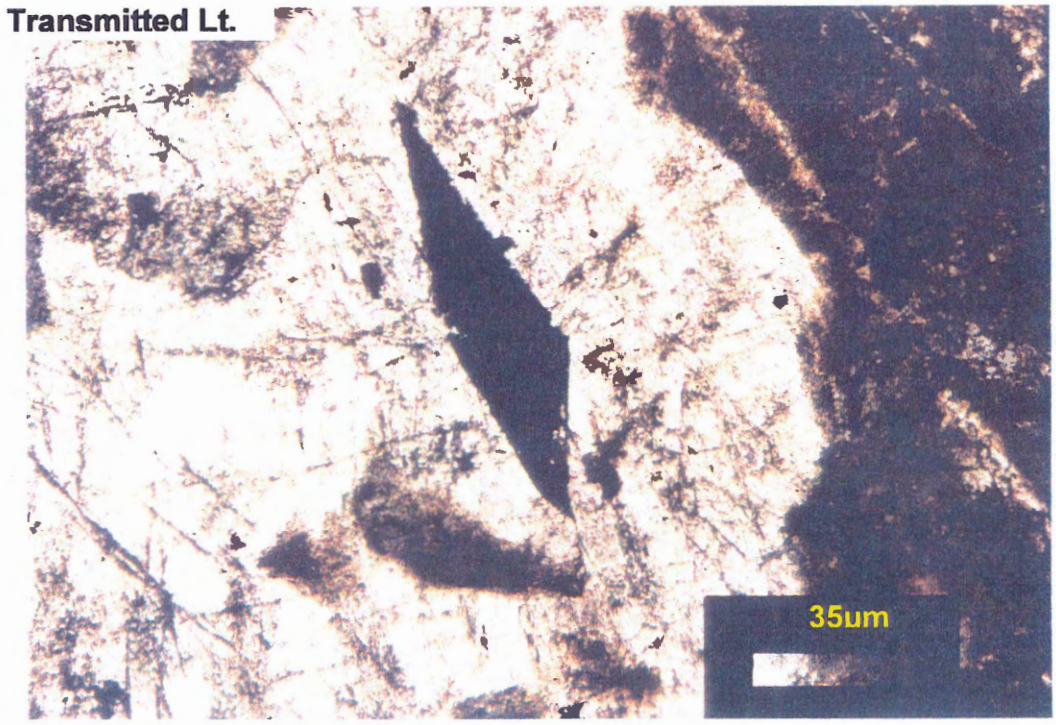

Figure 4.19: Sample CU1115. Transmitted light thin section of a titanite grain that has been completely altered to opaque minerals consisting predominantly of rutile.

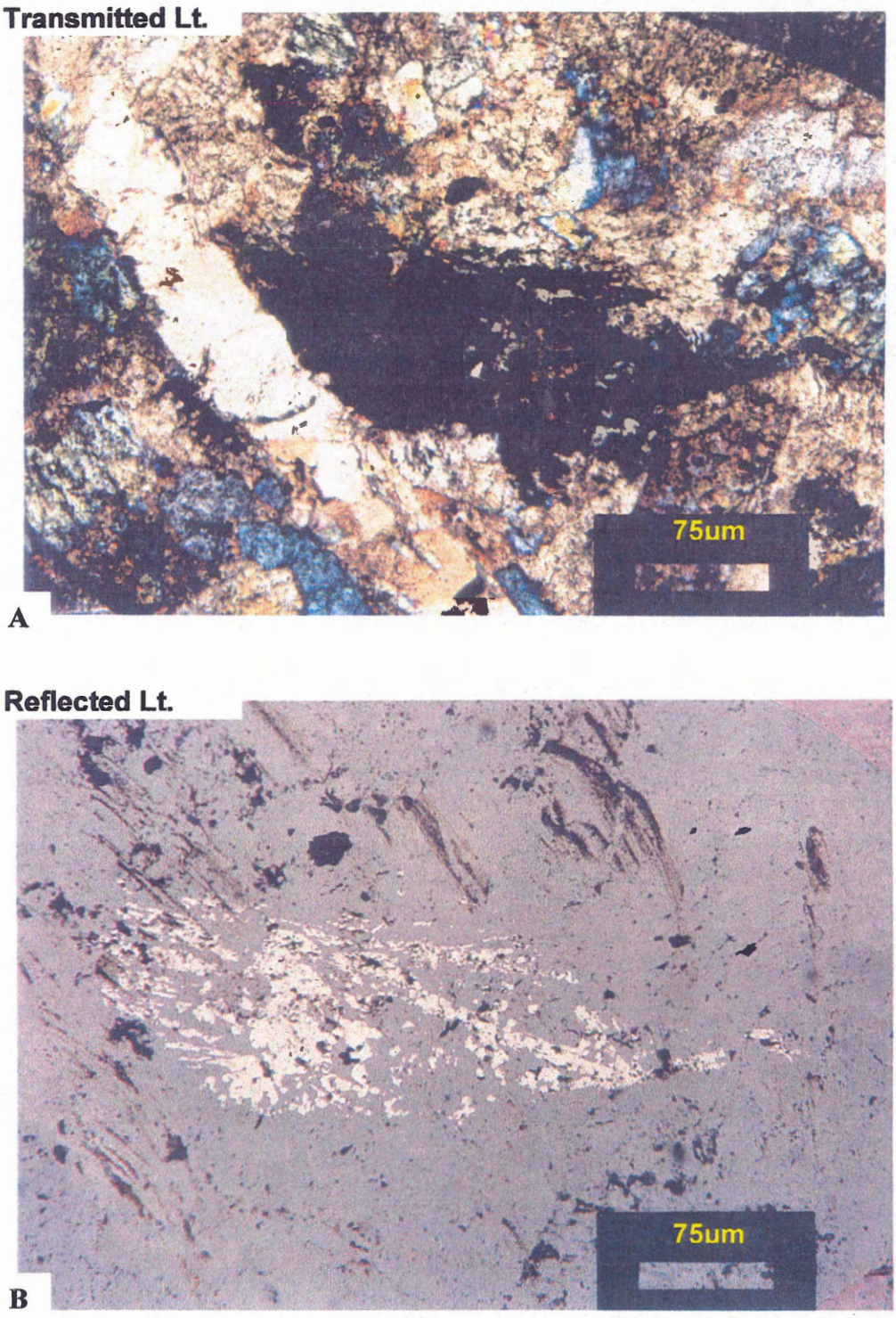

Figure 4.20: Sample CU1101. A) XN-Transmitted light thin section of an altered titanite mineral (Opaque) that has been cross-cut by a quartz vein (Left Center) that is characteristic of sericitic alteration. B) Reflected light view of same grain presented in A. Notice how the secondary rutile (Light Gray) forms skeletal grins and does not completely pseudomorph the primary titanite grain.

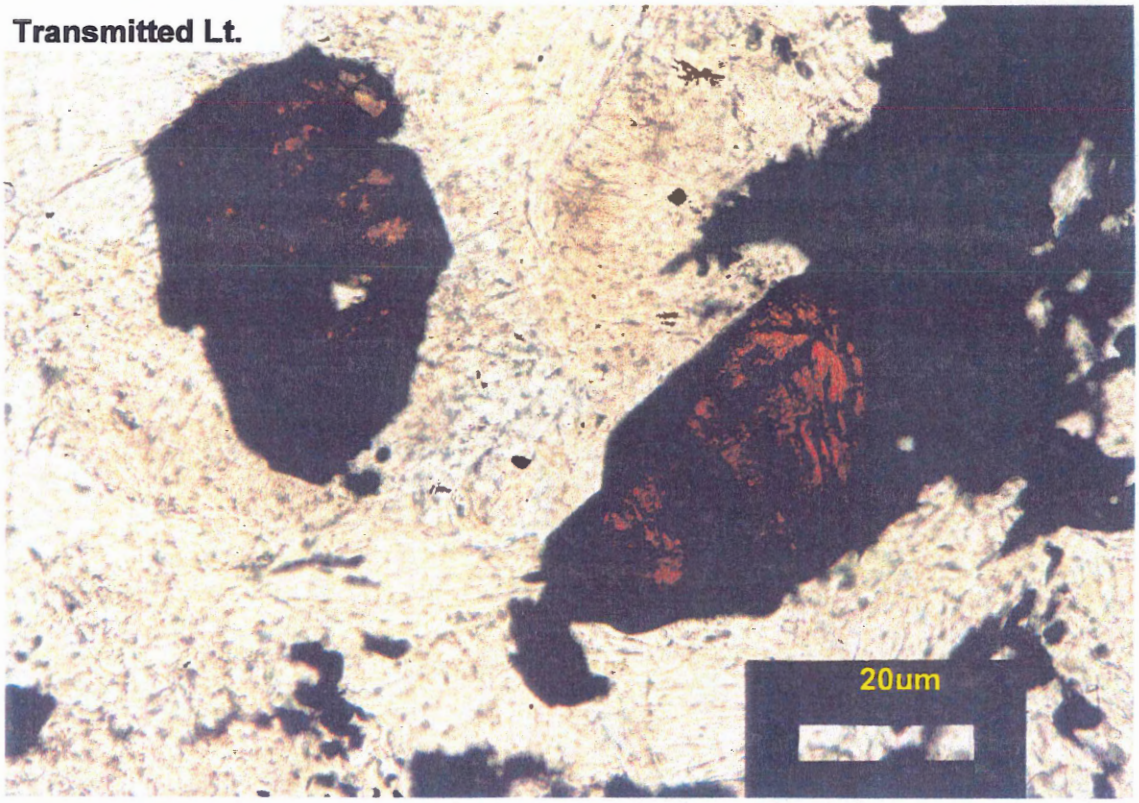

Figure 4.21: Sample CU448. Transmitted light thin section of two rutile grains (Deep Red) within a quartz-sericite matrix. Unlike the previous samples, the rutile here is exhibiting deep red internal reflections, which are characteristic of this mineral.

4.1.1. Geochemistry of titanium-bearing minerals

The majority of geochemical data was obtained via electron microprobe work previously conducted on a number of polished thin sections of rutile and titanite grains from the work of PhD student A. Arnott at Dalhousie University. The results of which are presented graphically in Figure 4.22. The major trend in this graph indicates that there are a higher percentage of trace elements in the unaltered titanite grains as opposed to the altered rutile grains, which generally contain very minor percentages f trace elements.

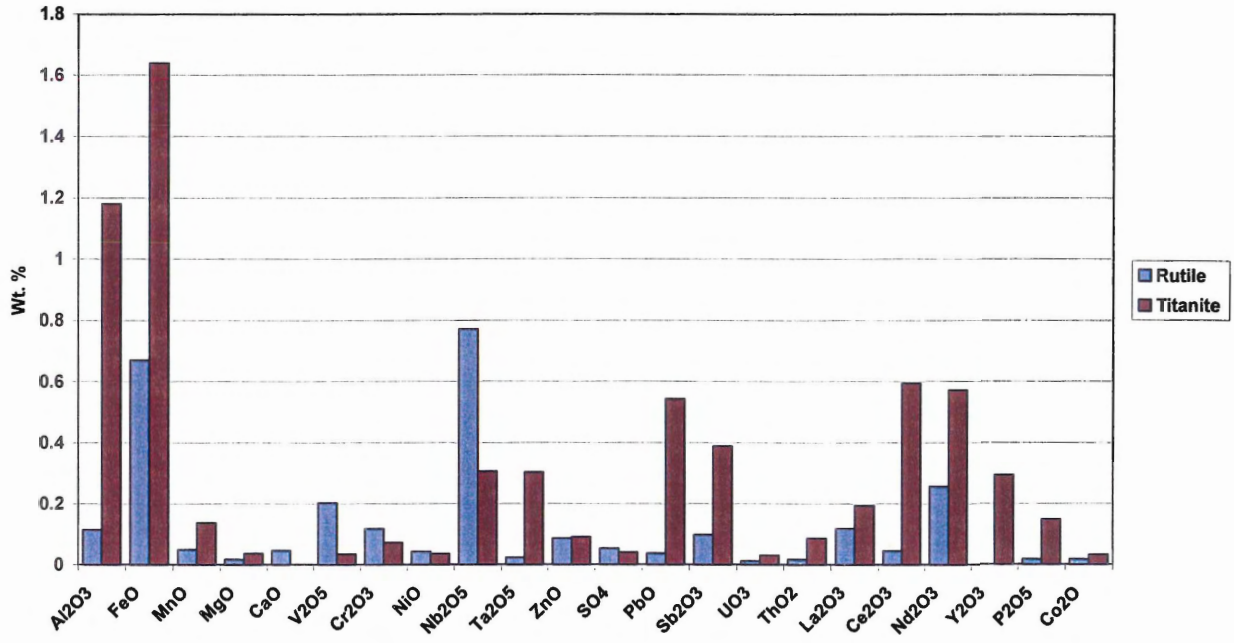

Figure 4.22: Comparison of average trace element compositions in primary titanite and hydrothermal rutile

4.3. Electron microprobe image analysis

4.3.1. Rutile image analysis

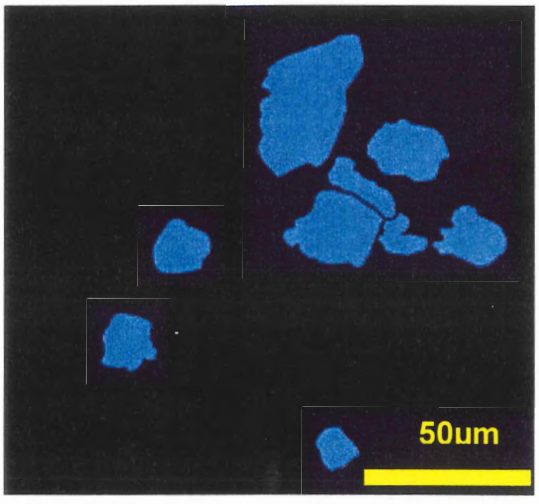

Figure 4.23: Positively identified rutile grains (blue) based on its characteristic grey level from the electron microprobe image analysis. After a positive identification is made, each of the grains are scanned for the various morphological features.

Image analysis via electron microprobe (Section 3.5) was conducted on rutile grains from a heavy mineral concentrate and composite sample from each of the three sample localities (Appendix 10). Once there is positive grain identification (Figure 4.23), they are scanned for different morphological features. In this case they include the area, aspect ratio, circularity, form factor, roundness and waddel diameter.

Area: The rutile in the samples that have undergone potassic alteration occupy a larger area than those that have been affected by the quartz-sericite alteration. The only exception to this relationship is the concentrate sample from Chuquicamata, which has a smaller area characteristic of rocks that have undergone quartz-sericite alteration.

Aspect Ratio: Aspect ratio can simply be defined as the length of the grain divided by its width. The aspect ratio for each of the six samples is very similar, with an average range of 1.720-1.900. This indicates that all of the rutile grains have lengths that are approximately twice the length of their widths, which would produce needle-like shapes.

Circularity: Circularity has the equation,

$$\frac{perimeter}{\left(2*\sqrt{(area*\pi)}\right)}$$

This equation equates the degree of spericity as a function of perimeter vs. area, where a value of one equals a disk. As with aspect ratio, the circularity of the rutile grains in each of the samples is very consistent, with an average range of 1.310-1.560, another indication of the grains elongation.

Form Factor: The equation for form factor is

$$\frac{(4*\pi*area)}{perimeter^2}$$

This function relates the area to the perimeter and is used to describe the equation of a circle. As the perimeter increases, the form factor decreases with increasingly higher irregularity. For a circle the form factor = 1, and for a square it equals 0.785. The average form factor is very similar for each sample and has an average range of 0.470-0.670. This indicates that the rutile has a high degree of irregular grain boundaries.

Roundness: The roundness of a grain can be found using the equation,

$$\frac{(4 * area)}{(\pi * length^2)}$$

The roundness is similar to the form factor in that it too is an equation for describing a circle. However, instead of perimeter, this equation uses the length to determine the degree of circularity. Again for a circle, the roundness equals one. The data obtained from this analysis was again very similar for each sample, with an average range of 0.380-0.490. This along with the form factor can be used to determine the degree of irregularities of the rutile grain boundaries.

Waddel Diameter: The waddel diameter takes into account all the grain irregularities defined by the roundness and the form factor and smoothes them out to a circular form in order to give a more accurate grain diameter. It can be found using the equation

$$2 * \sqrt{\left(\frac{area}{\pi}\right)}$$

The average waddel diameter for each of the samples follows the same pattern as the area data for each sample. In the least altered potassic rocks (RT) the grain diameter is larger (~22.5μm) than the more severely altered quartz-sericite rocks (MM), which has an average grain diameter of 14.0μm. The two Chuquicamata samples are very different

from each other. The composite sample has a grain diameter similar to the potassically-altered rocks of RT (~20.0μm), while the concentrate sample has an average grain diameter of only 14.0μm. This value is more consistent with the MM samples, indicating that this particular sample may have been affected by quartz-sericite alteration as well.

4.3.2. Molybdenite image analysis

Molybdenite is presently being mined at the Chuquicamata mine as a by-product of copper mining. The reason for its image analysis (Appendix 11) in this study is to serve as a morphological comparison to the rutile grains. Unlike the rutile present in each of the six grain mount samples, only one sample, the concentrate grain mount from Radomiro Tomic, contains a sufficient quantity of molybdenite grains to validate the use of image analysis.

A total of 84 grains were identified as molybdenite in this sample. The average area of the grains was 441.4 μm with an aspect ratio of 2.285. The average circularity was 1.47, while the form factor and roundness were 0.5842 and 0.3906 respectively. It was also interesting to note that the average waddel diameter was just 14.91 μm.

4.3.3. Grain size distribution of composite samples

The three composite samples, created from the CIMM heavy mineral concentrates, were crushed to represent typical run of the mill concentrate (Figure 4.24), however, the actual mesh size used at Chuquicamata is not known and this should serve only as an approximation.

The results of a grain size distribution (Appendix 12) shows that for all three samples the highest percentage of grains occur at about 100 microns or 100 mesh size. However image analysis has indicated that the average rutile grains are only about 15

microns wide when averaged over both zones of alteration. So, based on this distribution current milling of concentrate would only recover about 2.5 percent of the total rutile situated in this porphyry copper deposit.

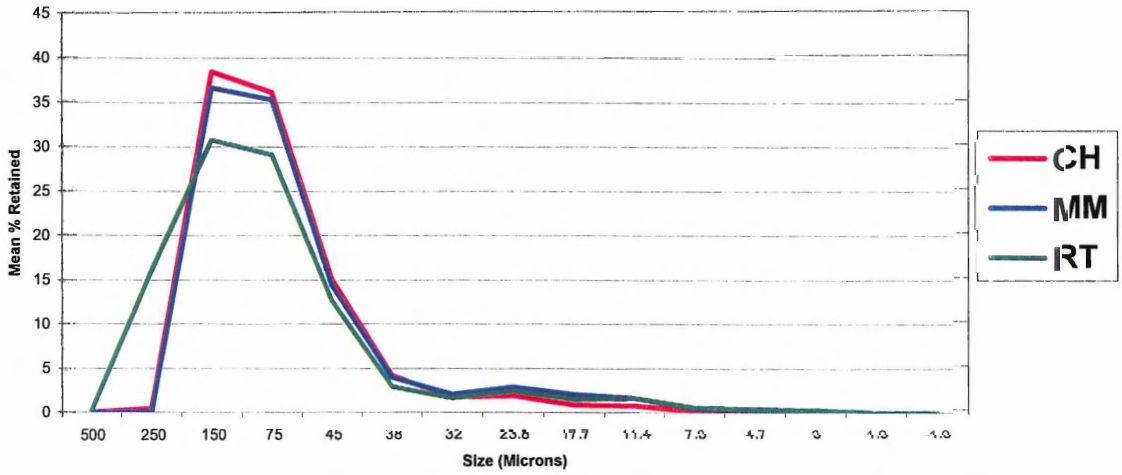

Figure 4.24: Grain Size Distribution of Composite Samples From Chuquicamata (CH), Mansa Mina (MM), and Radomiro Tomic (RT)

Chapter 5

Geological discussion and conclusions

5.1. Mineralogy of titanium-bearing minerals

The results of mineralogical studies carried out on polished sections and grain mounts from Chuquicamata, Radomiro Tomic, and Mansa Mina indicate that the majority of titanium present in this porphyry copper deposit is hosted in hydrothermal rutile. This rutile is a result of the alteration of the primary minerals biotite, titanite, and titanium-bearing magnetite by sulphur-bearing hydrothermal fluids.

Biotite: As a biotite cumulate begins to crystallize in a melt, it is common for the cations Al^{3+}, Fe^{3+}, and Ti^{4+} to substitute for Mg^{2+} and Fe^{2+} on the octahedral sites (Dymek, 1983). The percentage of titanium incorporated in these primary biotites is very minor, however, because of its great abundance in rocks of gronodioritic composition, it can be considered a significant host of elemental titanium.

Upon hydrothermal alteration, primary biotite interacts with S_2 from the hydrothermal fluids present [5.1]. This interaction produces the reaction:

Primary Biotite + Sulphur $\Rightarrow$ Phlogophitic Biotite + Pyrite + Rutile

$$K(Fe,Mg)_2(Fe,Al,Ti)Si_3AlO_{10}(OH,F)_2 + S_2 \Rightarrow K(Mg,Fe)_3Si_3AlO_{10}(OH,F)_2 + FeS_2 + TiO_2 \quad [5.1]$$

In a few of the altered biotite minerals, copper minerals such as chalcopyrite and bornite are present. This is because they too prefer mafite sites such as biotite for crystallization (Williams, and Cesbron, 1977).

Titanite: Force (1991) noted that the formation of rutile from the alteration of titanite was a function of CO_2 pressure, where a higher CO_2 pressure would force the

reaction to a rutile, quartz, and carbonate product. There is, however, no evidence of CO_2 interaction with the titanite from the samples at Chuquicamata. This being said, the most reasonable theory is to assume that the titanite reacted with HCl, a major constituent of hydrothermal fluids. This would force the reaction to a product consisting of quartz and rutile [5.2]. It would also produce water and calcium chloride. The aqueous calcium chloride would further react with sodium sulphate ($NaSO_4$) in solution to produce sodium chloride (NaCl) and anhydrite ($CaSO_4$), which is present at the Chuquicamata mine (Sillitoe et al., 1996).

Titanite + Hydrochloric Acid $\Rightarrow$ Rutile + Calcium Chloride + Quartz + Water

$$CaTiSiO_5 + 2HCl \Rightarrow TiO_2 + CaCl_2 + SiO_2 + H_20 \qquad [5.2]$$

Titanium-bearing magnetite: The term titanium-bearing magnetite is used here to represent the magnetite grains that contain exsolution lamellae of ilmenite. In magmatic magnetite dissolved Ti^{4+} can be very abundant, which causes it to be exsolved as ilmenite. Once exsolved the ilmenite tends to form lamellae that are parallel to the {111} plane of the magnetite (Ramdohr, 1980). In the presence of H_2S-bearing hydrothermal fluids, which is found in most ore-forming solutions, magnetite is transformed to pyrite [5.3] (Ramdohr, 1980). This would tend to leave behind the ilmenite lamellae; however, the H_2S-bearing fluid alters it as well, resulting in the formation of pyrite and rutile [5.4]. The alteration of magnetite can be explained by the equation:

Magnetite + Hydrogen Sulphide + Sulphur $\Rightarrow$ Pyrite + Sulphuric Acid

$$Fe_3O_4 + H_2S + 3S_2 \Rightarrow 3FeS_2 + H_2SO_4 \qquad [5.3]$$

As well, the alteration of the ilmenite lamellae can be explained by the redox equation:

Ilmenite + Hydrogen Sulphide + Sulphur $\Rightarrow$ Pyrite + Rutile + Sulphuric Acid

$$8FeTiO_3 + 2H_2S + 7S_2 \Rightarrow 8FeS_2 + 8TiO_2 + 2H_2SO_4 \quad [5.4]$$

A final, yet minor occurrence of rutile was observed in a grain mount sample from the sericitic rocks from Mansa Mina. This was the presence of rutile intergrown with the clay mineral pyrophyllite ($Al_2Si_4O_{10}(OH)_2$). This occurrence marks the first positive identification of the clay mineral in all of the rocks in the Chuquicamata district. In a typical porphyry copper deposit, pyrophyllite is a common mineral of the advanced argillic alteration zone (Section 2.1.1.4), in which it indicates an alteration temperature of above about 300°C, therefore its presence in samples that were thought to have undergone only quartz-sericite alteration may indicate a higher degree of alteration than was previously considered.

5.2. Geochemical abundance of titanium

Results of geochemical analyses of heavy mineral concentrates (Section 4.2) indicate the highest percentage of titanium occurs in the least altered rocks of the potassic zone of alteration. This is evidenced by an average content of approximately 1.4 wt.% in the Radomiro Tomic mine samples and 1.3 wt.% in the Chuquicamata mine samples. In contrast, the quartz-sericite altered rocks form the Mansa Mina mine samples averages approximately 0.35 wt.% titanium. This same trend is revealed in the mineralogical abundances of rutile in the same heavy mineral concentrate samples. The Radomiro Tomic mine samples contain approximately 1.0 vol.% and the Chuquicamata mine samples contain approximately 1.2 vol.%. Again, the Mansa Mina mine samples contain a significantly less, approximately 0.34 vol.% rutile. By taking a simple ratio of rutile to titanium (RU/Ti) and converting it to the percentage of rutile, another significant trend arises. The percentage of titanium incorporated into rutile in the least altered potassic

rocks represented by Radomiro Tomic is approximately 72%. The samples from Chuquicamata has approximately 92% of the titanium incorporated into the rutile and the highest degree of alteration from the Mansa Mina samples has approximately 97% of the titanium incorporated into the rutile. This trend shows in the least altered rocks of the potassic zone, a higher percentage of titanium is incorporated into the non-economic minerals biotite, titanite, and titanium-bearing magnetite. However, as hydrothermal alteration progresses into the quartz-sericite zone, these primary titanium-bearing minerals have all been transformed into their hydrothermal counterparts. This results in an increase to 97% of the total titanium present incorporated in the potentially economic rutile minerals. The downside is that there is approximately 68% less titanium and rutile present in the quartz-sericite samples. By averaging the percentage of rutile from the potassic zones of Chuquicamata and Radomiro Tomic, there is approximately 1.10 vol.% rutile. Assuming an average of 1.35 wt.% titanium in these two sample localities it can be deduced that approximately 82% of the titanium is incorporated into the rutile, and 82% percent of 1.10 vol.% is still 0.902%, a value three times the average amount of rutile from the quartz-sericite zone.

By examining the correlation data it becomes possible to better understand the distribution of titanium and rutile in this porphyry copper deposit. There is a high positive correlation between rutile and bornite in the least altered concentrates represented by Radomiro Tomic and a high positive correlation with chalcopyrite in the Chuquicamata and Mansa Mina concentrates. This trend is mimicked by a high positive correlation between titanium and copper in the Radomiro Tomic concentrates, however

the Mansa Mina and Chuquicamata concentrates do not exhibit this same trend. These concentrates show a slight negative trend between titanium and copper.

There is also a high negative correlation between rutile and pyrite in the least altered concentrates represented by Radomiro Tomic and Chuquicamata. This correlation is less significant in the more severely altered concentrates represented by Mansa Mina, however it still exists. This same trend is represented by the correlation of titanium to iron. The Radomiro Tomic concentrates have a very high negative trend with iron, which becomes less evident in the Chuquicamata and Mansa Mina concentrates that represent an increasing degree of alteration. The correlation between rutile and molybdenite does not seem to be significant in any of the samples, nor does the correlation between titanium and molybdenum, with exception to a high positive correlation from the most severely altered Mansa Mina samples.

Given the above data it can be inferred that upon hydrothermal alteration the titanium in this porphyry copper deposit was immobile. This is evidenced by a linear trend of a high to low titanium percentage in these concentrate samples from the least altered potassic zone to most altered quartz-sericite zone. This is indicative that the hydrothermal fluids circulated throughout this deposit and preferentially remobilized the elements surrounding the titanium (e.g. iron from biotite and titanium-bearing magnetite) while the titanium was left in situ to create rutile, because it is not stable in its metallic form. Hydrothermal fluids circulate outward from the potassic core to the quartz-sericite zone. If the titanium were mobilized one would expect to see a nonlinear trend in percentage of titanium between alteration zones because the hydrothermal fluids would

have incorporated it and precipitated it as rutile in the quartz-sericite zone, thus producing higher titanium values as alteration progressed.

The highest percentage of rutile occurs in the Chuquicamata mine. These samples show a slightly less titanium abundance than the least altered Radomiro Tomic rocks, however, because the rutile is the result of the destruction of primary titanium-bearing minerals by hydrothermal fluids the least altered rock has not yet liberated as much titanium to form rutile as the intermediately altered Chuquicamata rocks simply because it has not been affected by the hydrothermal fluids to the same degree. The quartz-sericite rocks from Mansa Mina contain the highest ratio of rutile to titanium (97%), however, have considerably less total titanium available to form rutile because of its immobile nature.

5.3. Titanite and rutile geochemical compositions

The microprobe data of the titanite and rutile grains (Appendix 4 and 5) suggest the majority of trace elements most likely originated in the titanite because in most cases the trace element content of the titanite grains are greater that that of the rutile grains (Figure 4.22). Exceptions to this are the amounts of vanadium, chromium, nickel, and niobium found in the rutile and titanite grains (Figure 4.22). The greater abundance of vanadium, chromium, and nickel in the rutile suggests that it does not originate from the titanite. These elements commonly occur in trace amounts in magnetite-bearing rocks. Therefore it is highly likely that they are incorporated into the rutile during hydrothermal alteration of the titanium-bearing magnetite minerals. Niobium is an incompatible element. It has a similar charge and atomic radius to titanium, for which it commonly

substitutes. Therefore, the niobium may substitute for titanium in any of the titanium-bearing minerals, thus its primary origin may actually be from several minerals.

5.4. Conclusions

A major part of this thesis was to determine the mineralogical distribution and geochemistry of titanium in the Chuquicamata porphyry copper deposit. In doing so, it allows for the evaluation of the possibility of a profitable recovery of titanium in the Chuquicamata porphyry copper deposit. As well, it allows for the study of the behavior of titanium in the porphyry copper environment, which was a secondary objective of this thesis. From the results of the CIMM database of major metals and mineralogical abundances, and the polished thin sections, the following conclusions can be made

1.) The majority (>90%) of all the titanium in the Chuquicamata deposit is in the form of hydrothermal rutile.

2.) The formation of hydrothermal rutile is a result of the chemical interaction between sulphur-rich hydrothermal fluids and the magmatic minerals titanite, biotite, and titanium-bearing magnetite.

3.)The statistical results of a large geochemical database of major metals in heavy mineral concentrates revealed that there is a decrease in the overall abundance of titanium as hydrothermal alteration progresses. There are two main hydrothermal alteration zones where ore is mined at Chuquicamata, the potassic, and the quartz-sericite zones. The least altered potassic rocks, represented by samples from the Radomiro Tomic and Chuquicamata mines had an average of 1.35 percent by weight, whereas the rocks exhibiting a higher quartz-sericite alteration only averaged 0.35 percent by weight.

4.) The hydrothermal rutile contains very low amounts of trace elements. Economically this is a great benefit, as a high percentage of trace elements will have negative effects if the rutile is to be used as a pigment. Also, the low trace element content is characteristic of porphyry copper deposits (Section 2.3.1.) and may warrant its use as a prospecting tool for other porphyry copper deposits in the area.

The results of this pilot study indicate that the mineralogical compositions of potentially economic elements play a major role in defining the economic viability of a certain commodity.

5.5. Future considerations

Since the concentrate samples for this study were collected from three different mine sites that are proposed to represent the most developed zones of hydrothermal alteration present at the Chuquicamata porphyry deposit, this study should be considered as a pilot study of the potential for rutile recovery from the potassic and quartz-sericite zones of a porphyry copper deposit. In order for detailed assessment of each of these deposits a greater number of samples from each area would be required in order to put greater confidence in these results.

A study of the rutile distribution in the local river and soil sediments may prove to be a valuable exploration tool for other porphyry copper deposits in the area (see above Section 2.3.1.).

A study of the titanite as a possible titanium source in the least altered rocks surrounding the mine may we warranted because it occurs as much larger grain sizes than

the secondary rutile, however at present times a process for the extraction of titanium from titanite is unavailable.

Chapter 6

Metallurgical discussion and conclusions

6.1. Image analysis and grain size distribution

The results of the electron microprobe image analysis of rutile grains representative of all sample localities has revealed that regardless of what alteration zone they are found in, they all have relatively the same morphological features (Appendix 10). This trait can be associated with the way in which the rutile is formed. As the primary titanium-bearing minerals are altered, the mobile elements are removed, leaving behind voids in the primary mineral structure. Because all of the rutile minerals were formed in this manner, it makes sense that they would all have the same morphological characteristics. The major difference in the rutile from different localities is in the grain size. Samples from Radomiro Tomic, the least altered potassic zone, have an average grain size of 22μm, whereas the grains from Mansa Mina average only 13.5μm. The Chuquicamata samples are divided. The Composite sample, which was created by Marcos Zentilli from concentrate samples that specifically showed the least amount of sericitic overprinting, has an average grain size consistent with the Radomiro Tomic samples. The concentrate sample, however, was not specifically selected to avoid any sericitic alteration. The result of this is a decrease in average grain size to that representative of the Mansa Mina samples. From these results it is clear that samples that have only undergone potassic alteration contain rutile grains that on average are larger than those that have been subject to quartz-sericite alteration.

To get a better understanding of the possibility of rutile recovery, molybdenite grains, that are presently being recovered, were subjected to the electron microprobe image analysis (Appendix 11). The results from this test indicated that on average these grains have a larger aspect ratio than the rutile grains (2.29 as opposed to 1.80), indicating that they are more needle-like than the rutile grains. This test also indicated that the molybdenite grains have an average waddel diameter of 14.9 μm and average area of 441 μm. The size of these grains are therefore similar to the rutile grains from the zones of quartz-sericite alteration, and are on average smaller than the rutile from the least altered potassic zones (Section 4.2.1). Section 6.1.2. (Below) provides an explanation of the process for the recovery of molybdenite from the Chuquicamata ore. It states that in order to economically recover molybdenite, the ore must go through a series of flotation cells (Chapter 7) and regrinding processes. This same process may potentially be used to recovered rutile from Chuquicamata.

6.2. Ore processing at the Chuquicamata mine

At the Chuquicamata mine site ore is hauled by truck to the primary mill (1), crushed to the size of coarse gravel, and sent to the surface via conveyer belts. Once at the surface it enters the secondary mill to be crushed again to the size of small pebbles and then to the concentrate plant (3) where it undergoes two processes. The first is a wet milling (4), where the ore is mixed with water and thousands of small steel balls inside large rotating cylinders (ball milling), which grinds the pebble size ore to a fine powder. By mixing this powder with water it forms a paste that flows into the second process at

Figure 6.1: (Following Page) Flow chart of the mining operation at the Chuquicamata porphyry copper deposit (After Turismo Y comunicaciones S.A., 1992).

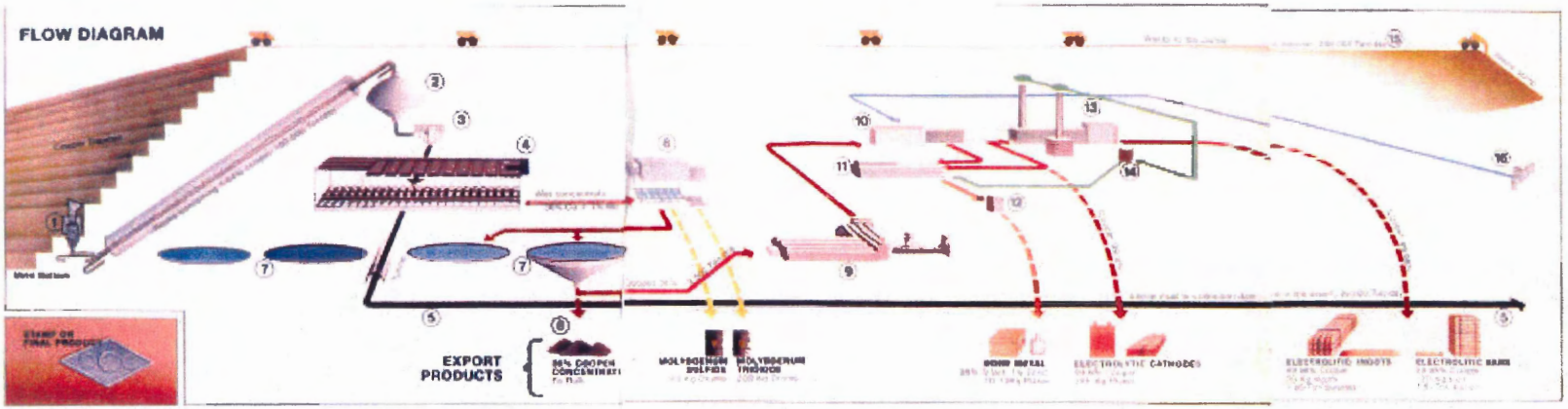
FLOW DIAGRAM
EXPORT PRODUCTS
ELECTROLYTIC CATHODES

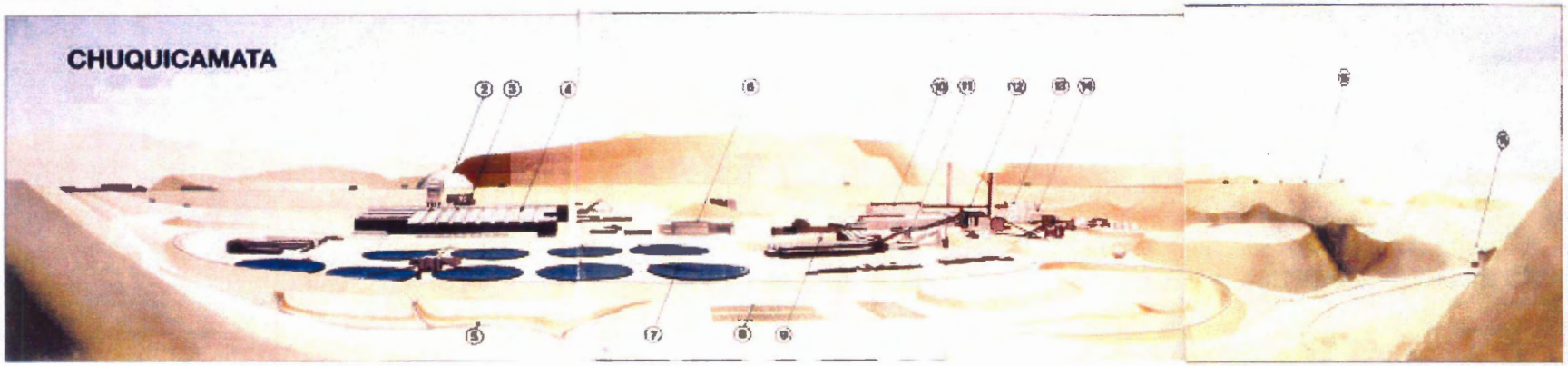
CHUQUICAMATA

the wet mill, the flotation cells (4). At these cells, more water is added to the paste, as well as the injection of air and chemicals. This produces froth that captures the copper-bearing minerals and floats them to the surface. This froth, called the collective concentrate, overflows into ducts and is comprised of approximately 37% copper, and 1% molybdenum, as well as minor amounts of gold, and silver. This method is referred to as froth flotation.

The minerals that are not picked up by the froth settle at the bottom of the cells, where they are extracted into the waste mud canal (5) and carried by gravity to the desert waste piles (15).

The collective concentrate is again introduced into a circuit of flotation cells, where the 1% molybdenum is extracted (6) (Section 6.3.1.). The final products then consist of molybdenite (MoS_2) that is obtained directly from the concentrate, and molybdenum trioxide (MoO_3) that is obtained by roasting the concentrate.

After the molybdenum is extracted, the collective concentrate is introduced into a number of settling tanks (7) where it settles to the bottom, now known as wet concentrate. From there it is either sent to a solar-drying plant (8), where it is sun-dried and sold to other refineries as copper concentrate, or (the majority) is sent to the drying plant (9). At the drying plant the wet concentrate is heated to a dry concentrate before being sent to the refinery (10, 11). Once the dry concentrate is refined it contains 99.8% copper, known as electrolytic cathodes. The waste product of this refining, known as anodal mud, is brought to the noble metals plant, where it is smelted into 10-12 kg plates of Doré metal, a compilation of 98% silver and 1% gold.

The electrolytic cathodes are then smelted in refining furnaces (13) to produce a final product of ingots and bars containing 99.98% copper and sold for most copper applications.

6.2.1. Molybdenum recovery at Chuquicamata

As described above the molybdenum, in the form of the mineral molybdenite (MoS_2), is extracted from the ore concentrate via froth flotation (Figure 6.2). The first molybdenite flotation circuit uses sodium hydrosulphide (NaHS) to depress the copper mineral in the concentrate. From this, the cleaner concentrate is reprocessed in four to seven stages in which 2.5 kg/ton of arsenic Nokes reagent is used to float the MoS_2.

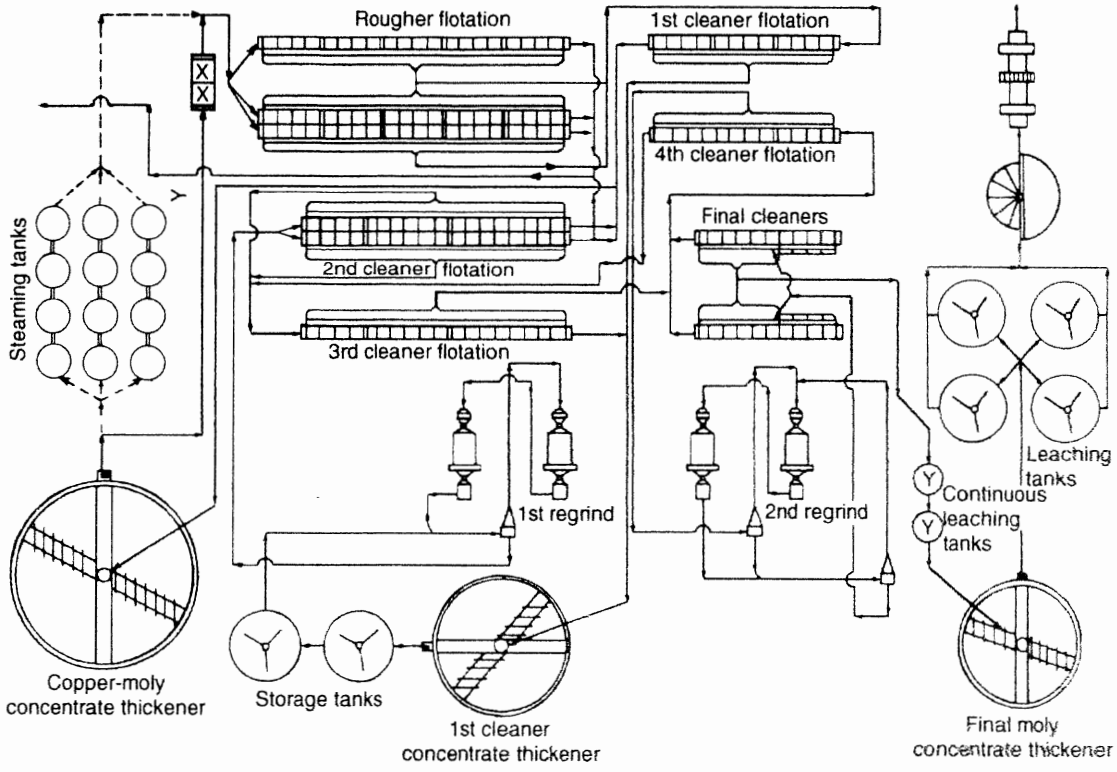

Figure 6.2: Flow sheet of Molybdenum extraction via froth flotation at the Chuquicamata mine (After Wills, 1997).

Regrinding also takes place after the first and fourth flotation stages, producing a concentrate of 55% Mo and 1-2% Cu. The concentrate is then leached with sodium cyanide (NaCN) to further reduce the copper content, primarily as chalcopyrite, to below 0.3%. The sodium cyanide is also is also added in the last two cleaning stages. Nitrogen is the gas used rather than oxygen as its reducing potential lowers the amount of depressant significantly.

6.3. Economic potential for rutile recovery

Under present milling conditions at Chuquicamata, the recovery of rutile would be very low and not justify the added costs. However, there is a significantly high positive correlation between titanium and copper in the least altered ore represented by the Radomiro Tomic heavy mineral concentrate samples (Figure 4.12), and a significantly high positive correlation between rutile and bornite in the same concentrate samples (Figure 4.9), as well there is a significantly high positive correlation between rutile and chalcopyrite in the Chuquicamata heavy mineral concentrate samples (Figure 4.7). Based on these positive correlations it can be assumed that titanium and rutile follow a relatively linear positive correlation with copper and the major ore minerals of copper.

In 1997, the Chuquicamata mine produced 481,000 tonnes of refined copper from 53,000,000 tonnes of sulphide ore containing an average grade of 1.05%Cu (Ossandón et al., 2001). If the average copper content, based on the heavy mineral concentrate samples from Radomiro Tomic and Chuquicamata, is approximately 17%, and an average of 1.34% titanium from the same samples, then based on the significantly positive correlation between titanium and copper in the least altered rocks, and the significantly

positive correlation between rutile and chalcopyrite and bornite, the average titanium grade (X) can be estimated by:

$$\frac{17\%}{1.34\%} = \frac{1.05\%}{X}$$

Where X = 0.083%

This grade is approximately 3.5 times the molybdenum grade of 0.024% (Kirkham and Sinclair, 1996), which is presently being recovered at Chuquicamata. Therefore, in terms of the 1997 production figures, approximately 43,990 tonnes of titanium was entering the tailings ponds. Not all of the titanium in this deposit occurs as rutile; therefore, by averaging the ratio of titanium to rutile, it turns out that approximately 82% of all the titanium is incorporated into the rutile. Therefore, of the total 43,990 tonnes of titanium present, 36,072 tonnes is present as rutile.

According to the USGS Minerals Yearbook (2001), the average price of rutile was approximately $550 US per tonne in 2001. This would equal to:

36,072 tonnes * 550.00$ = $19.8 million/year from rutile concentrate. Theoretically, rutile contains 60% titanium; therefore, 60% of 36,072 tonnes equals 21,643 tonnes of titanium. The average price of titanium sponge, the basic metal form of titanium, was $7.91 US/kg in 2001 (USGS Minerals Yearbook, 2001). This equates to approximately $171 million US/year being lost to the tailing ponds in the form of unrecovered rutile.

6.4. Conclusions

The primary objective of this thesis was to examine the possibility of recovering rutile as a by-product of porphyry copper mining. Image analysis via the electron microprobe has provided a powerful tool for grain size calculations, and comparisons

with molybdenite, which is presently being mined. Based on these results the following conclusions can be stated.

1.) The average grain size of rutile is larger in the rocks that have undergone the least amount of hydrothermal alteration

2.) The average size of the molybdenite grains taken from the least altered Radomiro Tomic heavy mineral concentrate sample was similar to the size of the rutile grains in the quartz-sericite sample, represented by Mansa Mina.

3.) When combined with the results of the grain size distribution, present milling conditions would only recover about 2 percent of the total contained rutile.

4.) At present times, based on the results of the grain size distribution and the average rutile grain diameter, full liberation would require excessively fine milling to -800 mesh (Appendix 13), which would cost far more than would be feasible to make a profit.

6.5. Future considerations

For future consideration it would be beneficial to carry out several flotation experiments, based on the information provided below in chapter 7, in order to determine the percentage of total rutile that may be recovered at a profit. There is also the possibility of a study on the feasibility of setting up a regrinding and flotation circuit near the wastepiles and mine tailings to recover rutile. The tailings especially, have had the majority of copper and molybdenum sulphides removed, therefore there may prove to be a higher concentration in the overall rutile grade. Another option may be the chemical leaching of pyrite and silicates surrounding the rutile for easier recovery.

Regardless of the method, if recovered, a study on the production of titanium metal would be necessary, as in this form it is much more valuable than copper or molybdenum metal.

Chapter 7

Froth flotation and its role in rutile recovery

7.1. Froth flotation

There are many different mineral separation techniques used to recover ore minerals from gangue minerals. A list of some of the most common ones is presented below in figure 7.1. Based on the excessively fine grain size, relatively low grades, and nonmagnetic nature of the rutile in this porphyry copper deposit, the most reasonable method of separation would be by froth flotation.

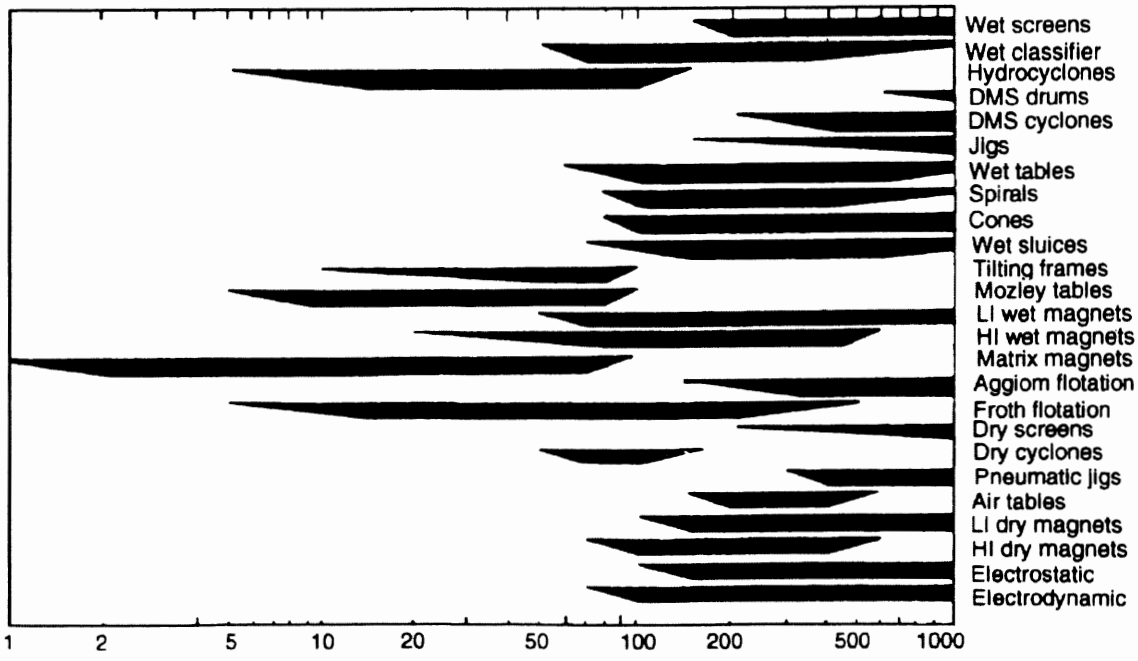

Figure 7.1: Effective range (in microns) of application of conventional mineral processing techniques (After Wills, 1997)

The theory of froth flotation is based on the differences in physico-chemical surface properties of minerals. Upon treatment by certain reagents, these differences between minerals in the pulp (the slurry of concentrate minerals in the flotation cell)

become apparent (Wills, 1997). This method is particularly attractive because it can only be applied to relatively fine particles because in order for the flotation to work a mineral grain must be able to attach itself to an air bubble so it can be floated to the surface (Wills, 1997). If the particles are too large, the attachment to the bubble will be weak, causing the grains to fall off.

In order for the air bubbles to attach to the mineral grains they have to be able to displace water from the grains surface, which is only possible if the mineral is water repellant, or hydrophobic (Wills, 1997). Once the grain is attached and reaches the surface, the bubble must be able to stay in tact to form froth, otherwise they burst and the grains sink back into the pulp. In nature most minerals are polar therefore they are not hydrophobic (Wills, 1997). In order for this to occur, certain chemical compounds known as flotation reagents must be used.

The most important group of reagents is the collectors. These compounds adsorb to the mineral surfaces, rendering them hydrophobic in order to initiate bubble attachment (Wills, 1997). Another important group of reagents are the frothers, which are responsible for the stability of the froth once the grains have been floated to the surface. The final group of reagents is the regulators, which are used to control the whole process. There are two types of regulators, the activators, which liberate grains into the liquid, and the depressants, which are used to selectively render certain minerals hydrophilic (water absorbing) in order to prevent their flotation (Wills, 1997).

A major problem with froth flotation is the occurrence of slime, a coagulation of fine mineral particles. In a crushed and ground ore slimes typically occur from particles below 20 μm (Wills, 1997). They can hinder flotation by coating the other larger

minerals and reducing collector adsorption. To overcome this problem a de-sliming method must be employed.

One possibility is to remove the slime-size particles before flotation, however, this may decrease the overall value of the concentrate, and epically in this case where a high percentage of rutile minerals are below the 20-μm mark. Another possibility is to apply a vigorous agitation to the flotation cells, or inject a slime dispersant chemical into the cells. One such dispersant is sodium silicate ($Na_2O*2SiO_2$), which when put in solution will increase the double-layer charge on particles causing the slime layers to readily disperse (Wills, 1997). This allows the now cleaned mineral surfaces to attach to the collectors for proper flotation. Sodium silicate can also act as a depressant for minerals such as the non-sulphide minerals like scheelite, calcite, and fluorite (Wills, 1997).

A number of variations of froth flotation have been developed for the flotation of ultra-fine mineral grains from the pulp. Those that will be discussed here include, electroflotation, carrier flotation, selective flocculation, and depressive flotation.

7.1.1. Electroflotation

For industrial purposes, froth flotation is rarely applied to particles below 10 μm in size because of the lack of control of air bubble size (Wills, 1997) because ultra-fine bubbles must be generated to improve attachment to the extremely fine particles. It is possible to generate these bubbles by in situ electrolysis in a modified flotation cell. A direct current is passed through the pulp by two electrodes, generating a stream of hydrogen and oxygen bubbles, the majority ranging in size from 10-60 μm (Wills, 1997). The bubble density can be controlled by the current density, which provides adequate

froth control and efficient distribution of the ultra-fine bubbles, whereas conventional froth flotation methods produce bubbles ranging from 0.6-1.0 mm in diameter and little size control (Wills, 1997). This process has not been used commercially for mineral separation. Its main use has been in the sewage treatment industry to float solids from suspension; as well it has been used in the food industry (Wills, 1997). This being said, the excellent control of bubble size may justify the use of electroflotation for the flotation of ultra-fine ore minerals.

7.2. Coagulation and flocculation

One method of overcoming the problem of ultra-fine particle flotation is to create aggregates of the specific ore mineral, thus making it easier to float under conventional methods. These aggregates can be attained through the coagulation or flocculation of the ultra-fine particles.

7.2.1. Coagulation

Coagulation of ultra-fine particles occurs when these particles adhere directly to each other under collisional forces (Wills, 1997). In a normal system the adhesion caused by the mutual attraction forces, known as the London-Van Der Waal's molecular forces, are only effective at short ranges and are prevented by an electrical charge surrounding each particle (Wills, 1997). The electrical charge around each grain will have the same sign throughout any given system, generating repulsion between two grains that are coming into contact with one another. Aqueous solutions of pH 4 or greater are generally negative, and strong acids of pH less than 4 are generally positive (Wills, 1997). It is this repulsion that prevents the particles form coagulating, but at the same time it also keeps them in motion and impedes the rate of settling (Wills, 1997).

The introduction of coagulants, which are electrolytes with an opposite charge to the particles in solution, causes a neutralization of charges when dispersed throughout the system. This will allow the particles to collide with each other and adhere as a result of the London-Van Der Waal's molecular forces (Wills, 1997). The most frequently used coagulants are cationic inorganic-salts such as Al^{3+}, Fe^{3+}, and Ca^{2+}. Depending on the surface charge of the particles, lime or sulphuric acid may also be used to promote coagulation (Wills, 1997).

7.2.2. Flocculation

Flocculation is similar to coagulation; however, it involves the formation of much more loosely bound agglomerates that is based on molecules of reagent forming bridges between separate suspended particles. These reagents are long-chain organic polymers, formerly natural minerals such as starch, glue, gelatine, and guar gum; however, synthetic materials, termed polyelectrolytes, are now more commonly used, the majority of which are anionic in character (Wills, 1997). The inorganic salts used for coagulation are not sufficient for flocculation, as they cannot perform the bridging function.

In order for the maximum flocculation of fine-grained minerals to occur, there are certain factors that must be considered, primarily an optimum dosage rate and pH (Wills, 1997). An excess of flocculant can actually cause a depression of particles because of floc breakdown. The physical factors also play an important role in the stability of the flocs; because they are so fragile particle-particle collisions created by a vigorous agitation of the slurry may in fact destroy the flocs. This can even occur during pumping of the slurry, however, mild agitation is essential for the primary depression of the grains in order for the flocculant to coat every individual grain (Wills, 1997). After the flocs

have been formed care should be taken to avoid vigorous agitation, which may rupture the long-chain molecules and destroy the flocs.

7.2.2.1. Selective flocculation

The treatment of finely disseminated ores often results in the production of ultra-fine particles, or slimes. These slimes respond poorly to conventional mineral separating techniques and are often lost to the tailings, thus reducing the percentage of recovered ore. The agglomeration of these ultra-fine particles in suspension may be obtained under high shear conditions (Wills, 1997). If the particles are hydrophobic, a shear field initiated by vigorous agitation of sufficient magnitude to overcome the energy barrier separating the particles may be necessary to bring them together (Wills, 1997).

In multi-mineral ore feeds, it is not enough to be able to agglomerate all the fine particles present in the slurry, as much of it will consist of unwanted gangue minerals. To avoid this problem selective flocculation of the ore minerals, followed by flotation of the aggregates may serve to be a favorable technique. In order for this process to be successful the mineral mixture must be stably dispersed before the addition of a high molecular weight polymer that will absorb on only one of the mineral species in the slurry. This is then followed by flotation of the selected mineral flocs from the mixture (Wills, 1997).

One example of this process in industry is the Cleveland Cliffs Iron Company's ten million tonne/year operation in the U.S (Wills, 1997). This mine treats fine-grained non-magnetic oxidized taconites in order to recover hematite. The hematite, which is finely intergrown with the host rock, is ground to 85% - 25um. Caustic soda and sodium

silicate is then added as depressants for the fine silica, and a cornstarch flocculant is added to selectively flocculate the hematite grains.

7.3. Carrier flotation

This method of flotation relies on particles of coarser grain size to be introduced into the pulp in order to recover the ultra-fine ore minerals. The ultra-fine ore minerals in the pulp will then attach to the newly introduced grains, forming larger amalgamations that can be floated off. This phenomenon is an important type of shear flocculation, in which a shear field caused by vigorous agitation overcomes the energy barrier separating the particles in order to adhere them to each other (Wills, 1997).

Another example of this method is the beneficiation of kaolin clay by the addition of minus 60 μm calcite grains to the flotation system with oleic acid as a collector. During conditioning the anatase (TiO_2) within the clay coats the calcite grains and is liberated when the calcite is floated off, leaving behind the kaolin (Wills, 1997).

The same mineral can some times be used as the carrier mineral. For example, coarse-grained hematite ore can be used as a carrier for the agglomeration of the fine hematite in the pulp. This method has been successful in a number of Chinese mines for the flotation of hematite, Cu-oxides, lead-zinc slimes, and tin slimes. In these cases the coarse grains are returned to the slime feed, where they act both as carriers, and as promoters for aggregation of the fines (Wills, 1997).

7.4. A modified flotation cell for fine-grained materials

The separation of clays and other fine minerals, particularly those that form natural slimes, by froth flotation is in part restricted by the potential energy barrier

preventing a mineral particle in the liquid phase of a pulp entering the liquid/air interface (Ranney, 1980).

A process derived by E.K. Cundy; U.S. patent 3,979,289; Sept. 7, 1976, was proposed for separating fine minerals from their impurities. According to Ranney (1980), the steps in which this process is accomplished are:

1. Conditioning the fine material with a deflocculant in an aqueous slurry.
2. Mixing in a collector for the mineral impurities before or during the conditioning phase.
3. Injection of this conditioned slurry into a froth flotation cell containing a central, internal, submerged impellor that has a base plate containing a plurality of blades in a radial arrangement, with a stationary cover plate that has a small clearance from the tips of the blades.
4. The impellor must have a minimum peripheral speed of 2000 ft/min in order to give the particles sufficient momentum to break through the energy barrier between it and an air bubble.

The flotation cell that was constructed to carry out this procedure is represented by figure 7.2. It is comprised of an impellor (1), which has a base plate (1A) with a plurality of blades radially attached (1B), all of which is driven by an electric motor (2). The motor is mounted on supporting steelwork (3) and activates the impellor through an arrangement of pulleys and belts (4) and a vertical shaft (5) that rotates is a bearing (6). The impellor is surrounded by a stationary cover plate in the form of a hood (7) and is supported by four diagonal baffles (8). The hood is separated from the tips of the blades usually by 1/24-1/30 the diameter of the impellor. The hood has an upper plate member

(7A) from which there is a plurality of fins (7B) extending radially from a position adjacent to and external of the periphery of the impellor to the periphery of the upper plate member.

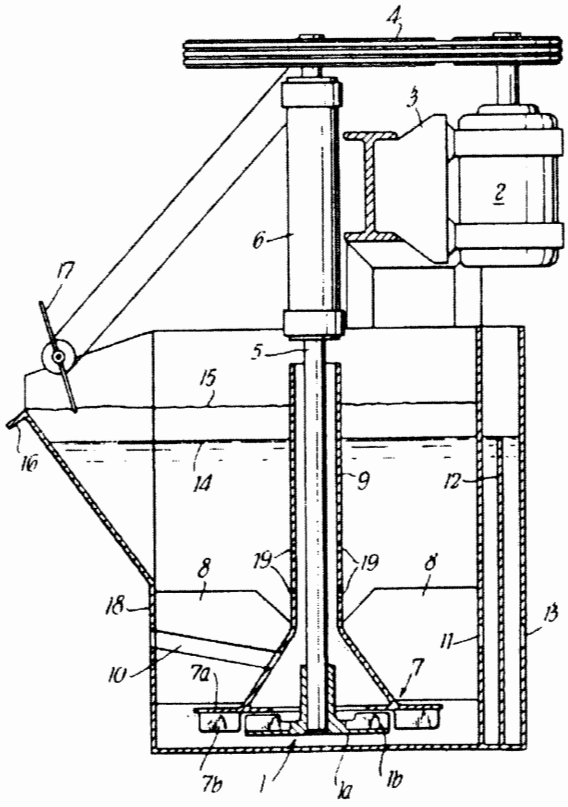

Figure 7.2: Flotation cell used to recover fine-grained material (After Ranney, 1980)

The shaft is surrounded by a cowling (9), which is attached to the hood and baffles. The feed of conditioned slurry is introduced into the cell by a pipe (10) that transports it to the inside of the cowling. It is then drawn down through a number of apertures in the hood by the impellor or circulated through the cowling by a series of holes (19). Simultaneously air is drawn into the cell via the impellor through the top of the cowling.

The discharge, or sink, material passes out of the cell through an orifice (11) and over a weir (12). Adding or removing wooden battens can adjust the height of the weir. Once

past the weir, the discharge finally leaves the cell by an outer orifice (13). The level of the conditioned slurry in the cell is represented by (14), and the top of the froth is represented by (15). The froth is skimmed off over a lip (16) by a rotating paddle (17), which is driven by the electric motor. The cell sides (18) are constructed from wood.

7.5. Froth flotation and rutile recovery

There have been numerous attempts to recover rutile via froth flotation. Purcell and Sun (1963) used unsaturated fatty acids (oleic, linoleic, and linolenic acids) and Marabini and Rinelli (1983) used the chelating agent N-benzoyl-N-phenyl-hydroxlamine (N-BPHA) as the collectors for rutile flotation, however, their results were less than satisfactory. A study by Ma (1989) obtained slightly better results and involved the flotation of rutile mixed with chlorite at a pH of 8-9 using sodium hydroxamate as the rutile collector, and sodium hexametaphosphate and carboxymethyl cellulose as gangue depressants. The floated concentrate was then roasted to remove the sulphur.

Until recently, the best rutile flotation results were obtained by using benzyl arsenic acid (BAA) as a collector (e.g. Cui et al., 1986). In this study hard rock rutile ore from the Zaoyang Rutile Mine in China was floated using sodium fluorosilicate (Na_2SiF_6) as a gangue depressant and BAA as the collector. Sulphuric acid was used to adjust the pH to 4.5. This method worked fine, however, BAA is a toxic substance and can cause many environmental problems. New restrictions were placed on its production and usage, resulting in high reagent costs and rendering the whole process only marginally economical (Liu and Peng, 1999).

Liu and Peng (1999) carried out a study to find a more cost effective and environmentally friendly substitution for the BAA. The results of this study revealed that

a composite collector blended with a 1:1 weight ratio of styryl phosphonic acid and octanol was most effective for the flotation of hard rock rutile ore. The octanol is not actually a collector, but it co-adsorbs to the rutile surfaces and increases the hydrophobicity in order to render it floatable. It was also found that the composite collector needed an emulsifier added at 1% of the total collector weight. The emulsifier was used because octanol is only slightly soluble in water, so it floated on top of the pulp and destroyed the froth. Therefore, in order for the composite collector to be useful, it was thoroughly emulsified by an ordinary mechanical agitator. The most effective recovery of rutile was produced at a pH of 4.5, the addition of 500 g/ton sodium fluorosilicate as a depressant, and the addition of 800 g/ton of the composite collector containing 1% emulsifier (labeled as E-3 in this study).

Bulatovic and Wyslouzil (1999) conducted a laboratory study on the flotation of rutile ore mixed mainly with ilmenorutile, quartz, dolomite, feldspar, and mica. Moderate amounts of clay minerals in the form of illite were also present. This gangue mineral assemblage is comparable to that of a porphyry copper deposit. The rutile grains were liberated at sizes ranging from 125-180 μm, and the flotation was carried out on the ground and deslimed ores.

The results of this study showed that the maximum rutile recovery by flotation was achieved with a collector comprised of a phosphonic acid ester modified with succinamate. A modification of the phosphonic acid ester with petroleum sulphonate gave similar metallurgical results, but with less recovery. It was possible to upgrade the rutile concentrate by reverse flotation of the residual silicates and dolomite, and the depression of the rutile with a caustic starch depressant.

In 1980 Llewellyn and Sullivan tackled the problem of floating rutile from the tailings of a porphyry copper deposit. To do this they first removed the sulphides and carbonates, and then floated the rutile by using a petroleum sulphonate as the collector in an acid circuit. The major problem encountered in this experiment was the formation of slimes that resulted from the fine rutile grain size. This problem resulted in a low rutile recovery and was deemed uneconomical.

Of great interest to this study is the study by Bertini et al. (1991), which investigates the recovery of the fine-grained titanium minerals rutile and ilmenite through selective flocculation. The results of their study indicate that by using a copolymer of 3,4-(methylenedioxy)benzyl acrylate with acrylic acid, excellent selective flocculation of these titanium minerals against gangue minerals such as quartz can be achieved. The rutile especially showed high flocculating stability. The water solubility and flocculating power of this copolymer was highly dependent on the pH values. If they were added at a basic pH, they acted as dispersants, however in an acid circuit, they were precipitated and showed a very high rate of flocculation. In this study the authors also investigate the effect of rutile flocculation at different copolymer composition and concentration at various pH levels. The results of which are given in table 7.1. To summarize these results, the best flocculation values were attained over a very limited acidic pH region. Outside this region the copolymer acted as a dispersant or was inert. This characteristic enables the pulp and the copolymer to be mixed under non-flocculating pH conditions and by carefully changing the pH one can control the gradual formation of rutile flocs, thereby limiting the contamination of the concentrate by unwanted mineral grains (Bertini et al., 1991).

Copolymer	PH	Concentration		
		10 ppm	50ppm	100ppm
I(0.1005)/AA(0.8995)	2.5	F 84	F 94	F 87
	3	F 76	F 89	F 78
	4.5	D 55	D 68	D 71
	7	D 38	D 50	D 55
	9	D31	D 51	D 54
I(0.1808)/AA(0.8192)	2.5	F 84	F 96	F 95
	3	F 68	F 86	F 84
	4.5	D 61	D 82	D 95
	7	D 8	D 5	D 11
	9	D 19	D 22	D 25
I(0.2841)/AA(0.7159)	2.5	F 65	F 87	F 87
	3	F 57	F 85	F 85
	4.5	D 42	D 56	D 60
	7	F 5	D 12	D 19
	9	0	D 13	D 9

Table 7.1: Flocculating power % (F) and dispersing power % (D) of 3,4-(methylenedioxy)benzyl acrylate (I) / acrylic acid (AA) for rutile based on different copolymer concentrations, compositions, and pH values (after Bertini, et al., 1991).

7.6. Rules for optimum mineral recovery

Barbery (1991, p.298-300) has compiled a list of rules that have been made by different authors at various times since mineral processing became a technical subject. The most applicable ones are listed here.

- "It is not practical to carry out liberation to completion; indeed, it is economically desirable to strike some happy medium between complete liberation and one that is metallurgically ineffective (...). The practice of discarding a clean tailing after comparatively coarse grinding, and of further

grinding and floating the concentrate should be encouraged because of the resulting economy in grinding" (Gaudin, 1932, in Barbery 1991).

- "Three important points in mill practice should now be apparent. First, it is not necessary to begin by grinding all the minerals to their fully liberated state in order to produce clean separation. Results can frequently be achieved in stages. First comes grinding, next separation into clean concentrate, clean tailing and "locked" particles. Finally the middling is unlocked by grinding and retreated. Second, the middling, or any fraction of it, can be held in a closed circuit if by so doing the work of separation is made more efficient. Third, a true middling always needs special treatment not provided for in the appliance, which has sent it out as a middling. After this special treatment it may be unsuitable for return to the sorting appliance. In the case just considered, if treatment depended on the mass of the particle, the ground fragments would probably be sent to a machine specially adapted to deal with their smaller size" (Pryor, 1965, in Barbery 1991).
- "The point will be repeatedly made that grade and recovery represent off; for a given sample of material, one can be obtained at the expense of the other. The concentration (...) is carried out in stages, described as roughing, scavenging, and cleaning. Roughing is the first stage, designed to remove the easily recovered liberated valuable as a rougher concentrate. The rougher tailings then pass to scavenging, where the emphasis is on recovery: the aim is to extract all the remaining valuable that is economically justifiable to recover (...). The scavenger concentrate is in principle recycled to recover the

valuable. Essentially it consists of middlings or unliberated particles, and unless further size reduction is applied to this concentrate, it is forced eventually to leave with the final tailings or the final concentrate. In the first instance, overall recovery is low, in the latter overall grade is low" (Kelly and Spottiswood, 1982, in Barbery 1991).

- "The correct degree of liberation is the key to success in mineral processing. The valuable mineral should be freed from the gangue, but only just freed. A process which overgrinds the ore is wasteful, since it needlessly consumes power and makes efficient recovery more difficult to attain. So important is it to avoid overgrinding, that (...) some ores are comminuted to a size coarser than their liberating size before initial concentration" (Wills, 1981, in Barbery 1991).
- "During the grinding of low-grade ore the bulk of the gangue is often liberated at a coarse size. In certain circumstances it may be economical to grind at a size much coarser than the optimum in order to produce in the subsequent concentration process a large middlings fraction and a tailings which can be discarded at a coarse grain size" (Wills, 1981, in Barbery 1991).

7.7. Introduction of a flotation circuit for rutile recovery at Chuquicamata

From the discussion on the recovery of copper sulphides and molybdenite from the Chuquicamata mine (Section one begins to realize where in the mining process the rutile recovery could be introduced. For instance, once the concentrate of copper sulphides and molybdenite are floated off, the remaining pulp is transported to the tailings pond. A rutile flotation circuit consisting of a series of ball mills and flotation

cells could be devised to intersect the tailings prior to it being discharged. The benefit of this method is that the raw ore has already undergone flotation for the copper-sulphides and molybdenite, therefore the absence of these minerals would potentially lead to easier flotation as there is less chance of cross-contamination with other minerals. The disadvantage of this method is that because rutile has not been studied in this milling process, it may be incorporated into the froth along with the copper-sulphides and molybdenite during the initial flotation process. If this happens the rutile flotation circuit will either have to be placed before the molybdenite circuit, before the copper-sulphide circuit, or after both have been extracted. This position will have to be further investigated, as there may be critical conflicts between the reagents used in each circumstance.

References

Anderson, C.A., Scholtz, E.A., and Strobell, J.D., Jr., 1955, Geology and ore deposits of the Bagdad area, Yavapai County, Arizona. United States Geological Survey Professional Paper 278, 103p.

Ballard, J.R., Palin, M.J., Williams, I.S., and Campbell, I.H., 2001, two ages of porphyry intrusion resolved for the super-giant Chuquicamata copper deposit of northern Chile by ELA-ICP-MS and SHRIMP. Geology, vol. 29, p. 383-386.

Barbery, G., 1991, Mineral liberation, 351 pp. Les Editions GB, Quebec, Canada.

Barnes, H.L., (ed), 1979, Geochemistry of hydrothermal ore deposits, John Wiley & Sons, Inc., Toronto, Ontario

Bertini, V., Pocci, M., Marabini, A.M., Barbaro, M., De Munno, A., and Picci, N., 1991, 3,4-(methylenedioxy)benzyl acrylate/acrylic acid copolymers as selective pH-controlled flocculants for finely divided titanium minerals. Colloids and Surfaces, vol. 60, p. 413-421.

Bish, D.L., and Reynolds Jr., R.C., 1989, Sample preparation for X-ray diffraction, Chapter 4. In: Modern powder diffraction, Ribbe, P.H. (ed), The mineralogical society of America, Washington, D.C.

Brooks, R.R., 1972 Geobotany and biogeochemistry in mineral exploration. Harper and Row Inc. New York

Bulatovic, S., and Wyslouzil, D.M., 1999, Process development for treatment of complex perovskite, ilmenite and rutile ores. Minerals Engineering, vol. 12, p. 1407-1417.

Carson, D.J.T., and Jambor, J.L., 1974, Mineralogy, zonal relationships and economic significance of hydrothermal alteration at porphyry copper deposits, Babine Lake area, British Columbia: CIM Bulletin, February, p. 110-133.

Clark, A.H., Archibald, D.A., Lee, A.W., Farrar, E., and Hodgson, C.J., 1998, Laser probe $^{40}Ar/^{39}Ar$ ages of early- and late- stage alteration assemblages, Rosario porphyry copper-molybdenum deposit, Collahuasi district, I Region, Chile. Economic geology, vol. 93, p. 326-337.

Craig, J.R., and Vaughan, D.J., 1994, Ore microscopy and ore petrography, John Wiley & Sons, Inc, Toronto.

Cuadra, P.C., Rojas, G.S., 2001, Oxide mineralization at the Radomiro Tomic porphyry copper deposit, northern Chile. Economic Geology, vol. 96, p. 387-400.

Cui, L., and Liu, J., 1986, Studies on the flotation separation of rutile from garnet (In Chinese). Chemical Mining Technology, vol. 5, p. 32-33.

Czamanzke, G.K., Force, E.R., and Moore, W.J., 1981, Some geologic and potential resource aspects of rutile in porphyry copper deposits: Economic Geology, v.70, p. 2240-2256.

Deer, W.A., Howie, R.A., and Zussman, J., 1992. An introduction to the rock-forming minerals, 2nd edition. John Wiley & Sons, Inc. New York 696p.

Dymek, R.F., 1983. Titanium, aluminum and interlayer cation substitutions in biotite from high-grade gneisses, West Greenland: American Mineralogist, v68, p. 880-899.

Force, E.R., 1991, Geology of titanium-mineral deposits, 112 pp. The geological society of America, Inc., Boulder, Colorado, U.S.A.

Force, E. R., Djaswadi, Sukirno, and Van Leeuwen, Theo, 1984, Exploration for porphyry metal deposits based on rutile distribution – a test in Sumatera: U.S. Geological Survey Bulletin 1558-A, p. A1-A9.

Force, E.R., 1976A, Titanium contents and titanium partitioning in rocks: U.S. Geological Survey Professional Paper 959-A

Force, E.R., 1976F, Titanium minerals in deposits of other minerals: U.S. Geological Survey Professional Paper 959-F

Gambogi, J., 1999, Titanium: U.S. Geological Survey Minerals Yearbook, p. 79.1-79.6.

Gaudin, A.M., 1932, Flotation, p. 120-155, McGraw Hill, New York, U.S.A.

Graves, M.C., and Zentilli, M. 1994, Trace element study of heavy mineral concentrates from Chuquicamata, Mansa Mina, and Radomiro Tomic deposits (appendix 9.1). CIMM Reports Selected Extracts: Chuquicamata Division, CODELCO.

Guilbert, J.M., and Park, C.F., Jr. 1986, The geology of ore deposits. W.H. Freeman and Company, New York

Hedenquist, J. W., and Lowenstern, J. B., 1994, The role of magmas in the formation of hydrothermal ore deposits. Nature, vol. 370, p.519-527.

Hibberd, J., and Smith, D., 1999, Nursing management in Canada, 2nd edition, W.B. Saunders Canada, Philadelphia.

Hummel, R.C., 2000. Titanium, Cambridge Scientific Abstracts, Retrieved October, 2001 from: http://www.csa.com/hottopics/titanium/overview.html

Kelly, E.G., and Spottiswood, D.J., 1982, Principles of mineral processing, Wiley, New York, U.S.A.

Kirkham, R.V., and Sinclair, W.D., 1996, Porphyry copper, gold, molybdenum, tungsten, tin, silver. In: Geology of Canadian mineral deposit types, Eckstrand, O.R., Sinclair, W.D., and Thorpe, R.I., Geological Survey of Canada, geology of Canada, no. 8, p. 421-446.

Lehmann, B., Dietrich, A., and Wallianos, A., 2000, From rocks to ore: International Journal of Earth Science, v.89, p. 284-294.

Lindsay, D.D., Zentilli, M., and Rojas, J., 1995. Evolution of an active ductile to brittle shear system controlling mineralization at the Chuquicamata porphyry copper deposit, northern Chile. International Geology Reviews, v.37, p. 945-958

Lindsay, D.D., 1998, Structural control and anisotropy of mineralization within the Chuquicamata porphyry copper deposit, northern Chile. Unpublished Ph.D. thesis, Dalhousie University, Halifax, NS, 381p.

Liu, Q., and Peng, Y., 1999, The development of a composite collector for the flotation of rutile. Minerals Engineering, vol. 12, p. 1419-1430.

Llewellyn, T.O., and Sullivan, G.V., 1980, Recovery of rutile from a porphyry copper tailings sample. United States Bureau of Mines Report of Investigations No. 8462, 21pp.

Lowell, D. J., and Guilbert, J. M., 1970, Lateral and vertical alteration-mineralization zoning in porphyry ore deposits: Economic Geology, v. 65, p. 373-407.

Ma, G., 1989, Studies on the flotation of fine and ultrafine metamorphic rutile ore (In Chinese). Non-ferrous Metals, vol. 3, p. 12-13.

Maksaev, V., and Zentilli, M., 1988, Marco metalogenico regional de los megadepositos de tipo porfido cuprifero del norte grande de Chile. V Congreso Geologico Chileno, Tomo I, p. B181-B212.

Marabini, A.M, and Rinelli, G., 1983, Development of a specific reagent for rutile flotation. Transactions of AIME, vol. 274, p. 1822-1827.

McQuillian, A.D., and McQuillian, M.K., 1956, Metallurgy of the rarer metals-4: Titanium, Butterworths Scientific Publications Ltd., Toronto, Canada

National Materials Advisory Board, 1983, Titanium—Past, present, and future: Washington, DC, National Academy Press, 209 p.

Ossandón, G.C., Fréraut, R.C., Lewis, G.B., Lindsay, D.D., and Zentilli, M., 2001, Geology of the Chuquicamata mine: a progress report: Economic Geology, v. 96, p. 249-270

Pemberton, G.B., 1997, Dating of alteration at the Radomiro Tomic porphyry copper deposit, northern Chile by the high precision $^{40}Ar/^{39}Ar$ method. Unpublished BSc thesis, Dalhousie University, Halifax, NS, 103p.

Petruk, W., 1990, Determining mineralogical characteristics by image analysis, Chapter 14. In: Advanced microscopic studies of ore minerals, Jambor, J.L., and Vaughn, D.J. (eds), Mineralogical association of Canada, Ottawa, Ontario

Pryor, E.J., 1965, Mineral processing, Elsevier, Amsterdam

Purcell, G., and Sun, S.C., 1963, Significance of double bonds in fatty acid flotation. Transactions of AIME, vol. 254, p. 13-16.

Ramdohr, P., 1980, The ore minerals and their intergrowths,. Vol. 2, (ed) Pergamon Press, Toronto, Ontario

Ranney, M.W., 1980, Flotation agents and processes, 372 pp, Noyes Data Corporation, Park Ridge, New Jersey, U.S.A.

Reed, S.J.B., 1995, Electron probe microanalysis, Chapter 2. In: Microprobe techniques in the earth sciences, Potts, P.J., Bowles, J.F.W., Reed, S.B.J., and Cave, M.R. (eds), Chapman and Hall, New York.

Reynolds, P., Ravenhurst, C., Zentilli, M., and Lindsay, D., 1998, High-precision $^{40}Ar/^{39}Ar$ dating of two consecutive hydrothermal events in the Chuquicamata porphyry copper system, Chile. Chemical Geology, vol. 148, p. 45-60.

Richards, J.P., Boyce, A.J., and Pringle, M.S., 2001, Geologic evolution of the Escondida area, northern Chile: a model for spatial and temporal localization of porphyry Cu mineralization: Economic Geology, v.96, p. 271-305.

Rose, E R, 1969. Geology of Titanium and Titaniferous Deposits of Canada, *Economic Geology Report No 25*, 177 pp (Department of Mines and Resources, Canada: Ottawa).

Sillitoe, R.H., Marquardt, J.C., Ramirez, F., Becerra, H., and Gómez, M., 1996, Geology of the concealed MM porphyry copper deposit, Chuquicamata district, northern Chile. In: Andean copper deposits: new discoveries, mineralization, styles and metallogeny. Camus, F., Sillitoe, R.H., and Petersen, R., (eds.), Society of Economic Geologists Special Publication No. 5, p. 59-70.

Spectra Research Corporation, 5835 Coopers Avenue, Mississauga, Ontario.

Turismo Y comunicaciones S.A., 1992, Chile: A remote corner on the earth. Empresas Cochrane, Chile 712p.

Udubasa, G., 1982, Rutile of postmagmatic mineral formation. p. 784-793. In: Ore genesis: The state of the art, Amstutz, G.C., El Goresy, A., Frenzel, G., Kluth, C., Moh, G., Wauschkuhn, A., Zimmermann, R.A. (eds), Springer-Verlag, New York.

Van Baalen, M.R., 1993, Titanium mobility in metamorphic systems: a review. Chemical Geology, v.110, p. 233-249.

Williams, S. A., and Cesbron, F. P., 1977, Rutile and apatite: useful prospecting guides for porphyry copper deposits: Mineralogical Magizine, v.41, p. 288-292.

Wills, B.A., 1981, Mineral processing technology, Pergamon Press, London.

Wills, B.A., 1997, Mineral processing technology, 486 pp. Butterworth-Heinemann, Boston, Massachusetts, U.S.A.

Winter, J.D., 1999, Igneous and metamorphic petrology. Prentice Hall

Major Titanium-Bearing Minerals, their Compositions, Physical Properties, Nature of Occurrence, and Abundance

Mineral	Chemical Composition	Physical Properties	Nature of Occurrence	Abundance
Rutile	TiO_2; Ti 60%, Fe impurity as much as 10%	Hard, reddish brown crystals, tetragonal	In ilmenite and sometimes biotite, in veins, as accessory grains, and in placer deposits	Most common form of TiO_2
	High Temperature Polymorph			
Ilmeno-rutile	Ferriferous rutile with Nb			
strüverite	Ferriferous rutile with Ta			
Brookite	TiO_2 ($Fe_2O_3 \cdot TiO_2$); Ti 60%	Like rutile, but Orthorhombic	Hydrothermal veins, accessory minerals, often secondary mineral with sphene, chlorite, etc., and placer deposits	Rare
Anatase (octahedrite)	TiO_2; Ti 60% Low Temperature Polymorph	Like rutile but of secondary origin, tetragonal	In altered titanium-bearing Rocks, and veins and druses in granite pegmatites.	Rare
Arizonite	$Fe_2O_3 \cdot 3TiO_2$; Ti 36%	Hard, dark steel grey, brown streaks	With gadolinite in pegmatite, Mohave County, Arizona	Rare
Ilmenite	$FeTiO_3$; Ti 31.6%, Fe 36.8%;	Hard, black, weakly magnetic, will cling to magnet when powdered, rhombohedral	In massive vein-dykes and disseminations in anorthosite and gabbroic anorthosite; also in placers	Abundant
Ferrian ilmenite	6-13% Fe_2O_3 in solid solution			
Magneto-ilmenite	Intergrowths of magnetite			
Hemo-magnetite	Ferrian ilmenite with inter-growths of titanhematite			
Geikielite, högbomite, pyrophanite, senaite, silicoilmenite?	(Mg,Fe) TiO_3, with Al, Fe, Mn, Pb, Si			

Perovskite Niobian perovskite (Oka) and other multiple oxide minerals (brannerite, davidite, etc.)	$CaTiO_3$; Ti 35.3% 25-56.2% TiO_2; Ti 15-30%	Hard, cubic crystals, perfect cleavage, isometric	In chlorite, talc, and serpentine rocks, and in basic and alkaline rocks	Not Abundant
Titanite (Sphene)	$CaTiSiO_5$; Ti 24.5%	Hard, brownish wedge-shaped crystals, good cleavage, monoclinic	Common accessory mineral, also in pegmatite, alkaline rocks, and contact deposits	Not Abundant
Ulvöspinel Mogensite	Fe_2TiO_4 ($2FeO \cdot TiO_2$); Fe 44%, Ti 16.8% Intergrowth of ulvöspinel in magnetite	Hard, dark, magnetic, Isometric	Intergrown with titanomagnetite, forms solid-solution series	Rare
Pseudobrookite	Fe_2TiO_5; Ti 12%	Dark brown tabular crystals, streak ochre yellow	In lavas of Europe, as at Vesuvius, and in artificial Melts	Rare
Titanomagnetite Ilmeno-magnetite	($FeTi_3O_4$); Fe 40-71%, Ti 1-15%; Titanomagnetite with inter growths of ilmenite or ferrian ilmenite	Hard, dark, strongly magnetic, isometric	Forms solid-solution series	Abundant
Titanhematite Ilmeno-hematite	$(FeTi)_2O_3$; Ti 1-10%; titanhematite with inter-growths of ferrian ilmenite or hemo-ilmenite	Hard, dark, weakly magnetic, rhombohedral	Forms solid-solution series with ilmenite	Widespread but not abundant
Leucoxene Brown Creamy white	A mixture of rutile, hematite and pseudobrookite, etc. A mixture of sphene altered feldspar, etc.	Hard, dark films Soft, creamy films	Alteration products coating Ti-bearing ores and sands Alteration products coating Ti-bearing rocks	Widespread but not abundant

Data taken from (Rose, 1969) and (Deer, Howie, and Zussman, 1992)

Appendix 2A

Geochemical Analysis of
Radomiro Tomic Mine Concentrate Samples

Sample #	Cu (%)	Fe (%)	Mo (%)	As (%)	Pb (%)	Zn (%)	Sb (%)	Ti (%)
4136-39	6.16	36.8	2.95	<0.005	0.01	0.008	<0.005	0.7
4136-40	35.8	18.8	0.1	<0.005	0.021	0.003	<0.005	<0.1
4136-41	29.4	24	0.19	<0.005	0.002	0.006	<0.005	1.3
4136-42	10.2	33	0.4	<0.005	0.006	0.016	<0.005	0.6
4136-43	1.24	42.1	0.072	<0.005	0.002	0.001	<0.005	<0.1
4136-44	39.87	10.3	3.67	<0.005	0.18	0.053	<0.005	1.9
4136-45	6.56	38	1.73	<0.005	0.009	0.004	<0.005	0.2
4136-46	3.45	38.9	2.26	<0.005	0.005	0.003	<0.005	0.7
4136-47	0.65	43.3	0.02	<0.005	0.026	0.001	<0.005	<0.1
4136-48	34.65	16.9	0.96	<0.005	0.028	0.073	<0.005	4.1
4136-49	23.67	17.2	0.39	0.18	0.01	0.067	0.034	2.1
4136-50	2.1	42.4	0.016	<0.005	0.002	0.002	<0.005	<0.1
4136-51	24.36	13.2	9.63	<0.005	0.019	0.098	<0.005	2.2
4136-52	23.8	26	1.04	<0.005	0.004	0.01	<0.005	1.2
4136-53	2.8	42.8	0.54	<0.005	0.007	0.001	<0.005	0.1
4136-55	4.47	40.3	1.16	<0.005	0.007	0.003	<0.005	0.1
4136-56	14.9	34.3	0.068	0.012	0.004	0.01	<0.005	0.9
4136-57	3.49	42.2	0.86	<0.005	0.004	0.017	<0.005	1.1
4136-61	10.2	39.9	0.43	<0.005	0.004	0.009	<0.005	0.6
4136-62	41.3	12.7	0.7	<0.005	0.014	0.06	<0.005	3.8
4136-63	21.08	32.4	0.51	<0.005	0.009	0.011	<0.005	1.9
4136-64	46.75	8.1	0.6	<0.005	0.018	0.22	<0.005	2.9
4136-65	6.51	39.7	1.55	<0.005	0.005	0.005	<0.005	0.4
4136-66	47.88	10.2	0.23	<0.005	0.018	0.46	<0.005	2.2
4136-67	12	39.2	0.94	<0.005	0.007	0.01	<0.005	0.4
4136-68	39.92	14	5.45	<0.005	0.38	0.38	<0.005	2
4136-69	21.22	30.2	1.68	<0.005	0.009	0.021	<0.005	1.2

Appendix 2B

Geochemical Analysis of Chuquicamata
Mine Concentrate Samples

Sample #	Cu (%)	Fe (%)	Mo (%)	As (%)	Pb (%)	Zn (%)	Sb (%)	Ti (%)
4136-19	20.6	22.7	0.048	0.044	0.18	1.56	0.005	0.9
4136-20	20.7	21.4	0.11	0.087	0.087	3.35	<0.005	0.9
4136-21	21	17.6	0.62	0.017	0.069	1.33	<0.005	0.7
4136-22	33.1	17.5	0.51	0.077	0.092	0.64	0.006	1.1
4136-23	29.4	20	0.25	0.085	0.12	1.1	0.005	1.3
4136-24	13.3	26.2	0.049	0.026	0.052	0.43	<0.005	1.8
4136-25	8.5	35.4	0.069	0.006	0.005	0.31	<0.005	2
4136-26	6.62	38.1	0.16	<0.005	0.006	0.15	<0.005	1.5
4136-27	21.7	27.3	0.16	0.28	0.089	2.57	0.012	0.5
4136-28	12.9	25.4	0.49	0.45	0.17	2.59	0.012	0.8
4136-29	18.4	29.1	0.16	0.042	0.015	0.45	<0.005	1.2
4136-30	27.9	19.4	0.56	0.007	0.04	0.31	<0.005	0.9
4136-31	47.5	12.6	0.13	0.054	0.012	0.066	<0.005	1
4136-32	20.4	23.8	0.2	0.15	0.013	0.59	<0.005	1.6
4136-33	15.4	27.8	0.089	<0.005	0.003	0.42	<0.005	1.3
4136-34	9.89	31.2	0.15	0.06	0.005	0.053	0.005	1.4
4136-35	3.14	32.4	<0.004	0.089	0.012	0.13	0.006	1.8
4136-36	3.75	34.5	0.028	0.02	0.098	0.1	<0.005	2.1
4136-37	13.8	29.9	0.011	<0.005	0.008	0.18	<0.005	1.4
4136-38	10.8	33	0.07	0.038	0.003	0.093	<0.005	1.2
4136-138	34.02	20.9	0.016	0.018	0.005	0.037	<0.005	1.4
4136-139	31.31	22.7	0.013	0.011	0.006	0.031	<0.005	1.7
4136-140	34.22	25	0.036	<0.005	0.003	0.023	<0.005	1.1
4136-141	21.84	26.9	0.022	<0.005	0.006	0.19	<0.005	2.1
4136-142	8.29	40.7	0.22	0.15	0.06	0.86	<0.005	0.1
4136-143	32.22	18.7	0.41	4.49	0.049	0.42	0.14	0.3
4136-144	13	36.8	0.24	0.4	0.054	0.36	0.021	0.2
4136-145	37.43	18.7	0.88	0.026	0.006	0.07	<0.005	1
4136-146	35.61	16.7	6.1	0.009	0.021	0.046	<0.005	0.9
4136-147	25.67	25.4	0.083	0.017	0.003	0.083	0.006	1
4136-148	20.98	28.8	0.052	<0.005	0.004	0.071	<0.005	1
4136-149	24.23	25.9	0.25	<0.005	0.005	0.054	<0.005	2
4136-150	13.8	37.4	0.047	0.022	<0.002	0.18	<0.005	0.7
4136-151	10	39.4	0.091	0.016	0.003	0.23	<0.005	0.3
4136-152	10.5	25.9	0.034	0.011	0.34	0.83	<0.005	1
4136-153	3.37	41.9	0.16	0.013	0.006	0.38	<0.005	1
4136-154	2.95	38.9	0.029	0.008	0.006	0.29	<0.005	0.9
4136-155ç	5.03	36.7	0.14	<0.005	0.004	0.92	<0.005	1.6
4136-156	6.27	29.5	0.16	0.006	0.005	1.36	<0.005	1.8

4136-157	2.94	36.4	0.077	<0.005	0.005	0.56	<0.005	2.2
4136-158	2.09	35.4	0.031	0.009	0.007	0.4	<0.005	1.9
4136-159	2.4	37.2	0.011	<0.005	0.004	0.35	<0.005	1.9
4136-160	2.39	37.5	<0.004	<0.005	0.005	0.15	<0.005	1.4
4136-161	5.43	35.4	0.007	<0.005	0.01	0.42	<0.005	1.3
4136-162ς	1.76	40.8	0.01	<0.005	0.005	0.24	<0.005	2.3
4136-163	1.14	43	0.005	<0.005	0.005	0.12	<0.005	1.9
4136-164	1.18	43.2	0.005	0.007	0.003	0.084	<0.005	0.6
4136-165	1.62	41.4	<0.004	0.023	0.005	0.12	<0.005	1.1
4136-166	3.55	39	0.005	<0.005	0.005	0.1	<0.005	0.8
4136-167	2.48	43.2	0.01	<0.005	0.003	0.047	<0.005	0.8
4136-168	4.07	39.5	0.004	0.018	0.007	0.097	<0.005	0.9
4136-169	2.69	39	0.005	<0.005	0.006	0.089	<0.005	2.2
4136-170	5.11	40	<0.004	0.035	0.004	0.039	<0.005	0.9
4136-171	6.52	36	0.019	0.011	0.005	0.069	<0.005	1.7
4136-172	21.07	27.4	0.11	0.01	0.007	0.12	<0.005	1.9
4136-173	13.4	34.7	0.011	0.008	0.003	0.056	<0.005	2
4136-174	10.8	33.9	0.039	0.021	0.003	0.069	<0.005	1.1
4136-175	6.47	34.3	0.008	0.04	0.004	0.039	<0.005	1
4136-176	4.73	38.5	<0.004	0.093	0.005	0.052	<0.005	0.8

Appendix 2C

Geochemical Analysis of
Mansa Mina Mine Concentrate Samples

Sample #	Cu (%)	Fe (%)	Mo (%)	As (%)	Pb (%)	Zn (%)	Sb (%)	Ti (%)
4136-1	7.25	35.6	0.027	1.8	0.046	0.41	0.053	0.3
4136-2	9.85	31.8	0.005	3.05	0.34	1.07	0.095	<0.1
4136-3	7.37	36.7	0.005	0.37	0.13	2.37	0.02	0.3
4136-4	12.3	32	0.006	2.58	0.033	0.26	0.17	0.3
4136-5	5.12	37.7	0.006	0.85	0.039	0.26	0.059	0.5
4136-6	8.7	34	0.009	0.97	0.05	0.4	0.12	0.6
4136-7	6.25	35.7	0.011	0.7	0.2	0.53	0.14	0.7
4136-8	16.3	32	0.044	0.12	0.12	0.23	<0.005	0.6
4136-9	2.85	32.9	0.24	0.018	0.33	5.04	<0.005	0.9
4136-10	19	30.7	0.026	0.43	0.098	0.55	<0.005	0.4
4136-11	16.5	27.2	0.3	0.98	0.44	1.93	0.021	1
4136-12	3.68	29.6	0.13	0.006	0.25	8.15	<0.005	0.7
4136-72	11.7	32.1	<0.004	3.04	0.022	0.17	0.069	0.2
4136-73	8.26	36.9	0.019	0.45	0.028	0.044	0.023	0.4
4136-74	15.8	31.6	0.011	0.5	0.053	0.087	0.069	0.2
4136-75	12.1	30.2	<0.004	2.98	0.076	0.63	0.051	0.2
4136-76	9.52	35.7	0.019	0.56	0.054	0.67	0.009	0.3
4136-77	20.9	27.7	0.035	0.29	0.23	10.27	<0.005	0.2
4136-78	14.1	28.2	0.098	0.27	0.34	5.74	<0.005	0.5
4136-79	17.1	28.1	0.024	0.15	0.18	3.69	0.016	0.3
4136-80	16.8	31.3	0.009	0.74	0.11	0.62	0.005	0.3
4136-81	9.84	32.4	0.023	0.041	0.13	5.8	<0.005	0.3
4136-82	11.9	32.2	<0.004	0.45	0.054	0.039	0.025	0.4
4136-83	31.8	16.7	<0.004	4.69	0.016	0.079	0.35	0.4
4136-84	30.3	22.3	<0.004	0.87	0.024	0.43	0.08	0.4
4136-85	13.3	33.7	0.013	1.23	0.022	0.19	0.051	0.1
4136-86	9.6	35.9	0.012	0.51	0.06	0.28	0.024	0.2
4136-87	20.8	24.8	0.038	2.43	0.058	0.46	0.18	0.2
4136-88	39.6	16.7	0.086	1.27	0.034	0.76	0.15	0.1
4136-89	23.9	24.8	0.054	0.61	0.032	0.5	0.24	0.1
4136-90	30.4	18.3	0.016	4.29	0.027	0.24	0.54	0.1
4136-91	37.8	18.1	0.007	1.31	0.057	0.24	0.22	0.1
4136-92	15.6	16.2	<0.004	1.12	0.067	0.63	0.53	0.6
4136-93	25.7	11.5	<0.004	2.06	0.046	0.64	0.49	0.3
4136-94	26.1	14.4	<0.004	3.18	0.15	3	0.53	0.3
4136-95	26	18.8	0.004	3.03	0.041	0.56	0.28	0.4
4136-96	22.1	30.3	<0.004	0.032	0.015	0.017	0.012	0.1
4136-97	13.2	32.4	0.078	0.006	0.03	0.016	0.01	0.5
4136-98	16.8	26.6	0.096	0.1	0.072	0.18	0.28	0.6

4136-99	9.94	26.6	0.015	0.014	0.075	0.075	<0.005	1
4136-100	10.4	31.8	1.03	<0.005	0.024	0.12	<0.005	0.5
4136-101	11.6	26.4	0.44	0.032	0.018	0.046	<0.005	0.8
4136-102	16.2	22.1	0.011	1.56	0.055	0.024	0.049	0.3
4136-103	26.7	30.8	0.005	0.34	0.065	0.11	0.012	0.4
4136-104	22.8	28.4	0.005	0.079	0.076	0.14	0.007	0.3
4136-105	6.83	39	0.005	0.028	0.043	0.058	<0.005	0.2
4136-106	14.8	33.4	0.004	0.54	0.016	0.22	0.041	0.2
4136-107	29.4	22.8	<0.004	0.69	0.02	0.01	0.098	0.3
4136-108	13.3	31.9	0.004	1.47	0.058	0.048	0.055	0.2
4136-109	19.7	29.9	0.004	1.25	0.063	0.18	0.049	0.2
4136-110	25.1	24.6	0.008	0.88	0.088	0.99	0.12	0.5
4136-111	23.4	25.1	0.017	0.17	0.073	0.16	0.25	0.2
4136-112	10.8	35.2	0.005	0.72	0.029	0.074	0.035	0.3
4136-113	29.7	21.4	0.014	2.66	0.05	0.27	0.44	0.2
4136-114	31.3	19.4	0.012	2.89	0.1	0.31	0.29	0.1
4136-115	22.9	22.9	0.046	2.04	0.06	0.29	0.2	0.2
4136-116	47.2	3.5	<0.004	11.2	0.027	0.45	1.17	<0.1
4136-117	48.2	3.9	<0.004	10.1	0.029	0.15	1.04	<0.1
4136-118	26.3	16.3	<0.004	5.01	0.06	0.11	0.64	0.3
4136-119	16.4	22.4	0.006	2.96	0.04	0.11	0.37	0.4
4136-120	18.7	26.4	<0.004	5.24	0.013	0.018	0.38	0.5
4136-121	14.5	29.3	<0.004	3.07	0.014	0.071	0.31	0.2
4136-122	35.9	20.9	<0.004	1.19	0.01	0.051	0.18	0.3
4136-123	18.8	27.4	<0.004	2.15	0.012	0.031	0.16	0.3
4136-124	27.3	26	<0.004	1.58	0.011	0.19	0.078	0.2
4136-125	23.2	29.1	<0.004	0.81	0.012	0.065	0.032	0.3
4136-126	33.1	20.5	0.006	3.19	0.018	0.12	0.22	0.3
4136-127	28.5	24.8	0.008	1.84	0.027	0.13	0.15	0.2
4136-128	18.2	26.5	0.018	2.69	0.11	0.4	0.15	0.2
4136-129	26.8	23.8	<0.004	2.09	0.026	0.14	0.11	0.3
4136-130	37.4	13.2	<0.004	4.28	0.028	0.16	0.32	0.1
4136-131	14.4	29.6	<0.004	2.28	0.018	0.035	0.075	0.3
4136-132	12.2	27.4	<0.004	2.99	0.021	0.02	0.098	0.4
4136-133	18.3	30.1	<0.004	0.83	0.04	0.13	0.054	0.5
4136-134	31.6	17.8	0.004	1.4	0.05	0.044	0.07	0.4
4136-135	34.2	19.9	0.004	1.98	0.016	0.036	0.14	0.3
4136-136	22.8	28.2	0.004	0.63	0.046	0.081	0.035	0.4
4136-137	16.2	29.9	0.006	0.2	0.039	0.1	0.033	0.6

Appendix 3A

Radomiro Tomic Mine Mineralogical Data (Vol. %)

Sample #	CP	CC	DI	CV	BN	PY	MO	SPH	GA	RU	HE	GN
4136-39	8.72	0.48		0.06	5.32	74.16	6.09	0.1	0.27	0.35		4.08
4136-40	6.24	0.2	0.07	50.24		38.92	0.06					4.27
4136-41	58.68	0.68		1.24	12.23	5.37	0.7			2.7		18.3
4136-42	21.3	0.53	0.15		6.72	47.31	0.63	0.43		1.34		16.39
4136-43		1.1		0.53		89.48		0.29	0.08	0.18		3.1
4136-44	3.45	16.17			20.05	14.68	5.97				6.21	33.46
4136-45	10.51	0.1		4.19		72.61	1.93			0.32		10.23
4136-46	5.15	0.42	0.36	0.05	2.48	77.26	4.97	0.04		0.67		8.51
4136-47		0.34	0.08	0.34	0.08	95.74				0.06		3.36
4136-48	11.67	3.43			43.98	10.37	0.92			2.08	4.84	22.71
4136-53	3.02		0.08	2.78	0.03	84.89	1.12			0.34		7.74
4136-55	3.93			4.6		84.1	1.95			0.15		5.27
4136-56	40.57			0.11	0.31	46.45		0.1		0.72		11.46
4136-57	3.87	0.64		0.39	2.14	83.84	5.78			0.35	0.73	2.26
4136-61	19.49	0.94		1.91	2.36	69.57	0.48			0.16	0.16	4.92
4136-62	8.17	3.02		0.34	56.65	6.47	0.64			4.09	0.64	19.98
4136-63	31.13	1.09		0.41	14.46	42.08	0.54	0.1		0.21		9.99
4136-64	2.27	17.29		1.48	49.16	1.09	1.71			1.59	0.61	24.8
4136-65	5.43	1.91		1.38	3.48	77.22	1.79	0.18				8.61
4136-66	3.17	1.65		3.55	67.2	3.05	1.66			2.9	0.5	16.31
4136-67	33.4	0.07		0.61		58.74	1.35	0.29				5.55
4136-68	2.53	3.29			57.5	8.08	8.5		0.38		1.4	18.32
4136-69	26.23	3.44		0.47	17.46	39.94	2.83			0.22	0.93	8.48

Mineral Abbreviations

CP	Chalcopyrite ($CuFeS_2$)
CC	Chalcocite (Cu_2S)
CV	Covellite (CuS)
BN	Bornite (Cu_5FeS_4)
EN	Enargite (Cu_3AsS_4)
PY	Pyrite (FeS_2)
MO	Molybdenite (MoS)
SPH	Sphalerite (ZnS)
RU	Rutile (TiO_2)
GA	Gangue
HE	Hematite (Fe_2O_3)
GN	Galena (PbS)
DI	Digenite (Cu_9S_5)
CU.OX	Copper Oxide (Supergene)
MG	Magnetite (Fe_3O_4)

Appendix 3B

Chuquicamata Mine Mineralogical Data (Vol. %)

Sample #	CP	CC	DI	CV	BN	EN	PY	MO	SPH	GA	RU	HE	GN	MG
4136-19	1.39	10.16	0.4	16.27	0.18	0.12	56.95	0.12	3.25	0.07	0.29	0.05	10.75	
4136-20	4.06	17.72	1.33	3.75	0.53		53.8	0.05	6.24		0.54		11.98	
4136-21	22.29	13.21	10.03	3.89	14.76		25.72	1.45	2.04		0.2		6.41	
4136-22	22.54	6.31	1.39	8.89	24.84	0.12	22.1	1.28	0.41	0.07	1.18	0.24	10.62	
4136-23	32.78	2.8	5.72	7.22	10.94	0.14	20.71	0.44	3.06	TR	1.8	2.07	12.32	
4136-24	38.08		0.19	0.25	3.18	0.29	18.59	0.15	1.07		2.34	10.52	25.34	
4136-25	30.68	1.11	TR	TR		TR	19.62	0.08			2.95	25.03	20.52	
4136-26	21.08	0.61	TR	TR	TR		18.02	0.5			1.74	35.66	22.39	
4136-27	4.16	22.46	4.25	1.46	0.16	1.57	52.63	1.82	3.51		0.73	0.63	6.62	
4136-28	9.02	0.57	0.46	12.82	2.04	2.72	54.02	0.8	3.67	0.37	1.68	0.21	11.51	
4136-29	59.61	0.15		0.12	0.23	0.04	19.06	0.51	0.5		1.93	5.72	11.75	
4136-30	16.89	6.78	12.44	3.41	10.45		35.44	0.37	0.53		1.22	0.07	12.39	
4136-31	21.92	2.99	2.9	1.08	61.15	0.14	1.37	0.11	0.03		1.65	0.37	6.28	
4136-32	64.83	1.64	0.07	TR	0.29		10.87	0.86	1.15	TR	3.19	0.9	16.03	
4136-33	46.76	0.2	0.07	TR	0.06		32.9	0.17	0.57		2.04	0.55	16.68	
4136-34	36.71	TR		TR	0.04	0.11	17.95	0.68			1.22	19.74	23.53	
4136-35	12.62				0.35	0.3	24.35				0.58	24.25	37.55	
4136-36	9.77	0.05			0.13		21.44	0.04	0.35		0.7	44.58	22.94	
4136-37	34.79	0.39	0.5	1.3	2.69		37.2		0.12		1.48	1.93	19.54	
4136-38	34.87	0.22	0.09	0.15	TR	0.24	38.99	0.04			1.72	4.47	19.2	
4136-138	58.85	0.57	0.99	6.16	13.16		1.36			0.06	1.32		17.49	
4136-139	66.4	1.57		3.19	7.82		1.24	0.12					18.39	
4136-140	72.41	2.76		5.43	5.33		1.24						12.48	
4136-141	45.47	0.53	0.53	0.48	7.76		11.62	0.05			1.4		29.15	
4136-142	2.3	5.46	1.56	2.13		0.56	83.99	0.3	0.29	0.08	0.18		3.1	
4136-143	11.21	11.75	1.01	4.09	4.16	26.53	30.2	0.74	0.33		0.31		9.66	
4136-144	6.01	4.17	2.02	2.52	5.6	1.56	74.26	0.35	0.17		0.36		2.96	
4136-145	40.86	1.97	3.82	2.93	26.38	0.05	6.64	1.78	0.09		1.18		14.2	
4136-146	36.49	4	4.51	0.6	24.94		5.71	7.87	0.08		1.89		13.91	
4136-147	66.29	1.09		2.45	0.28		6				1.66		22.04	
4136-148	57.2			1.5	0.24		19.19	0.16			1.12		20.41	
4136-149	64.1	1.14	0.07	1.27	0.32		2.63	0.35	0.05		2.74		25.85	
4136-150	30.71		0.63	2.39	0.11		62.72	0.05			0.7		2.69	
4136-151	21.35	0.06	1.46	4.35	0.75		69.2	0.19			0.5		2.15	
4136-152	15.29	2.9	0.66	3.53	0.04		43.49		0.2		1.36		32.26	
4136-153	1.55	2.78	0.17	0.54		0.13	70.71	0.21	0.3		0.87	7.54	11.42	3.77
4136-154	2.43	1.75		0.94	0.09		69.48				0.43	8.32	15.68	0.89
4136-155	12.32	0.79		0.21			35.03	0.33	0.14		1.12	16.04	29.25	4.46
4136-156	14.37	1.34		0.13	0.21		25.83	0.33	0.17		0.29	6.77	36.88	13.69
4136-157	7.39	0.51					22.65	0.09	0.04		0.66	4.63	40.57	23.45
4136-158	5.11	0.33		0.26	0.05		40.8				0.88	9.59	36.21	6.78
4136-159	6.19	0.22		0.09			38.64		0.15		1.54	10.87	31.22	11.07
4136-160	6.28	0.24		0.05			43.2		0.09		0.81	10.61	32.67	6.05
4136-161	9.54	2.68					48.99				0.97	0.73	30.07	7.03
4136-162	4.68	0.2					26.11				1.34	2.89	36.71	28.07
4136-163	3.2			0.06			42.48	0.23			1.08	4.6	24.93	23.4
4136-164	2.69	0.32					82.24				0.52	1.4	8.8	4.03
4136-165	2.14	0.49	0.43	0.25			53.32				0.41	2.76	29.7	10.49
4136-166	8.28	0.49	0.07	0.28	0.06		74.27				0.87	0.82	12.95	1.9
4136-167	7.11						73.46				0.72	1.33	9.47	7.65
4136-168	9.93	0.15		0.35	0.46		66.38		0.05		1.02	2.06	18.22	1.4
4136-169	7.35	0.11		0.09			45.56				1.25	17.59	23.58	4.45
4136-170	8.04	1.74		1.15	0.35	0.08	69.66				0.52	2.31	15.21	0.79
4136-171	11.95	1.36		1.89			49.97		0.15		2.08	7.05	23.68	1.39
4136-172	52.49	2.11	1.05	0.43	0.13		14.73	0.12	0.32		2.16	4.05	21.23	1.17
4136-173	35.78	0.4	0.81	0.11			43.48				0.94	2.02	16.1	0.37
4136-174	23.57	2	0.52	0.57	0.46		49.99				0.9	1.53	20.45	
4136-175	16.58	0.07	0.07	0.39	0.43		53.71				0.3	0.94	25.73	1.5
4136-176	9.19	0.19	0.07	0.53	1.3		71.47				0.53	0.53	15.73	

Appendix 3C

Mansa Mina Mine Mineralogical Data (Vol. %)

Sample #	CP	CC	CV	BN	EN	PY	MO	SPH	GA	RU	HE	GN	DI	CU OX.
4136-72		1.47			11.23	79.46	0.06	0.15		0.11	0.2	5.78	TR	
4136-73		6.73	TR	TR	5.24	84.37	0.05			0.14		3.19	0.07	
4136-74	0.04	11.94		0.05	4.23	76.87						6.32	0.12	
4136-75	0.11	4.88	0.06	0.13	13.89	66.6		0.2				10.18		
4136-76	0.04	12		0.31	0.53	82.2		0.52		0.13		3.09	0.17	
4136-77	0.19	27.35	TR	0.28	1.4	62.23		1.38	0.07			7.1	TR	
4136-78	6.89	11.7	0.04	3.28	0.15	61.06	0.16	10.03	0.32	0.4		5.89		
4136-79	6.46	16.12		3.4		60.85	0.08	6.65	0.07	0.07		5.96		
4136-80	20.44	0.72	TR	9.63		59.57		0.43	TR	0.41		5.12	TR	
4136-81	23.61	0.11	0.04	4.1	0.04	59.33	TR	8.4	TR	0.48		3.68		
4136-82	0.04	10.63	TR	0.14	2.06	76.32				0.27		8.29		
4136-83	TR	18.41		0.45	34.51	40.2		0.08		0.21		5.51		
4136-84		32.33		0.06	5.37	55.83		0.34		0.35		5.17		
4136-85		9.78		0.05	5.37	80.32		0.16		0.08		3.66		
4136-86	0.05	9.62		0.11	1.26	85.12	0.05	0.04		0.32		3.42		
4136-87		15.99		0.2	11.74	64.32		0.04		0.08		6.67		
4136-88	0.04	44.15			7.4	41.57				0.18		4.74		
4136-89		26.13		0.39	5.66	61.79		0.04				5.46		
4136-90	0.04	20.5		0.1	29.93	44.35				0.08		4.99		
4136-91	0.06	40.76		1.95	9.29	43.39		0.03		0.06		4.4		
4136-92	TR	5.58	TR	0.11	20.6	44.81		0.29		0.31		27.72		
4136-93	TR	16.79		1.15	30.6	27.38		0.75	TR	0.11		23.04		
4136-94	TR	11.16	TR	0.18	39.96	33.64		4.08	TR	0.15		10.32		
4136-95		21.1		3.02	17.82	43.1		0.86		0.3	0.11	13.64		
4136-96	0.95	4.38		26.96	0.07	63.6		0.03		0.14		3.86		
4136-97	3.43	1.04		16.52	0.04	70.99	0.27			0.61		7.06		
4136-98	12.75	1.39		19.73	0.06	52.2	0.06	0.2		0.86	0.4	12.11		
4136-99	36.5	0.32	TR	0.4		37.48	0.05			1.87	0.06	23.31		
4136-100	34.93		0.05			42.74	2.86	0.49		0.7	2.76	14.8		
4136-101	50.32				0.06	26.67	0.05			1.02	6.69	14.91		
4136-102		11.79			11.36	72.72				0.25		3.46		
4136-103		30.92	0.04		2.16	59.66		0.04		0.51		6.63		
4136-104		26.76	0.22	0.12	0.47	65.87		0.24		0.35		5.99		
4136-105		8.71			0.07	87.18				0.07		3.91		
4136-106		15.73			3.05	75.05		0.35		0.31		5.5		
4136-107		32.44		1.3	3.41	53.99		0.15				8.71		
4136-108		9.47	0.09		8.4	74.87		0.08		0.24		6.76		
4136-109	0.04	18.49		0.21	6.06	69.23		0.49	TR	0.39		4.9		
4136-110	0.05	26.55			4.74	60.93				0.5		6.93		
4136-111		23.34		0.3	7.31	60.22		0.05		0.05	0.06	7.69		
4136-112	0.04	11.17	TR	0.14	3.61	77.06		0.04		0.3		7.36		
4136-113	0.08	26.75	0.05	0.41	12.74	50.71		0.2			0.05	7.79		
4136-114	TR	29.22		0.15	12.84	45.43		0.34		0.08		9.87		
4136-115	0.04	22.69		0.57	9.83	52.4		0.37		0.09		13.35		
4136-116		9.45		TR	64.86	5.38		0.47				4.24	0.06	
4136-117		19.81		0.19	63.17	8.37						5.89	TR	
4136-118	0.05	11.29	TR	TR	33.2	40.06		0.96		0.59		11.85	0.06	
4136-119		5.48			23.35	51.64		0.09		0.6		13.85	0.06	
4136-120	TR	1.36	TR	0.06	32.42	62.62				0.05		3.33		
4136-121	0.04	2.33		0.05	22.26	67.5		0.04		1.17		5.2	0.06	
4136-122	TR	38.79		0.27	5.68	52.03		TR		0.52		1.91	TR	
4136-123	TR	17.18	TR	1.53	13.97	58.59		0.16		0.76		7.57	0.11	
4136-124	0.14	22.96		5.21	7.67	61.37		0.04	TR	0.09		2.52		
4136-125	TR	26.74	0.93	1.66	5	61.78		0.41		0.13		3.29	0.06	
4136-126		25.41	0.88	3.49	15.62	50.57		0.48		0.3		2.34	0.29	
4136-127	0.04	27.47	1.26	0.65	9.2	57.92		0.71		0.08		2.23	0.39	
4136-128	0.22	14.04	TR	0.09	9.32	40.56		0.07		0.22		15.25	TR	1.05
4136-129	0.04	26.82	TR	0.05	7.79	57.7		0.04		0.58		3.65	0.11	
4136-130		32.7		TR	20.93	30.24						12.04	TR	
4136-131	0.22	9.17		TR	10.24	71.36				0.22		7.37	TR	
4136-132		0.66			11.47	71.47				0.21		16.14		
4136-133	1.91	0.74			3.66	71.55		0.1	TR			4.9	17.14	
4136-134		14.28	5.97	0.06	5.51	54.42		0.27		0.33		6.55	12.39	
4136-135		15.41	2.6	0.3	10.24	52.13				0.04		4.78	14.28	
4136-136	0.04	21.27	0.36	0.1	2.74	68.65		0.12		0.2		3.42	3	
4136-137		13.44	0.19	0.05	0.74	75.76		0.21		0.31		5.38	3.88	

Rutile Microprobe Analysis

Sample	SiO2	TiO2	Al2O3	FeO	MnO	MgO	CaO	V2O5	Cr2O3	NiO	Nb2O5	Ta2O5	ZnO	SO4	PbO	Sb2O3	UO3	ThO2	La2O3	Ce2O3	Nd2O3	Y2O3	P2O5	Co2O	Total
Cu1101-1	2.00	96.18	0.00	0.35	0.06	0.00	0.03	1.14	0.06	0.18	0.21	0.00	0.00	0.05	0.00	0.04	0.00	0.00	0.00	0.00	0.24	0.00	0.00	0.00	99.66
Cu1101-2	1.07	98.15	0.07	0.16	0.00	0.05	0.00	0.53	0.27	0.07	0.20	0.00	0.00	0.00	0.08	0.00	0.00	0.00	0.00	0.00	0.32	0.00	0.00	0.00	100.01
Cu1101-3	1.70	96.34	0.00	0.44	0.09	0.00	0.00	0.58	0.11	0.13	0.10	0.00	0.00	0.02	0.00	0.05	0.00	0.00	0.00	0.01	0.10	0.00	0.00	0.00	99.06
Cu1101-4	1.67	95.87	0.00	0.16	0.15	0.00	0.00	0.48	0.11	0.00	0.00	0.00	0.00	0.10	0.00	0.22	0.00	0.00	0.00	0.00	0.34	0.00	0.00	0.09	98.23
Cu1101-5	1.32	96.72	0.03	0.41	0.03	0.00	0.09	0.52	0.00	0.00	0.23	0.00	0.00	0.07	0.01	0.11	0.00	0.00	0.20	0.00	0.28	0.00	0.00	0.00	98.97
Cu1115-4	0.43	98.36	0.04	0.75	0.03	0.06	0.05	0.00	0.20	0.02	0.49	0.00	0.00	0.02	0.02	0.01	0.00	0.00	0.08	0.00	0.22	0.00	0.00	0.00	100.02
Cu1115-5	0.29	98.91	0.00	0.48	0.08	0.05	0.07	0.00	0.22	0.02	0.62	0.00	0.00	0.08	0.00	0.01	0.06	0.00	0.34	0.30	0.36	0.00	0.00	0.00	100.23
Cu1115-6	0.30	97.04	0.07	0.90	0.10	0.00	0.08	0.00	0.14	0.00	1.09	0.00	0.03	0.00	0.07	0.04	0.00	0.00	0.00	0.00	0.51	0.00	0.00	0.00	99.55
Cu1115-7	0.33	99.23	0.07	0.43	0.00	0.05	0.00	0.00	0.20	0.00	0.55	0.00	0.04	0.06	0.04	0.04	0.09	0.00	0.12	0.03	0.19	0.00	0.01	0.00	100.21
Cu1115-8	0.45	94.67	0.07	1.66	0.11	0.00	0.10	0.00	0.08	0.05	2.70	0.21	0.25	0.00	0.26	0.06	0.00	0.26	0.00	0.00	0.20	0.00	0.10	0.04	99.79
Cu1115-9	0.80	97.26	0.13	0.74	0.00	0.00	0.00	0.00	0.20	0.12	0.81	0.00	0.03	0.09	0.09	0.00	0.00	0.00	0.00	0.00	0.48	0.00	0.00	0.02	100.09
Cu1115-10	0.34	97.54	0.08	0.64	0.00	0.05	0.01	0.00	0.11	0.00	0.78	0.00	0.27	0.05	0.00	0.16	0.00	0.00	0.64	0.34	0.19	0.00	0.00	0.08	98.96
CU1115-11	0.45	95.57	0.19	1.39	0.05	0.00	0.06	0.00	0.05	0.12	2.25	0.17	0.17	0.08	0.00	0.00	0.02	0.00	0.00	0.00	0.14	0.00	0.00	0.00	100.01
Cu1115-12	3.03	95.62	1.00	0.73	0.00	0.03	0.17	0.00	0.07	0.00	0.70	0.00	0.35	0.12	0.00	0.49	0.00	0.00	0.03	0.01	0.17	0.00	0.06	0.05	101.74
Cu1115-13	0.73	95.03	0.07	0.81	0.00	0.00	0.04	0.00	0.05	0.00	0.94	0.00	0.04	0.04	0.00	0.20	0.00	0.00	0.00	0.00	0.38	0.00	0.07	0.00	97.50
Cu1115-17	0.43	97.71	0.00	0.67	0.16	0.00	0.03	0.00	0.00	0.00	0.67	0.00	0.19	0.06	0.00	0.12	0.00	0.00	0.49	0.03	0.00	0.00	0.03	0.00	99.48

Titanite Microprobe Analysis

Sample	SiO2	TiO2	Al2O3	FeO	MnO	MgO	CaO	V2O5	Cr2O3	NiO	Nb2O5	Ta2O5	ZnO	SO4	PbO	Sb2O3	UO3	ThO2	La2O3	Ce2O3	Nd2O3	Y2O3	P2O5	Co2O	Total
Cu769-2	28.99	35.75	1.08	1.72	0.11	0.00	26.96	0.00	0.02	0.00	0.40	0.02	0.00	0.05	0.00	0.85	0.00	0.02	0.28	1.06	0.94	0.57	0.10	0.08	97.92
Cu769-3	29.36	35.88	0.98	1.70	0.30	0.08	26.86	0.00	0.00	0.20	0.70	0.06	0.00	0.00	0.27	0.10	0.00	0.00	0.42	1.05	0.62	0.69	0.09	0.00	98.13
Cu769-4	28.01	31.86	1.31	2.74	0.20	0.04	26.52	0.00	0.10	0.07	1.42	0.23	0.00	0.00	0.00	0.59	0.08	0.43	0.37	1.19	0.42	0.00	0.89	0.00	94.76
Cu769-5	28.76	34.74	1.36	2.26	0.24	0.02	26.88	0.00	0.04	0.04	0.29	0.00	0.00	0.00	0.00	0.51	0.08	0.00	0.09	0.95	0.93	0.47	0.18	0.02	96.59
Cu769-6	30.78	36.88	1.35	1.30	0.16	0.00	28.36	0.08	0.11	0.00	0.11	0.02	0.22	0.00	0.00	0.63	0.02	0.16	0.00	0.13	0.27	0.35	0.11	0.00	99.66
Cu769-7	29.71	36.78	1.23	1.31	0.15	0.04	28.39	0.00	0.15	0.02	0.18	0.00	0.23	0.00	0.05	0.26	0.25	0.00	0.00	0.28	0.42	0.07	0.16	0.00	97.42
Cu769-8	30.12	37.06	1.18	1.17	0.05	0.06	28.40	0.00	0.09	0.00	0.24	0.00	0.00	0.08	0.00	0.16	0.00	0.09	0.00	0.00	0.45	0.36	0.00	0.00	98.74
Cu769-9	30.02	37.28	1.20	1.08	0.00	0.00	28.44	0.00	0.13	0.00	0.35	0.01	0.00	0.00	0.05	0.43	0.08	0.00	0.15	0.53	0.21	0.04	0.11	0.16	98.54
Cu769-10	29.09	35.87	1.07	1.71	0.22	0.05	26.54	0.00	0.15	0.00	0.29	0.11	0.00	0.00	0.08	0.17	0.09	0.12	0.26	1.04	0.76	0.55	0.01	0.05	96.95
Cu769-11	29.25	35.56	1.05	1.70	0.03	0.02	26.82	0.11	0.15	0.00	0.56	0.06	0.09	0.00	0.02	0.44	0.00	0.00	0.46	1.03	1.09	0.58	0.29	0.00	97.63
Cu769-12	29.24	36.16	1.10	1.60	0.07	0.00	27.29	0.00	0.00	0.00	0.19	0.04	0.14	0.00	0.00	0.57	0.06	0.11	0.01	0.58	1.06	0.55	0.11	0.16	98.14
Cu769-13	28.70	35.65	1.25	1.85	0.12	0.12	26.63	0.00	0.00	0.05	0.23	0.07	0.07	0.00	0.03	0.69	0.00	0.00	0.41	1.04	1.11	0.55	0.08	0.08	97.48
Cu769-14	29.54	35.94	1.09	1.62	0.24	0.05	26.57	0.00	0.11	0.03	0.36	0.09	0.00	0.00	0.08	0.30	0.05	0.00	0.40	1.21	0.67	0.51	0.08	0.12	97.50
Cu769-15	29.94	36.42	1.16	1.60	0.20	0.02	27.36	0.19	0.00	0.00	0.13	0.00	0.03	0.00	0.00	0.22	0.03	0.00	0.19	0.62	0.72	0.17	0.15	0.00	97.82
Cu769-16	30.04	36.99	1.41	1.25	0.20	0.00	28.51	0.02	0.21	0.00	0.24	0.00	0.00	0.00	0.05	0.29	0.00	0.01	0.00	0.21	0.38	0.04	0.15	0.00	98.41
Cu769-17	29.45	36.53	1.23	1.71	0.11	0.05	27.64	0.00	0.17	0.04	0.09	0.02	0.16	0.00	0.00	0.36	0.00	0.14	0.06	0.48	0.69	0.32	0.01	0.00	97.73
Cu769-18	28.69	36.91	1.01	1.05	0.07	0.00	26.35	0.00	0.09	0.14	0.31	0.00	0.08	0.26	0.00	0.62	0.00	0.28	0.13	0.28	0.44	0.16	0.20	0.00	94.89
Cu046-1	29.88	37.68	1.10	1.29	0.12	0.00	28.95	0.08	0.00	0.04	0.23	0.00	0.14	0.00	0.11	0.14	0.00	0.16	0.00	0.15	0.28	0.22	0.11	0.00	98.90
Cu046-2	30.86	37.66	1.19	1.43	0.00	0.07	29.18	0.00	0.06	0.18	0.17	0.00	0.29	0.03	0.06	0.44	0.00	0.04	0.00	0.00	0.26	0.14	0.12	0.03	100.31
Cu046-3	30.29	37.65	1.13	1.30	0.14	0.04	29.07	0.00	0.20	0.02	0.17	0.00	0.16	0.05	0.08	0.15	0.05	0.10	0.13	0.17	0.31	0.30	0.05	0.00	99.44
Cu046-4	30.04	37.32	1.07	1.24	0.18	0.00	28.58	0.00	0.00	0.03	0.12	0.05	0.00	0.00	0.14	0.22	0.08	0.26	0.05	0.30	0.25	0.00	0.35	0.02	98.59
Cu769*-1	29.98	36.29	1.26	1.49	0.28	0.05	28.01	0.00	0.11	0.11	0.23	0.02	0.15	0.00	0.00	0.45	0.00	0.07	0.24	0.72	0.65	0.38	0.06	0.00	99.06
Cu769*-2	28.96	37.07	1.11	1.21	0.16	0.03	27.74	0.03	0.07	0.00	0.11	0.01	0.16	0.00	0.00	0.29	0.00	0.00	0.09	0.45	0.42	0.12	0.00	0.00	96.53
Cu769*-3	30.06	36.11	1.05	1.69	0.19	0.08	27.48	0.02	0.00	0.02	0.47	0.00	0.06	0.00	0.12	0.46	0.00	0.12	0.24	0.62	0.61	0.29	0.03	0.00	98.10
Cu746-2t	22.00	20.28	2.26	5.01	0.00	0.24	16.70	0.00	0.00	0.00	0.01	1.32	0.05	0.64	14.81	n/a	0.00	0.18	0.19	0.39	0.26	0.04	0.32	0.00	83.26
Cu746-3t	29.63	36.72	1.17	1.63	0.10	0.04	27.78	0.00	0.04	0.00	0.27	0.90	0.10	0.01	0.09	n/a	0.03	0.00	0.49	0.97	0.46	0.35	0.16	0.08	98.24
Cu746-t5	28.94	38.09	0.76	1.09	0.00	0.00	27.97	0.20	0.00	0.00	0.10	2.29	0.28	0.03	0.00	n/a	0.00	0.08	0.00	0.25	0.72	0.36	0.00	0.00	100.21
Cu746-6t	28.96	36.40	1.27	1.72	0.16	0.00	28.08	0.07	0.02	0.05	0.21	1.80	0.06	0.00	0.16	n/a	0.00	0.05	0.09	0.38	0.48	0.30	0.15	0.11	98.70
Cu746-8t	29.63	37.00	0.92	1.15	0.19	0.00	28.03	0.22	0.01	0.00	0.41	0.91	0.02	0.00	0.03	n/a	0.00	0.00	0.45	0.56	0.64	0.12	0.17	0.00	97.92
Cu746-9t	28.79	36.30	0.90	1.49	0.15	0.00	26.90	0.00	0.15	0.00	0.55	1.07	0.20	0.04	0.07	n/a	0.01	0.15	0.61	1.19	0.66	0.26	0.27	0.06	96.79

Statistical Terms Presented Throughout This Thesis

Statistical Term	Definition	Equation
N **Valid**	Number of samples with values greater than 0	
Missing	Number of samples that contain no data	
Mean	A measure of central tendency. The arithmetic average; the sum divided by the number of cases	$\bar{x} = \frac{1}{n}\sum x_i$
Std. Error of Mean	A measure of how much the value of the mean may vary from sample to sample taken from the same distribution. It is defined as the standard deviation divided by the square root of the number of valid samples	$SE_{\bar{x}} = \frac{s}{\sqrt{n}}$
Median	The value above and below which half the cases fall, the 50th percentile. If there is an even number of cases, the median is the average of the two middle cases when they are sorted in ascending or descending order. The median is a measure of central tendency not sensitive to outlying values, unlike the mean, which can be affected by a few extremely high or low values	
Mode	The most frequently occurring value. If several values share the greatest frequency of occurrence, each of them is a mode	
Standard Deviation	A measure of dispersion around the mean. In a normal distribution, 68% of cases fall within one SD of the mean and 95% of cases fall within 2 SD	$s = \sqrt{\frac{1}{n-1}\sum(x_i - \bar{x})^2}$
Variance	Refers to the average of the squares of the standard deviations of the observations from their means. Both variance and standard deviation are measures of spread.	$s^2 = \frac{1}{n-1}\sum(x_i - \bar{x})^2$
Skewness	A measure of the asymmetry of a distribution. The normal distribution is symmetric, and has a skewness value of zero. A distribution with a significant positive skewness has a long right tail. A distribution with a significant negative skewness has a long left tail. As a rough guide, a skewness value more than twice it's standard error is taken to indicate a departure from symmetry	Skewness = $n*M_3/[(n-1)*(n-2)*s^3]$ where M_3 is equal to: $\sum (x_i\text{-Mean}_x)^3$
Standard Error of Skewness	The ratio of skewness to its standard error can be used as a test of normality (that is, you can reject normality if the ratio is less than -2 or greater than +2). A large positive value for skewness indicates a long right tail; an extreme negative value, a long left tail.	

Kurtosis	A measure of the extent to which observations cluster around a central point. For a normal distribution, the value of the kurtosis statistic is 0. Positive kurtosis indicates that the observations cluster more and have longer tails than those in the normal distribution and negative kurtosis indicates the observations cluster less and have shorter tails	Kurtosis = $[n*(n+1)*M_4 - 3*M_2*M_2*(n-1)]/[(n-1)*(n-2)*(n-3)*s^4]$ where: M_j is equal to: $\sum (x_i - Mean_x)^j$
Standard Error of Kurtosis	The ratio of kurtosis to its standard error can be used as a test of normality (that is, you can reject normality if the ratio is less than -2 or greater than +2). A large positive value for kurtosis indicates that the tails of the distribution are longer than those of a normal distribution; a negative value for kurtosis indicates shorter tails (becoming like those of a box-shaped uniform distribution).	
Range	The difference between the largest and smallest values of a numeric variable; the maximum minus the minimum	
Minimum	The smallest value of a numeric variable	
Maximum	The largest value of a numeric variable	
Percentiles	Values of a quantitative variable that divide the ordered data into groups so that a certain percentage is above and another percentage is below. Quartiles (the 25th, 50th, and 75th percentiles) divide the observations into four groups of equal size	

(All definitions from SPSS 10.1™)

Appendix 7

Table of Significance for Correlation Values (r)

Degrees of Freedom	r				
	0.1	0.05	0.02	0.01	0.001
1	0.988	0.997	0.999	1	1
2	0.9	0.95	0.98	0.99	0.999
3	0.805	0.878	0.934	0.959	0.992
4	0.729	0.811	0.882	0.917	0.974
5	0.669	0.754	0.833	0.874	0.951
6	0.621	0.707	0.789	0.834	0.925
7	0.582	0.666	0.75	0.798	0.898
8	0.549	0.632	0.716	0.765	0.872
9	0.521	0.602	0.685	0.735	0.847
10	0.497	0.576	0.658	0.708	0.823
11	0.476	0.553	0.634	0.684	0.801
12	0.457	0.532	0.612	0.661	0.78
13	0.441	0.514	0.592	0.641	0.76
14	0.426	0.497	0.574	0.623	0.742
15	0.412	0.482	0.558	0.606	0.725
16	0.4	0.468	0.543	0.59	0.708
17	0.389	0.456	0.528	0.575	0.693
18	0.378	0.444	0.516	0.561	0.679
19	0.369	0.433	0.503	0.549	0.665
20	0.36	0.423	0.492	0.537	0.652
25	0.323	0.381	0.445	0.487	0.597
30	0.296	0.349	0.409	0.449	0.554
35	0.275	0.325	0.381	0.418	0.519
40	0.257	0.304	0.358	0.393	0.49
45	0.243	0.287	0.338	0.372	0.465
50	0.231	0.273	0.322	0.354	0.443
60	0.211	0.25	0.295	0.325	0.408
70	0.195	0.232	0.274	0.302	0.38
80	0.183	0.217	0.256	0.283	0.357
90	0.173	0.205	0.242	0.267	0.337
100	0.164	0.195	0.23	0.254	0.321

Appendix 8A

Significance Table for Radomiro Tomic Concentrates

All Values against Rutile (vol.%)

Mineral	Pearson Correlation	Number of Pairs (N)	Significance
CP	0.074	16	NS
CC	0.212	15	NS
DI	0.322	4	NS
CV	0.006	16	NS
BN	0.787	15	S**
CU.G	1	2	S**
PY	-0.826	18	S**
MO	-0.38	15	NS
SPH	0.517	6	NS
GA	1	2	S**
HE	0.13	7	NS
LIM	0.895	4	S
GN	0.789	18	S**

Note: Classification of significance is based on Brooks et al., (1972), as follows:
Probability greater than 0.1, not significant (NS)
Probability between 0.10 and 0.05, possibly significant (PS)
Probability between 0.05 and 0.01, significant (S)
Probability between 0.01 and 0.001, highly significant (S*)
Probability less than 0.001, very highly significant (S**)
Note: a. Cannot be computed because at least one of the variables is constant

Appendix 8B

Significance Table for Chuquicamata Concentrates

All Values against Rutile (vol.%)

Mineral	Pearson Correlation	Number of Pairs (N)	Significance
CP	0.654	57	S**
CC	-0.297	50	S
DI	-0.119	33	NS
CV	-0.089	45	NS
BN	0.132	39	NS
EN	-0.306	17	NS
PY	-0.591	57	S**
MO	0.09	34	NS
SPH	-0.159	31	NS
GA	0.601	5	NS
LI	0.619	7	PS
HE	0.095	42	NS
GN	0.137	57	NS
CU.G	0.827	4	S
MG	-0.021	22	NS

Note: Classification of significance is based on Brooks et al., (1972), as follows:
Probability greater than 0.1, not significant (NS)
Probability between 0.10 and 0.05, possibly significant (PS)
Probability between 0.05 and 0.01, significant (S)
Probability between 0.01 and 0.001, highly significant (S*)
Probability less than 0.001, very highly significant (S**)

Appendix 8C

Significance Table for Mansa Mina Concentrates

All Values against Rutile (vol.%)

Mineral	Pearson Correlation	Number of Pairs (N)	Significance
CP	0.642	28	S**
CC	-0.271	54	S
CV	-0.295	13	NS
BN	0.117	41	NS
CU.G	0.081	40	NS
EN	-0.092	52	NS
PY	-0.256	56	S
MO	0.049	10	NS
SPH	-0.005	41	NS
GA	1	2	S**
LI	-0.311	14	NS
HE	0.216	7	NS
GN	0.376	56	S*
DI	-0.326	14	NS
CU.OX	a	1	NS

Note: Classification of significance is based on Brooks et al., (1972), as follows:
Probability greater than 0.1, not significant (NS)
Probability between 0.10 and 0.05, possibly significant (PS)
Probability between 0.05 and 0.01, significant (S)
Probability between 0.01 and 0.001, highly significant (S*)
Probability less than 0.001, very highly significant (S**)
Note: a. Cannot be computed because at least one of the variables is constant

Appendix 9A

Significance Table for RT Major Elements

All Values against Ti (wt.%)

Element (%)	Pearson Correlation	Number of Pairs (N)	Significance
Cu	0.821	23	S**
Fe	-0.83	23	S**
Mo	0.115	23	NS
As	1	2	S**
Pb	0.202	23	NS
Zn	0.443	23	S
Sb	a	1	NS

Note: Classification of significance is based on Brooks et al., (1972), as follows:
Probability greater than 0.1, not significant (NS)
Probability between 0.10 and 0.05, possibly significant (PS)
Probability between 0.05 and 0.01, significant (S)
Probability between 0.01 and 0.001, highly significant (S*)
Probability less than 0.001, very highly significant (S**)
Note: a. Cannot be computed because at least one of the variables is constant

Appendix 9B

Significance Table for Chuquicamata Major Elements

All Values against Ti (wt.%)

Element (%)	Pearson Correlation	Number of Pairs (N)	Significance
Cu	-0.207	59	NS
Fe	0.089	59	NS
Mo	-0.157	54	NS
As	-0.303	42	PS
Pb	-0.241	58	PS
Zn	-0.23	59	PS
Sb	-0.525	10	PS

Note: Classification of significance is based on Brooks et al., (1972), as follows:
Probability greater than 0.1, not significant (NS)
Probability between 0.10 and 0.05, possibly significant (PS)
Probability between 0.05 and 0.01, significant (S)
Probability between 0.01 and 0.001, highly significant (S*)
Probability less than 0.001, very highly significant (S**)
Note: a. Cannot be computed because at least one of the variables is constant

Appendix 9C

Significance Table for Mansa Mina Major Elements

All Values against Ti (wt.%)

Element (%)	Pearson Correlation	Number of Pairs (N)	Significance
Cu	-0.432	75	S**
Fe	0.171	75	NS
Mo	0.358	53	S*
As	-0.314	74	S*
Pb	0.478	75	S**
Zn	0.177	75	NS
Sb	-0.088	64	NS

Note: Classification of significance is based on Brooks et al., (1972), as follows:
Probability greater than 0.1, not significant (NS)
Probability between 0.10 and 0.05, possibly significant (PS)
Probability between 0.05 and 0.01, significant (S)
Probability between 0.01 and 0.001, highly significant (S*)
Probability less than 0.001, very highly significant (S**)
Note: a. Cannot be computed because at least one of the variables is constant

Appendix 10

Summary of Selected Morphological Measurements Based on Rutile Image Analysis

Sample: TF1 CH Composite

Measurement	# of Grains	Mean	Median	Min	Max	Std. Dev.
Area (μm^2)	26	607.8	142.7	12.2	4757	1103
Aspect Ratio	26	1.785	1.543	1.165	5.609	0.8283
Circularity	26	1.418	1.247	1.022	2.547	0.4241
Compactness	26	0.7787	0.8176	0.3825	0.9457	0.1369
Form Factor	26	0.6019	0.6425	0.1542	0.9579	0.247
Roundness	26	0.4612	0.4644	0.1647	0.7763	0.1538
Waddel Diameter (µm)	26	19.92	13.36	3.941	77.83	19.42

Sample: TF1A CH Concentrate

Measurement	# of Grains	Mean	Median	Min	Max	Std. Dev.
Area (μm^2)	103	288.7	89.56	8.713	4628	644.4
Aspect Ratio	103	1.897	1.72	1.126	4.57	0.6484
Circularity	103	1.376	1.269	1.021	2.505	0.3224
Form Factor	103	0.6003	0.6218	0.1593	0.9601	0.2145
Roundness	103	0.4403	0.4623	0.1357	0.6869	0.1432
Waddel Diameter (µm)	103	14.28	10.12	3.331	76.77	12.79

Sample: TF2 MM Composite

Measurement	# of Grains	Mean	Median	Min	Max	Std. Dev.
Area (μm^2)	23	215.5	115.2	8.713	1478	355.2
Aspect Ratio	23	1.894	1.812	1.147	2.887	0.5316
Circularity	23	1.556	1.487	1.044	2.764	0.4207
Form Factor	23	0.4989	0.4553	0.1309	0.9174	0.232
Roundness	23	0.3791	0.4026	0.157	0.6938	0.158
Waddel Diameter (µm)	23	13.23	12.24	3.331	43.38	9.962

Sample: TF2A MM Concentrate

Measurement	# of Grains	Mean	Median	Min	Max	Std. Dev.
Area (μm^2)	50	367.1	66.45	10.46	7476	1094
Aspect Ratio	50	1.719	1.667	1.194	3.367	0.4594
Circularity	50	1.313	1.185	1.013	3.382	0.4186
Form Factor	50	0.6745	0.7325	0.0874	0.974	0.219
Roundness	50	0.4906	0.5013	0.1975	0.7376	0.1409
Waddel Diameter (µm)	50	14.86	9.049	3.649	97.56	15.71

Appendix 10

Sample: TF3 RT Composite

Measurement	# of Grains	Mean	Median	Min	Max	Std. Dev.
Area (μm^2)	5	466	438.3	101.1	1147	373.2
Aspect Ratio	5	1.796	1.448	1.347	2.647	0.5032
Circularity	5	1.539	1.471	1.229	2.132	0.312
Form Factor	5	0.4656	0.4618	0.22	0.6617	0.1453
Roundness	5	0.4194	0.4328	0.2948	0.5723	0.1045
Waddel Diameter (μm)	5	22.42	23.64	11.34	38.21	9.516

Sample: TF3A RT Concentrate

Measurement	# of Grains	Mean	Median	Min	Max	Std. Dev.
Area (μm^2)	164	751.5	215.8	8.713	11843	1572
Aspect Ratio	164	1.749	1.63	1.115	4.335	0.5587
Circularity	164	1.383	1.243	1.02	3.571	0.4007
Form Factor	164	0.6107	0.6462	0.0784	0.9621	0.2188
Roundness	164	0.4743	0.4759	0.0503	0.7747	0.1494
Waddel Diameter (μm)	164	22.94	16.17	3.331	122.8	20.75

Appendix 11

Summary of Selected Morphological Measurements Based on Molybdenite Image Analysis

Sample: TF3A

Measurem	# data	Mean	Median	Min	Max	sd.
Area (μm^2)	84	441.4	12.9	1.383	4608	927.7
Aspect rati	84	2.285	1.838	1.127	7.74	1.139
Circularity	84	1.47	1.287	1.013	3.341	0.4863
Form facto	84	0.5842	0.6048	0.0896	0.974	0.2702
Roundness	84	0.3906	0.4036	0.0938	0.7293	0.1479
Waddel dia	84	14.91	5.279	1.327	76.6	18.43

Appendix 12

DALHOUSIE
University

MINERALS ENGINEERING CENTRE

DalTech
P.O. Box 1000
Halifax, Nova Scotia
B3J 2X4

Tel: 902.494.3955
Fax: 902.425.1037
E-mail: mec@dal.ca

November 20, 2001

Department of Earth Sciences
Dalhousie University

Attention: Dr. M. Zentilli

Re: Results of Size Analysis on Submitted Samples.

Sample:	CH		MM		RT	
	%		%		%	
Microns	Retained	Cumulat Passing	Retained	Cumulat Passing	Retained	Cumulat Passing
500	0.00	100.00	0.00	100.00	0.00	100.00
250	0.44	99.56	0.09	99.91	16.06	83.94
150	38.50	61.06	36.69	63.22	30.81	53.13
75	36.19	24.87	35.34	27.88	29.16	23.97
45	15.13	9.74	14.42	13.46	12.66	11.31
38	4.16	5.58	3.98	9.48	2.94	8.37
32	1.72	3.86	2.06	7.42	1.61	6.76
23.8	1.89	1.97	2.88	4.54	2.43	4.33
17.7	0.82	1.15	2.07	2.47	1.48	2.85
11.4	0.77	0.38	1.63	0.84	1.63	1.22
7.3	0.16	0.22	0.42	0.42	0.59	0.63
4.7	0.17	0.05	0.28	0.14	0.38	0.25
3.0	0.05	0.00	0.14	0.00	0.25	0.00
1.9	0.00	0.00	0.00	0.00	0.00	0.00
-1.9	0.00		0.00		0.00	
Total	100.00		100.00		100.00	

Cyril Cole

Appendix 13

Mesh Size Conversion Chart

Mesh	*Micron*	*mm*	*Inches*
4	5205	5.205	0.2030
8	2487	2.487	0.0970
10	1923	1.923	0.0750
14	1307	1.307	0.0510
18	1000	1.000	0.0394
20	840	0.840	0.0331
25	710	0.710	0.0280
30	590	0.590	0.0232
35	500	0.500	0.0197
40	420	0.420	0.0165
45	350	0.350	0.0138
50	297	0.297	0.0117
60	250	0.250	0.0098
70	210	0.210	0.0083
80	177	0.177	0.0070
100	149	0.149	0.0059
120	125	0.125	0.0049
140	105	0.105	0.0041
170	88	0.088	0.0035
200	74	0.074	0.0029
230	62	0.062	0.0024
270	53	0.053	0.0021
325	44	0.044	0.0017
400	37	0.037	0.0015*
550	25	0.025	0.0009
800	15	0.015	0.0006
1250	10	0.010	0.0004
...	5	0.005	0.0002
...	1	0.001	0.000039

*Threshold of Visibility